DEVELOPMENT OF DOXORUBICIN LOADED LIPOSOMES SELF-ASSEMBLED WITH POLYSACCHARIDES FOR BREAST CANCER THERAPY

A Thesis Submitted to
the Graduate School of Engineering and Sciences of
İzmir Institute of Technology
in Partial Fulfillment of the Requirements for the Degree of

MASTER OF SCIENCE

in Biotechnology

by
Ayşenur Başar ÖNOL

July 2023
İZMİR

We approve the thesis of **Ayşenur Başar ÖNOL.**

Examining Committee Members:

_____

Assoc. Prof. Dr. Sevgi KILIÇ ÖZDEMİR

Department of Chemical Engineering, İzmir Institute of Technology

_____

Prof. Dr. Volga BULMUŞ ZAREIE

Department of Bioengineering, İzmir Institute of Technology

_____

Prof. Dr. Zekiye SULTAN ALTUN

Department of Basic Oncology, Dokuz Eylül University

20 July 2023

_____

Assoc. Prof. Dr. Sevgi KILIÇ ÖZDEMİR
Supervisor, Department of
Chemical Engineering
İzmir Institute of Technology

_____

Prof. Dr. Hürriyet POLAT
Co-Supervisor, Department of
Chemistry
İzmir Institute of Technology

_____

Assoc. Prof. Dr. Ali Oğuz BÜYÜKKİLECİ
Chair, Biotechnology
Graduate Programme
İzmir Institute of Technology

_____

Prof. Dr. Mehtap EANES
Dean of the Graduate School
Engineering and Sciences
İzmir Institute of Technology

ACKNOWLEDGEMENTS

I want to express my sincere gratitude to my thesis advisor, Assoc. Prof. Dr. Sevgi KILIÇ ÖZDEMİR, for her guidance, thoughtful advice, and continuous encouragement during the course of this work. I want to thank Prof. Dr.Hürriyet POLAT for her co-advising during my thesis. I would also like to thank Prof. Dr. Ekrem ÖZDEMİR for his guidance and support. I would also like to thank Prof. Dr. Zekiye SULTAN ALTUN and Ph.D. Selen KUM ÖZŞENGEZER for conducting in-vitro studies.

I would also like to thank my examining committee members, Prof. Dr.Volga BULMUŞ ZAREIE and Prof. Dr. Zekiye SULTAN ALTUN, for their suggestions and help.

I thank Dr. Sedef TAMBURACI, Burcu SIRMA TARIM, and İrem Yakar for an unbelievable year together and also Anılcan KUŞ for his support while writing my thesis. I extend my special thanks to lab member Ezgi İrem SAĞLAM.

I would like to also thank The Scientific and Technological Research Council of Turkey (TÜBİTAK) for the financial support throughout the project with grant number 121M625.

Finally, I would like to express my heartfelt gratitude, especially to my mother, Bahar ÖNOL, for always believing in me and supporting me in reaching my dreams (my journey is just starting now) and my father, Kamil Müsavat ÖNOL, who was always with me despite the distance, for their unconditional love, encouragement, sacrifices and unshakable faith in me and endless support over my whole life.

ABSTRACT

DEVELOPMENT OF DOXORUBICIN-LOADED LIPOSOMES SELF-ASSEMBLED WITH POLYSACCHARIDES FOR BREAST CANCER THERAPY

This thesis aimed to develop Tariquidar and Doxorubicin-loaded liposomes decorated by Fucoidan coating for breast cancer treatment. Fucoidan is a negatively charged polysaccharide with a special affinity to p-selectins expressed on MDA-MB-231 breast cancer cells and, at the same time, possesses anti-cancer activity. Different liposomes were prepared by extrusion method from the DSPC, Cholesterol, and cationic lipid DSTAP mixtures for coating negatively charged Fucoidan. The most stable liposomes with a size of 200 nm were obtained at a molar ratio of DSPC/Cholesterol/DSTAP:55/30/15, exhibiting a zeta potential above +30 mV. Tariquidar was encapsulated into the liposome bilayer by passive loading, and Doxorubicin into the core of the liposome by active loading. In the final step, liposomes were coated with Fucoidan by electrostatic interaction. Tariquidar loading was determined by UV-Vis spectrophotometry, indicating an optimum TRQ/Lipid molar ratio of 0.012 with encapsulation and loading efficiencies of 50% and 20%, respectively. Fluorescence spectrophotometry determined Doxorubicin loading, showing insignificant encapsulation efficiency change (exhibiting around 70%) by neither Tariquidar content in the bilayer nor DSTAP% in the formulation. An optimum amount of Fucoidan was determined by incubating the liposomes with varying amounts of fucoidan at different dilutions. Size and zeta potential measurements monitored the coating of liposomes with Fucoidan. Our finding showed that zeta potentials of liposomes go from positive to negative with increasing fucoidan, while no trend was observed in the size of liposomes. However, smaller sizes were observed when incubation was performed in diluted solutions.

ÖZET

MEME KANSERİ TEDAVİSİ İÇİN POLİSAKKARİTLERLE BİRLEŞTİRİLMİŞ DOKSORUBİSİN YÜKLÜ LİPOZOMLARIN GELİŞTİRİLMESİ

Bu tezde, meme kanseri tedavisi için Fucoidan kaplama ile dekore edilmiş Tariquidar ve Doksorubisin yüklü lipozomların geliştirilmesi amaçlanmıştır. Fucoidan, MDA-MB-231 meme kanseri hücrelerinde eksprese edilen p-selektinlere özel bir afiniteye sahip ve aynı zamanda anti-kanser özelliğe sahip negatif yüklü bir polisakkarittir. Farklı Lipozomlar, DSPC, Kolesterol ve negatif yüklü Fucoidan'ın kaplanması için katyonik lipid DSTAP karışımlarından ekstrüzyon yöntemiyle hazırlandı. En stabil lipozomlar, 200 nm boyutunda ve +30 mV'nin üzerinde bir zeta potansiyeli sergileyen DSPC/Kolesterol/DSTAP:55/30/15 molar oranında elde edildi. Tariquidar, pasif yükleme ile lipozom çift katmanına ve Doksorubisin, aktif yükleme ile lipozomun çekirdeğine enkapsüle edildi. Son aşamada ise, lipozomlar elektrostatik etkileşim yardımıyla Fucoidan ile kaplandı. Tariquidar yüklemesi, UV-Vis spektrofotometresi ile belirlendi ve sırasıyla %50 ve %20'lik enkapsülasyon ve yükleme verimlilikleriyle TRQ/Lipid molar oranında 0,012'lik bir optimum gösterdi. Doksorubisin yüklemesi Fluoresence spektrofotometri ile belirlendi ve enkapsülasyon verimliliğinin ne çift tabakadaki Tariqidar içeriğinden ne de formülasyondaki %DSTAP içeriğinden önemli ölçüde etkilenmeyerek %70 civarında bir enkapsülasyon verimliliği gösterdiği gözlemlendi. Optimum Fucoidan miktarı, lipozomların farklı dilüsyonlarda değişen miktarlarda fucoidan ile inkübe edilmesiyle belirlendi. Lipozomların Fucoidan ile kaplanması boyut ve zeta potansiyeli ölçümleriyle izlendi. Elde edilen sonuçlar, lipozomların zeta potansiyellerinin, artan fucoidan ile pozitiften negatife gittiğini, lipozomların boyutlarında ise herhangi bir trend olmadığını gösterdi. Ancak, seyreltilmiş çözeltilerde inkübasyon yapıldığında daha küçük boyutlar gözlendi.

To my family and for my dreams;

TABLE OF CONTENTS

LIST OF FIGURES

Figure **Page**

LIST OF TABLES

Table **Page**

LIST OF EQUATIONS

CHAPTER 1

INTRODUCTION

Targeted drug delivery systems are prevalent in this century. Chemotherapeutic chemicals used in conventional cancer treatment are not selective since they spread to normal cells in addition to the target tumor site, which reduces the effective dose in the tumor. Nanoparticles can increase the intracellular concentration of drugs in cancer cells and reduce or inhibit the toxicity of healthy cells. These intelligent drug delivery systems can also be created to be more specific to provide key-lock compatibility with specific unique cell receptors. (Ross et al., 2004; Larsen et al., 2000). Liposomes are the kind of nanoparticles that carry drug and are frequently used for this purpose.

Doxorubicin hydrochloride (DOX-HCl) is a commonly used anticancer agent, an anthracyclic antibiotic widely used to treat many types of cancer. DOX in the free form has many side effects, such as Hand–foot syndrome (HFS), cardiotoxicity, etc. However, liposomal doxorubicin has lower than free form. Several advantages include reducing the risk of immune system response, allowing the drug to remain in the bloodstream long-term, and providing a targeted drug delivery to only specific tumor cells but not to healthy cells (Allen & Cullis, 2004; Torchilin, 2005). Myocardial damage may lead to congestive heart failure and may occur as the total cumulative dose of doxorubicin HCl approaches 550 mg/m^2.

Multidrug resistance (MDR) is acquired resistance to chemotherapy medications in cancer cells and bacteria characterized by various chemical structures and modes of action. The overexpression of several proteins that expel chemotherapeutics from cells and reduce their concentration below the therapeutic level leads to MDR. The targeting of P-glycoprotein (P-gp), known as transmembrane transporter, mediates MDR in cancer and is the efflux pump commonly known, as an innovative strategy for overcoming multidrug resistance. According to research by Matzneller et al. (2018), the third-

generation P-gp inhibitor tariquidar (XR9576) enhances the brain distribution of P-gp substrate medicines in humans (Matzneller et al., 2018).

Key-lock conformation is an important keyword in targeted drug delivery systems. This key-lock conformation illustrates receptor–ligand interaction—for example, CD44 antigen to Hyaluronic acid and p-selectin to Fucoidan. Long-chain sulfated polysaccharide called Fucoidan is present in some species of brown algae. This study used the Fucus Vesiculosis form of Fucoidan to target the liposomes to p-selectin expressed in breast cancer cells.

This study aimed to design a targeted drug delivery system comprising DOX as an anticancer agent and Tariquidar as a p-glycoprotein inhibitor. Liposomes were used as Drug delivery agents because of its benefit besides the free form of drugs.

CHAPTER 2

LITERATURE SURVEY

2.1 Cancer

Cancers are linked to improper cell proliferation. The fundamental abnormality resulting in cancer development is the continual unregulated proliferation of cancer cells. Rather than responding appropriately to the signals that control normal cell behavior, cancer cells grow and divide uncontrolled, invading normal tissues and organs and eventually spreading throughout the body. The generalized loss of growth control exhibited by cancer cells is the net result of accumulated abnormalities in multiple cell regulatory systems. It is reflected in several aspects of cell behavior that distinguish cancer cells from their normal counterparts. Some crucial signals necessary for cell growth and development have deteriorated, causing this unusual growth. Cell division that is out of control is the basis of cancer. Cancer is diverse because cancer cells have complex genotypes and phenotypes. Cancer can result from abnormal proliferation of any of the different kinds of cells in the body, so there are more than a hundred distinct types of cancer, which can vary substantially in their behavior and response to treatment. The most critical issue in cancer pathology is the distinction between benign and malignant tumors. A tumor is any abnormal proliferation of cells, which may be benign or malignant. A benign tumor, such as a common skin wart, remains confined to its original location, neither invading surrounding normal tissue nor spreading to distant body sites. A malignant tumor, however, can invade surrounding normal tissue and spread throughout the body via the circulatory or lymphatic systems (metastasis). Only malignant tumors are correctly referred to as cancers, and their ability to invade and metastasize makes cancer dangerous.

Figure 1 indicates the various vital changes that occur in a cancer cell are-capacity

to proliferate without any growth signals, resistance to growth-inhibiting signals, resistance to regular cell death mechanisms, formation of new blood supply, ability to involve surrounding tissues, metastasis to distant organs and failure in the repair of damaged DNA.

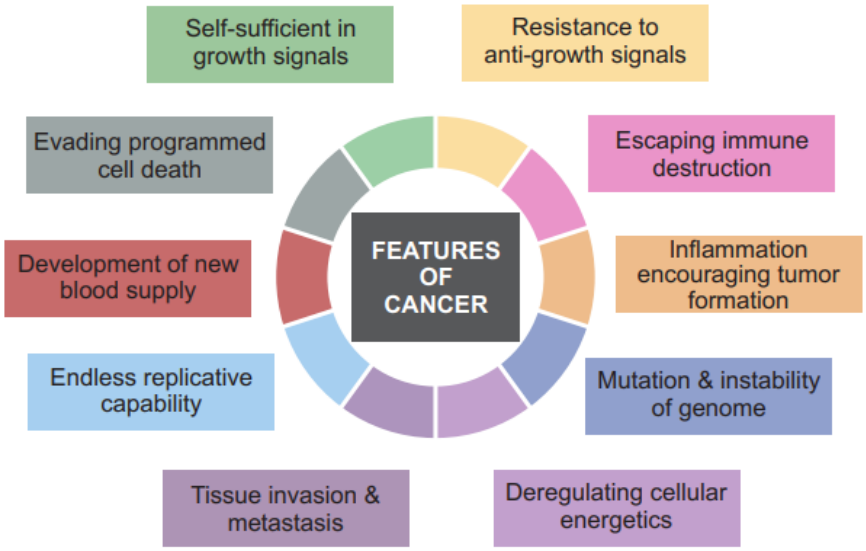

Figure 1. Features of Cancer – Major changes occurring in a cell undergoing malignant change.

At the cellular level, cancer development is viewed as a multistep process involving mutation and selection for cells with progressively increasing capacity for proliferation, survival, invasion, and metastasis (Figure 2). The first step in the process, tumor initiation, is thought to result from a genetic alteration leading to the abnormal proliferation of a single cell. Cell proliferation then leads to the outgrowth of clonally derived tumor cells. Tumor progression continues as additional mutations occur within cells of the tumor population. Some of these mutations confer a selective advantage to the cell, such as more rapid growth, and the descendants of a cell bearing such a mutation will consequently become dominant within the tumor population. The process is called clonal selection since a new clone of tumor cells has evolved based on its increased growth rate or other properties (such as survival, invasion, or metastasis) that confer a selective

advantage. The clonal selection continues throughout tumor development, so tumors continuously grow rapidly and become increasingly malignant. Metastasis is the last step. Cancer cells can spread to other parts of the body through a complicated process called metastasis, in which they separate from the initial tumor and move through the bloodstream or lymphatic system. The cells continue to divide into new places, eventually producing more tumors of cells that resemble the original tissue. The lethality of malignancies, such as pancreatic and uveal tumors, is largely influenced by their capacity to spread.

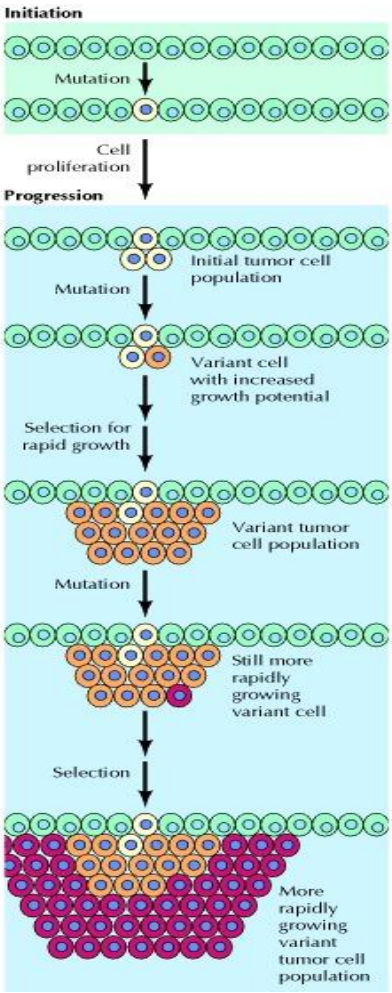

Figure 2. Stages of tumor development(Mohamed et al. 2021).

2.2 Breast Cancer

Breast cancer is the most prevalent cancer for men and women in most countries worldwide (Bray et al., 2011).

Breast tissue mainly consists of glands for milk production, called lobules, ducts carrying milk from lobules to the nipple, and stroma, composed of surrounding fatty tissue and connective tissue. Invasive and non-invasive breast cancer are both possible. Breast cancer that has spread to nearby tissues or distant organs is referred to as invasive breast cancer. Breast lobules or milk ducts are the limits of non-invasive breast cancer. Breast cancers come in various forms and are categorized according to how they appear under a microscope.

- Ductal cancer: This is the most typical form of breast cancer.
- Ductal carcinoma in situ (DCIS): This non-invasive malignancy is contained to the duct alone and has not spread outside.
- Infiltrating or invasive ductal carcinoma: This malignancy has migrated beyond the ducts or lobules.
- Lobular cancer with invasion: Breast cancer that has migrated outside of the ducts or lobules is a less frequent kind.

Table 1 shows the subclasses and mutation status of various breast cancer cell lines. As seen, there are three main subclasses of breast cancer cells.

- **Hormone receptor-positive:** Tumors expressing ER and PR in the breast are considered "hormone receptor-positive." The expression "ER-positive" implies tumors that express estrogen receptors. Tumors expressing progesterone receptors are referred to as "PR positive." Estrogen or progesterone may be essential to developing this particular form of cancer. Progesterone antiandrogen receptors can be found in around two-thirds of breast tumors. Those cancers that lack these receptors are called "hormone receptor-negative." Hormone therapy is frequently utilized to treat breast cancers that contain hormone receptors.

- **HER2 positive:** The human epidermal growth factor receptor 2 (HER2) gene is necessary to develop 10% to 20% of breast tumors. The expression "HER2 positive" applies to particular tumors. The HER2 protein, which is present in cancer cells and is essential for tumor cell proliferation, is produced by the HER2 gene. Breast tumors that are HER2-positive spread more quickly. They can also have either positive or negative hormone receptors. "HER2 negative" cancers either lack or have meager amounts of the HER2 protein and the HER2 gene.
- **Triple-negative:** A tumor is called "triple negative" if it lacks the expression of ER, PR, and HER2. Between 10% and 20% of invasive breast cancers are triple-negative.

Table 1 Breast Cancer Cell Lines (Warchal, Dawson, and Carragher 2016)

Cell line	Subclass	Mutation Status	
		PTEN	PI3K
MCF7	ER	WT	E545K
T47D	ER	WT	H1047R
MDA-MB-231	TN	WT	WT
MDA-MB-157	TN	WT	WT
HCC1569	HER2	WT	WT
SKBR3	HER2	WT	WT
HCC1954	HER2	-	H1047R
KPL4	HER2	-	H1047R

PTEN: Phosphatase and tensin homolog.

PI3K: Phosphoinsitide-3-kinase.

ER: Estrogen receptor.

WT: Wild type.

TN: Triple negative. f

HER2: Human epidermal growth factor receptor 2. (Warchal, Dawson, and Carragher 2016)

MDA-MB-231 cells are one of the most commonly used breast cancer cell lines in medical research laboratories. They were first isolated from the pleural effusion of a 51-year-old woman with breast adenocarcinoma, as seen in Figure 3. In a cell with a non-normal karyotype, the number of chromosomes in the line is unstable. The number of chromosomes in karyotype analysis is close to triploid values. It has been observed to have a small number of standard and a very small number of da chromosomes; there are no N8 and N15 chromosomes. The mentioned chromosomes are used as markers within the scope of cytogenetic analysis. Karyotype analyses have shown that cell populations are not homogeneous regarding chromosome numbers and structures. This cell line, which models specific properties of breast cancer cells, is a very suitable model for studying invasive cancer in vitro conditions. MDA-MB231 cells, which are ER-negative, have lost the properties shown by normal breast cells. The changes in MDA-MB-231 cells are related to tumor progression, metastasis formation, and resistance to programmed cell death.

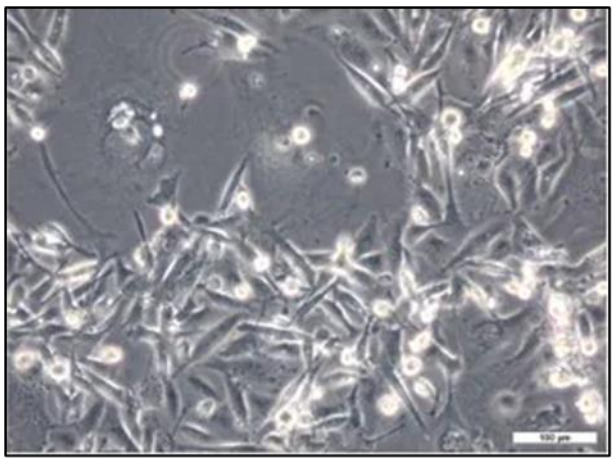

Figure 3. MDA-MB-231 Breast Cancer Cell.

2.3 Treatment of Cancer

Cancer is sometimes considered not a treatable illness; however, improvements in Medicine and the invention of modern medicines help overcome cancer more

efficiently. There are many methods, but the main ones are surgery and modern technologies such as radiation therapy, chemotherapy, immunotherapy, hormonal therapy, and targeted drug delivery applications (Sudhakar, 2009). Radiation therapy and surgery are the first options for a treatment method, but both result in misleadings. (Brizel et al., 1994). Most people have a combination of treatments, such as surgery with chemotherapy and radiation therapy.

- Surgery: A surgeon performs surgery to eliminate cancer from the body.
- Radiation therapy: High doses of radiation are used in radiation therapy, a type of cancer treatment, to destroy cancer cells and reduce tumor size.
- Chemotherapy: Drugs are used in chemotherapy, a type of cancer treatment, to destroy cancer cells.
- Immunotherapy: Immunotherapy is a cancer treatment that supports the immune system's ability to combat cancer.
- Hormone therapy: Breast and prostate cancers that utilize hormones to grow can be treated with hormone therapy to delay or stop their growth.
- Targeted therapy: A type of cancer treatment known as targeted therapy focuses on the alterations cancer cells undergo to multiply, proliferate, and spread.
- Stem cell transplants: Patients with cancer who had their blood-forming stem cells destroyed by extremely high doses of chemotherapy or radiation therapy can have their stem cells replaced through stem cell transplant procedures.
- Practical therapy: Precision medicine enables clinicians to choose the most likely to benefit their patients based on a genetic understanding of their ailment.

2.4 Chemotherapy

Chemotherapy is a commonly used cancer treatment that involves the use of medication to destroy cancer cells. Chemotherapy drugs come in various forms, but they all function similarly. They block cancer cells from multiplying, which stops them from developing and spreading throughout the body. Chemotherapy may be given by mouth, injection, infusion, or on the skin, depending on the type and stage of the cancer being treated. Although chemotherapy seems the best option, it also has limitations. Chaplin et

al. mentioned that the success of chemotherapy depends on the reaching tumor site because only a small amount, about 2% of the drug injected, reaches the target area, and the rest of the chemotherapeutic drug redistribute throughout the body (Chaplin et al.,1996).

2.5 Chemotherapeutic Drugs

The majority of chemotherapeutic drugs and pharmaceuticals act by preventing DNA production or function. Different cell cycle stages are affected differently by each chemotherapy medication. Chemotherapy medicines can be categorized as cell-cycle-specific (effective during certain stages of the cell cycle) or nonspecific (effective during all cell cycle phases), depending on how they work.

There are four main steps in the cytotoxic action of a chemotherapeutic drug on a cell:

- The drug enters or is actively taken up by the cell.
- The drug is activated (or its activity is preserved) within the cell.
- The drug affects its target(s) within the cell.
- If the damage caused is irreparable, cell death may be induced(Redmond et al.,2008; Stavrovskaya, 2000).

Chemotherapy agents can be classified as alkylating agents, antimetabolites, anthracyclines, antitumor antibiotics, monoclonal antibodies, platinum, or plant alkaloids, depending on their properties and kind of therapy seen in

Figure 4. Most cancer medications come from natural sources like bacteria and plants, while others come from synthetic or semi-synthetic methods.

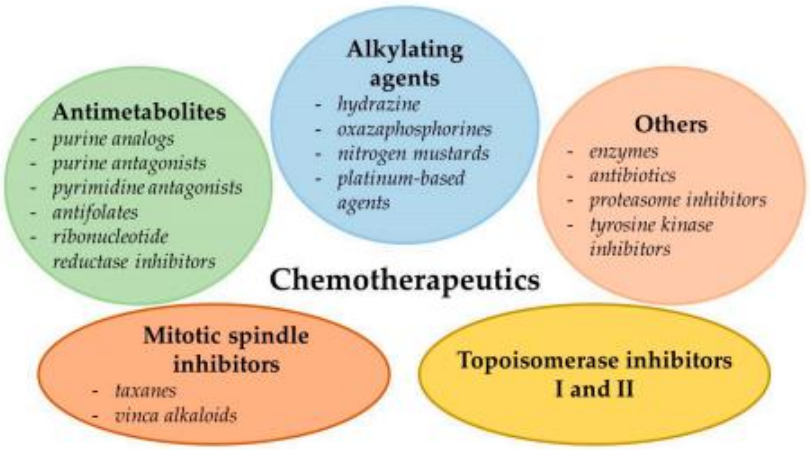

Figure 4. Classification of commonly used chemotherapeutics depends on their action mechanism (Bukowski, Kciuk, and Kontek 2020; Luqmani 2005).

Alkylating agents include the platinum-based substances (cisplatin, carboplatin, and oxaliplatin), nitrogen mustards (busulfan, chlorambucil, and melphalan), hydrazine (temozolomide), and novel, still-under-research off-on-type alkylating agents like vinyl-quinazolinone (VQ). Chemotherapeutics in this family of substances either construct inter- or intra-strand cross-links or transfer alkyl groups to DNA's guanine residues, causing mispairing to develop in DNA bases and impeding strand separation during DNA synthesis (Luqmani, 2005; Nussbaumer et al., 2011).

Inhibitors of pyrimidine synthesis include cytarabine, gemcitabine, capecitabine, and 5-fluorouracil (5-FU). Purine analogs include fludarabine, 6-mercaptopurine, azathioprine, and cladribine. Antifolates include methotrexate, pemetrexed, and pralatrexate. Hydroxyurea is a purine antagonist that inhibits the enzyme ribonucleotide reductase. By incorporating false structural analogs of pyrimidine/purine into DNA, these anticancer medications inhibit particular enzymes (dihydrofolate reductase, ribonucleotide reductase, and DNA polymerase), disrupt DNA/RNA synthesis, or lead to the development of DNA strand breaks (Bukowski et al., 2020; Luqmani, 2005; Nussbaumer et al., 2011).

Topoisomerase II inhibitors (etoposides, teniposide, and anthracyclines, such as idarubicin, daunorubicin, and doxorubicin (DOX) and topoisomerase I inhibitors (irinotecan and topotecan) disrupt topoisomerases' activities involved in DNA replication

and result in DNA strand breaks(Bax et al. 2019; Lara et al. 2018; Nussbaumer et al. 2011; Luqmani 2005).

Mitotic spindle inhibitors, such as taxanes (docetaxel and paclitaxel) and vinca alkaloids (vincristine (VCR) and vinblastine), affect the function/formation of spindle microtubules and result in cell death by preventing nuclear division (mitotic arrest in metaphase) (Luqmani, 2005; Nussbaumer et al., 2011). One of the recently synthesized N-carbonyl acridines was shown to disrupt tubulin polymerization and have strong antiproliferative effects on MB-468 human mammary gland/breast cancer cells, according to recent research by Peng et al. (Peng et al., 2020).

2.6 Doxorubicin

Doxorubicin (DOX), commercially marketed as Adriamycin, is an anthracycline-containing isolated from Streptomyces peucetius var. caesius in the 1970s, water-soluble, orange to red colored (at neutral pH), photosensitive chemotherapeutic drug which is possessing a superior antitumor activity against a wide myriad of solid tumors.

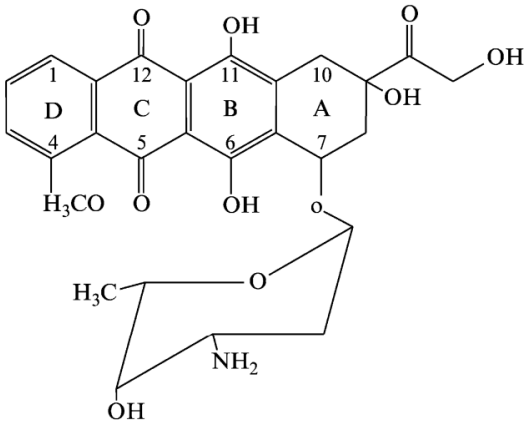

Figure 5. The chemical structure of doxorubicin. (Abraham et al. 2005a)

The chemical structure of the amphipathic DOX molecule illustrated in Figure 5, is made up of a water-soluble group, amino-sugar (Daunosamine: $C_6H_{13}NO_3$), and a water-insoluble aglycone (Adriamycin: C21H18O9) group. Of note, doxorubicin has three significant prototropic functions with associated pKas: (1) the amino group in the sugar moiety (pK1 = 8.15), (2) the phenolic group at C11 (pK2 = 10.16), and (3) the phenolic group at C6 (pK3 = 13.2).

Mechanistically, Doxorubicin is thought to act on cancer cells by two mechanisms: intercalation into DNA, which disrupts topoisomerase II-mediated DNA repair, and the creation of free radicals, which causes damage to cellular membranes, DNA, and proteins. Despite its therapeutic efficiency, DOX has negative systemic side effects such as cardiac cytotoxicity and nonselective death of quickly developing cells. These issues can arise during therapy or occasionally months or years after receiving doxorubicin. Heart issues can sometimes be unfixable. Congestive heart failure may result from myocardial injury, which can happen if the cumulative total dosage of doxorubicin HCl exceeds 550 mg/m^2 (Thorn et al. 2011a).

2.7 Multi-Drug Resistance (MDR)

MDR results from the overexpression of various proteins that extrude the chemotherapic from the cell, lowering its concentration below the effective one. Over 90% of cancer patients receiving conventional chemotherapeutics or cutting-edge, targeted medicines die due to multidrug resistance (MDR). After prolonged treatment, MDR commonly develops, leading to resistant malignancy and cancer recurrence. Another crucial factor to consider is that cancer cells with acquired MDR frequently develop cross-resistance to chemically unrelated chemotherapy medicines. Theoretical mechanisms for MDR have been proposed for a variety of cellular and non-cellular pathways, including decreased uptake of water-soluble drugs, increased enzyme levels of xenobiotic metabolism (e.g., glutathione-S-transferase), numerous changes in cells that affect the ability of cytotoxic drugs to kill them, and removal of hydrophobic drugs from cells due to increased energy-dependent efflux as seen in Figure 6.

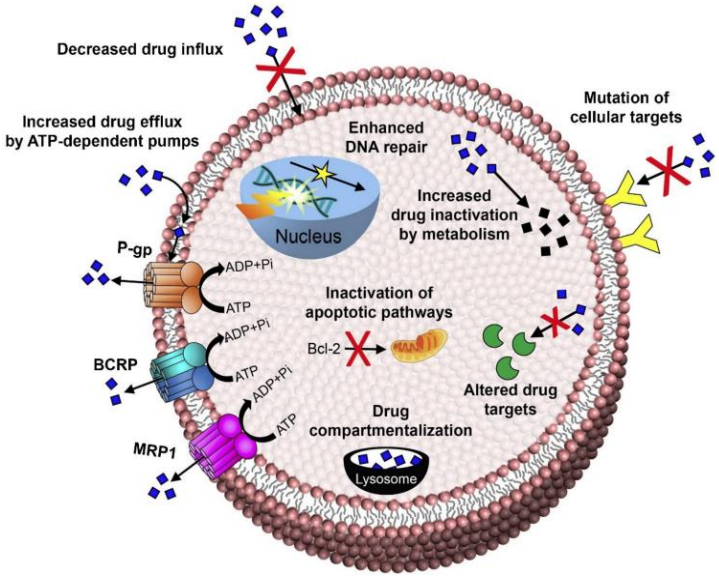

Figure 6. Schematic presentation of possible drug resistance mechanisms in cancer (Gote et al. 2021).

MDR is mainly related to the expression of the ATP-binding cassette (ABC) transporters. These proteins actively transport various structurally different substrates, such as hydrophobic drugs and lipids, from the inner to the outer leaflet of the cell membrane of the tumor cells, thereby decreasing their intracellular concentrations. The 48 human ABC transporter genes are classified into seven subfamilies (from ABCA to ABCG). Among them, P-glycoprotein is a well-known protein associated with multi-drug resistance. It belongs to the human ABCB (MDR/TAP) family and is also known as ABCB1 or breast cancer resistance protein, BCRP (ABCG2). Human ABCB1 transporter was the first recognized ABC transporter: its overexpression in cancer cells reduces the concentration of drugs in the cell and allows it to develop resistance to chemotherapic several medicines, such as taxanes (paclitaxel), vinca alkaloids (vinblastine), and anthracyclines (daunorubicin).

Even though resistance is a problem that restricts the use of doxorubicin, it is still a useful clinical antineoplastic drug, along with issues with cardiotoxicity. ABCB1 (MDR1, Pgp) (Cole et al. 1992) and ABCC1 (MRP1), as well as other transporters (ABCC2, ABCC3, ABCG2, and RALBP1), are all part of the resistance mechanism. The amplification of TOP2A (Thorn et al. 2011b), which has been established to impact the treatment response, is another route of doxorubicin resistance(Oakman et al. 2009).

An exponentially growing number of biomedical investigations aims to develop chemotherapeutics that can avoid or reverse MDR (Fugit et al. 2015).

According to several reports, melatonin affects P-gp expression by enhancing the sensitivity of colon cancer cells to chemotherapy. The researchers primarily studied melatonin's impact on the doxorubicin resistance of LoVo colon cancer cells. According to their findings, various amounts of MLT and DOX enhanced the proportion of cells expressing P-gp (Fic et al., 2017).

Based on their potency, selectivity, and drug interaction patterns, the numerous P-gp inhibitors created thus far are now divided into four generations, as shown in Table 2. These inhibitors work in a variety of ways, including blocking ATP hydrolysis, impairing the integrity of cell membrane lipids, or inhibiting the substrate binding site(s) by competitive, noncompetitive inhibition, and allosteric modification (Mondal and Ilies 2021).

Table 2. Different generations of P-gp efflux pump inhibitors(Mondal and Ilies 2021)

Generation	Drugs
First generation	Verapamil, quinine, quinidine, tamoxifen and toremifen flupenthixol, chlorpromazine, cyclosporin A, reserpine,
Second generation	Dexverapamil, valspodar, biricodar, timcodar, dofequidar, dexniguldipine, quinine homodimer Q2
Third generation	Elacridar, tariquidar, zosuquidar, laniquidar, DP7, PGP-4008, CBT-1, annamycin and mitotane
Fourth generation	Natural products Peptidomimetics Surfactants and lipids Dual ligands

In comparison to first-generation P-gp inhibitors like valspodar, tariquidar has a potency that is ten times greater in vitro and reverses both intrinsic and acquired resistance to doxorubicin, vincristine, and paclitaxel (Fox et al. 2015).

Tariquidar is one of the most effective P-glycoprotein (P-gp, ABCB1) drug pump inhibitors (Gillet and Gottesman 2010). As seen from Figure 7, it is a multi-drug resistant derivative of an anthranilamide that inhibits the transmembrane transport of anticancer medications by non-competitively binding to the p-glycoprotein transporter. Inhibition of transmembrane transport may increase anticancer drug's intracellular concentrations, thereby increasing its cytotoxicity.

In vitro, tariquidar reverses intrinsic and acquired resistance to doxorubicin, vincristine, and paclitaxel with a potency 10-fold greater than first-generation P-gp inhibitors, including valspodar (Fox et al. 2015). Tariquidar and structural analogs also inhibit Breast Cancer Resistance Protein (BCRP/ABCG2) (Mao and Unadkat 2015).

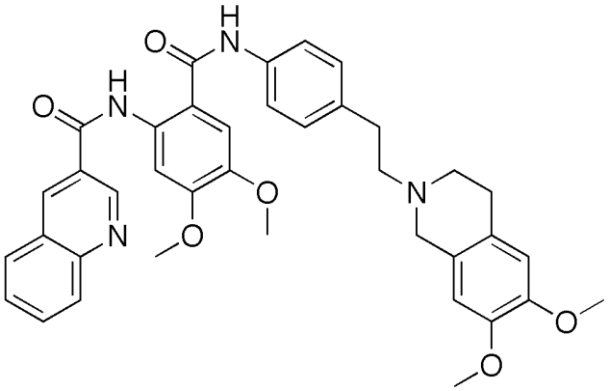

Figure 7. Structure of Tariquidar.

Tariquidar plays a significant role in MDR, as mentioned before, and literature has numerous research on Tariquidar, Doxorubicin, Tariquidar, and Paclitaxel combinations for overcoming different cancers. Yuquiong et al. reported a study on resistant ovarian cancer cells, multidrug resistance, and pH-sensitive liposomes. They prepared liposomes of TQR and DOX with the drug to lipid ratios of 0.05 and 0.10. Liposomal formulation with 0.05 almost inhibits the MDR of OVCAR8/ADR cells(Xia et al. 2018). Zhang et al. employed liposomes to transport paclitaxel and TQR (1/1 w/w)

and allowed the half inhibitory concentration (IC50) of paclitaxel to decline to nmol level (2-10 nM) from micromole level (1-2 M), overcoming ovarian cancer cell resistance(Y. Zhang et al. 2016).

Moreover, Patel et al. reported that the IC50 values for paclitaxel in SKOV-3 and SKOV-3TR cells were 27.11 nM and 2743 nM, respectively, when cells were treated with paclitaxel alone. As a result, a 100-fold greater dosage of paclitaxel is required to cause the same toxicity in SKOV-3TR cells as in SKOV-3 cells. When cells were treated with tariquidar- and paclitaxel-co-loaded liposomes, the IC50 values for paclitaxel were 17.68 nM and 34 nM, respectively, in SKOV-3 and SKOV-3TR cells. Their results show that a similar dosage of paclitaxel induces identical toxicity in both cell lines when tariquidar and paclitaxel are delivered simultaneously in long-circulating liposomes, suggesting MDR reversal by liposomal tariquidar (Patel et al. 2011a).

In another study, cancer stem cells (CSCs)-specific targeted $mSiO_2$-dPG nanocarriers simultaneous delivery chemotherapy drug DOX along with the P-glycoprotein (P-gp) inhibitor tariquidar for enhanced chemotherapy to overcome MDR in breast CSCs. The chemotherapeutic effectiveness against breast CSCs was improved due to the accumulation of DOX supplied by the $mSiO_2$-dPG nanocarriers being significantly increased in the three-dimensional, drug-resistant mammosphere of breast CSCs (Pan et al. 2021).

2.8 Drug Delivery Systems

Systems for delivering medications into or throughout the body are known as drug delivery systems. Drug "packaging"—such as a micelle or a nanoparticle—that shields the drug from deterioration and enables it to reach wherever it is needed in the body is referred to as a drug delivery system. A drug delivery system (DDS) is a method or process that releases the drug at a pre-selected site in a controlled manner to achieve a therapeutic effect. Drug delivery systems can, in principle, provide enhanced efficacy and reduced toxicity for a therapeutic agent. However, Conventional drug delivery systems (DDS) often have systematic side effects due to non-specific biological distribution and uncontrolled drug release characteristics. An ideal DDS in cancer

achieves two goals: tumor-specific delivery and tumor-specific drug release from delivery systems.

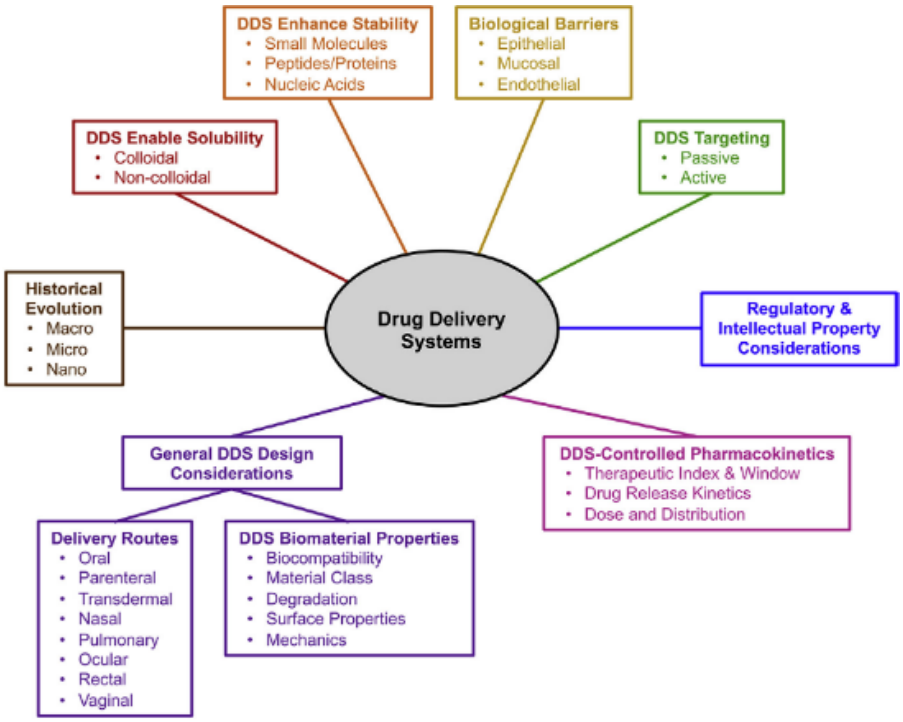

Figure 8. Overview of developing the drug delivery system (DDS) (Park 2014).

Cancer patients typically have significant cytotoxic side effects from anticancer medications, which restricts their options for therapy. Most anticancer treatments are administered at the highest permissible dose. Smart drug delivery systems (SDDSs) increase the therapeutic window of anticancer treatments by allowing lower drug dosages while retaining effective intracellular concentrations for longer. As a result, in addition to having more precise localization, patients' compliance, fewer hazardous side effects, and regulated biodistribution are also benefits of SDDSs.

SDDSs have the following advantages over conventional systems:

- The possibility of maintaining the plasma drug levels, which is therapeutically desirable,

- The possibility of eliminating or reducing side effects from systemic administration
- The possibility of improving and facilitating drug administration in areas with poor medical,
- The possibility of prescribing drugs with a short half-life in the body.
- Reduction of pain caused by high doses,
- The possibility of increasing patient compliance, and
- The possibility of producing a relatively low-cost product and fewer drugs release their load at the targeted site.

Most reported nanocarriers: liposomes, micelles, dendrimers, mesoporous silica nanoparticles (MSNs), gold nanoparticles (GNPs), superparamagnetic iron oxide nanoparticles (SPIONs), carbon nanotubes (CNTs), and quantum dots (QDs), vitamins (Folic acid (B9) (Rana and Bhatnagar 2021a)and Biotin (B7) (Saha et al. 2013) and monoclonal antibodies. These systems (Figure 9) can be used for many purposes, such as cosmetic, gene therapy, treatment of infectious diseases, and dermatological diseases, especially for drug transportation.

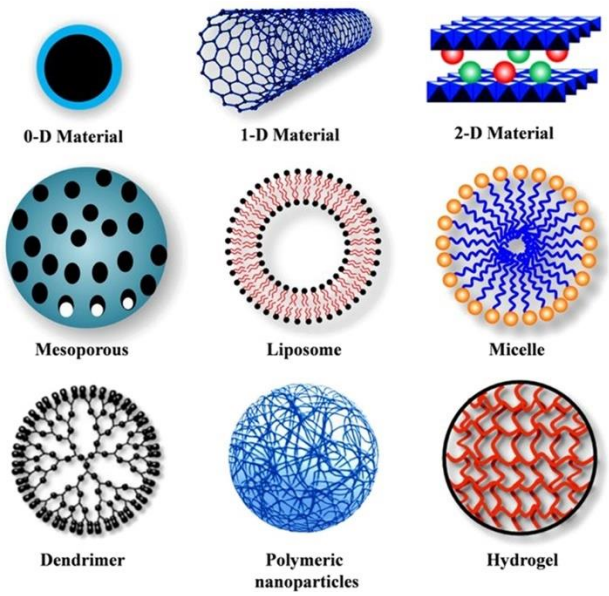

Figure 9. Types of nanocarriers (Monteiro et al. 2014a).

2.9 Targeted Drug Delivery

In 1906, Ehrlich first mentioned the target drug delivery (TDD) method based on the phrase "magic bullet." (Tewabe et al. 2021). The central concept of a targeted drug delivery system was based on three fundamental principles: identifying the specific target for the disease, identifying the drug that will effectively treat the disease, and choosing suitable target vehicles to carry the drug in stable form while avoiding other interactions and harm to the healthy tissues. Targeted drug delivery is an intelligent method in which a predetermined quantity of therapeutic material is continuously administered to a patient's body at a specific location (Valent et al. 2016). Most diseases require efficient, safe, and specifically targeted medications, including cancers, autoimmune diseases, neurological disorders, lung diseases, and cardiovascular diseases.

TDD systems should ideally contain the following characteristics;

- physically and chemically stable *in vivo* and *in vitro* circumstances,
- biochemically inert (nontoxic), non-immunogenic,
- capability of homogeneous capillary distribution,
- controlled medication delivery to the targeted cells, tissues, or organs.
- should have predictable and regulated drug release rates,
- zero order release kinetics,
- releasing drugs in a therapeutic amount,
- minimize drug leakage during circulation.

The carriers used should be easily and quickly removed from the body by biodegradation. The delivery system should also be easy to prepare and at least reasonably simple, reproducible, and economical.

There are six strategies for drug targeting the desired organ/tissue of interest: Passive Targeting, Active Targeting, Inverse Targeting, Physical Targeting, Dual Targeting, and Double Targeting. Among these, active and passive targeting are the most frequently used strategies.

2.9.1 Passive Targeting

Since the discovery of the Enhanced Permeability and Retention (EPR) effect in the 1980s by Maeda et al., many efforts have been made to understand the significance of this phenomenon in tumor targeting. Tumor blood vessels are generally characterized by abnormalities such as a high proportion of proliferating endothelial cells, pericyte deficiency, and aberrant basement membrane formation leading to an enhanced vascular permeability (Figure 10). When the tumor mass begins to develop locally and requires new blood vessels that can provide nutrition and oxygen, a process known as angiogenesis starts causing the cancer cells to release growth factors and hormones to create these new blood vessels (López Mendoza & Alcántara Quintana, 2022). The extravasation mechanism allows the delivery systems to pass through the leaky pores (100-800 nm) that result from the fast development of these blood vessels. Particles, such as nanocarriers (in the size range of 20–200 nm), can extravasate and accumulate inside the interstitial space. Endothelial pores have sizes varying from 10 to 1000 nm. Moreover, lymphatic vessels are absent or non-functional in the tumor, contributing to inefficient drainage from the tumor tissue (Danhier, Feron, and Préat 2010). Delivery systems accumulate at cancerous sites more than healthy organs or tissues. As a result, there is an increase in cellular uptake and release into the cellular cytoplasm, which results in increased toxicity in cancer cells(Alavi and Hamidi 2019).

The weak point in passive delivery is the suggestion that the retention only occurs in tumor sites (solid tumors); nevertheless, when a liquid tumor or metastasis cancer cells are treated, there is a lack of such an affinity(López Mendoza and Alcántara Quintana 2022).

Using this EPR effect, it is possible to increase the concentration of anti-cancer medications in the tumor much more than in healthy human tissue. According to Kommareddy et al., the passive targeting of gelatin (typeB) -based nanoparticles (NPs) successfully delivered genes at cancer areas. In another study, NP-based DDSs containing plasmid DNA (pDNA) were also made using gelatin (type B) for cancer treatment (Kaul and Amiji 2002).

pDNA-expressed green fluorescent proteins and -galactosidase were more effectively targeted *in vitro* and *in vivo* when DNA was encapsulated with PEGylated gelatine NPs. Additionally, lung carcinomas' DNA moieties have been targeted using

PEGylated gelatin nanoparticles, which have been shown to inhibit breast cancer cells' angiogenesis and tumor growth (Das et al. 2020).

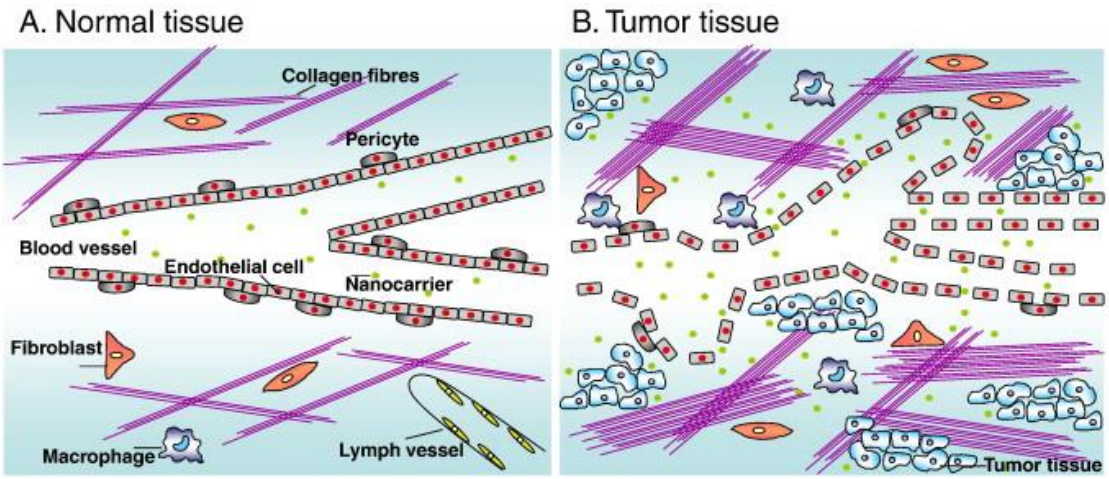

Figure 10. The enhanced Permeability and Retention effect explains the passive targeting of nanocarriers by differences between normal and malignant tissues (Danhier et al., 2010).

2.9.2 Active targeting

Active targeting comprises the detection of cancer cells, which increases drug accumulation and cellular internalization (Kim et al., 2018). In other words, active targeting refers to the accurate contact of the drug or drug carrier with the target cells via ligand-receptor interactions for intracellular localization, which only occurs after blood circulation and extravasations.

In active drug targeting, peptides, antibody fragments, and pharmaceuticals are combined to act as homing devices for antibodies, antibody fragments, and receptor structures expressed in the target area (Figure 11). Nanoparticles with a high surface-area-to-volume ratio, possible to achieve high ligand density on the surface for targeting purposes (Tewabe et al. 2021).

There are three main degrees of targeting for this strategy.

1) First-order targeting, also known as compartmental targeting, refers to the dispersion of the drug in the capillaries of general target areas, including lymphatics, peritoneal cavities, multiple cavities, cerebral ventricles, and joints.

2) Second-order targeting, in which drugs are delivered selectively to particular cell types, such as tumor cells, rather than to normal cells; an example is the delivery of drugs specifically to the liver's Kupffer cells.

3) Third-order targeting, a particular method of drug delivery, targets the drug intracellularly by endocytosis or through receptor-based ligand interactions at the location (Rani, Paliwal, and Kirti 2014).

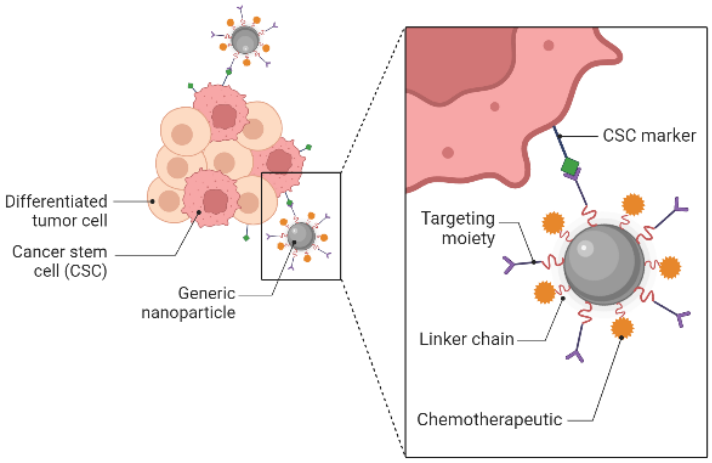

Figure 11. Actively targeting cancer stem cells with nanoparticles. The nanoparticles are made to carry therapeutic drugs attached to NPs via a linker chain and target molecules (both linked to NPs via a linker chain) that specifically target a specific CSC marker (Marei 2022)

Water-soluble vitamin B9 folate interacts with the folate receptor to facilitate cellular absorption. The folate receptor has the benefit of having modest expression in healthy tissues. Still, it is substantially expressed in various cancers, especially those affecting women, such as ovarian, breast, and cervical cancer. Compared to healthy

epithelial or fibroblast cells, folic acid binds to tumor cells 20 times more strongly. Due to these desirable characteristics, foliate conjugation has been a prominent strategy used in drug delivery systems (Rana and Bhatnagar 2021b).

The first targeted nanomedicine to start clinical trials was MCC-465 (immunoliposome-encapsulated doxorubicin). The formulation was a doxorubicin-encapsulated immunoliposome tagged with an F(ab′)2 fragment of human monoclonal antibody GAH, allowing malignant stomach tissues to be preferentially targeted over normal tissues. MCC-465 produced good results in phase I studies (Hamaguchi et al. 2004).

A dominant negative mutation of the human cyclin-G1 gene, which induces cell death through apoptotic pathways, is carried by the retroviral vector Rexin-G, a nonreplicated tumor-targeting agent. By decorating the nanoparticles with collagen-binding peptides, the wounded tissues exposed to collagen, such as malignant lesions, are given a preference for nanoparticle delivery. A 10-year survivor of gemcitabine-resistant pancreatic adenocarcinoma demonstrated the efficacy of the nanomedicine in phase I and phase II studies against chemotherapy-resistant metastatic sarcoma, pancreatic cancer, and breast cancer (Chawla et al. 2010).

2.9.3 Liposomes

Dr. Alec D. Bangham discovered liposomes in 1964 at the University of Cambridge's Babraham Institute. The Greek words "Lipos" (fat) and "Soma" (body) were combined to form the word liposome(Daraee et al. 2016). These biological structures have been used as drug carriers, especially for the last 50 years (Sercombe et al., 2015; Pozzi et al., 1996; Nomura et al., 2001). The liposomal bilayer typically consists of natural, non-toxic phospholipids, sphingolipids, cholesterol, and hydrophilic polymers.

Phospholipids typically have acyl chains and hydrophobic fatty acid tails, whereas their head groups are hydrophilic. Due to the hydrophobic impact of hydrophobic acyl chains when exposed to an aqueous environment, phospholipids have an amphiphilic character and produce polar shells in aqueous solutions(Monteiro et al. 2014b). Due to hydrogen bonds, van der Waals forces, and other electrostatic interactions, this process is thermodynamically advantageous.

Liposomes are helpful for drug administration because they are biocompatible, biodegradable, have low toxicity, and can alter the pharmacokinetic profile of the medication they contain. On the other hand, the potential to resemble cell membranes in structure and chemistry makes them appealing drug delivery mechanisms. Targeted medication distribution is made possible by these beneficial characteristics. While liposomes have been employed as drug-delivery systems for many years, more development is required to enable specific targeting at the cellular and molecular levels (Liu, Chen, and Zhang 2022).

The chemical properties of phospholipids used to prepare liposomes significantly affect the properties of liposomes. The biodistribution, clearance, drug release permeability, and liposome surface charge depend on phospholipids' chemical properties. Similarly, liposome encapsulation efficiency, toxicity, and stability are also affected by the types of phospholipids used in their preparation. Lipophilic hydrophilic balance has become a valuable index to predict the vesicle-forming ability of amphiphilic liposomes(Parchekani et al., 2022).

The phospholipid head groups determine the surface charge of liposomes(Nikolova, Kumar, and Chavali 2022a). In contrast to neutral phospholipids, negatively charged phospholipids are more quickly detected by macrophages. Additionally, small negative charges on neutral liposomes stabilize them by enhancing the repelling electrostatic forces that alter the aggregation-dependent process of phagocytic uptake(Olusanya et al. 2018). Because the uptake of positively charged liposomes appeared to be higher than that of negatively charged, most FDA-approved liposomes are negatively charged(Nikolova, Kumar, and Chavali 2022a). Additionally, cationic liposomes inhibit interactions with tumor cells, and their accumulation in the tumor stroma serves as a drug depot (Nikolova, Kumar, and Chavali 2022b).

Sterols are substances found in cell membranes. Their presence in the membrane alters the bilayer's permeability, fluidity, and stability. One of the most popular sterols used to increase the stability of liposomes is cholesterol (Figure 12).

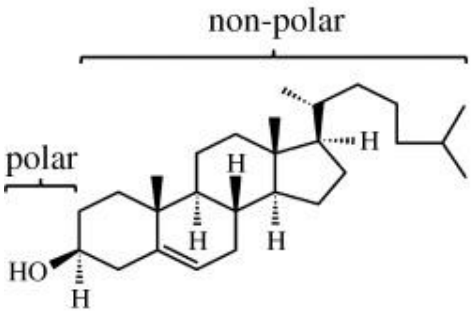

Figure 12. Structure of Cholesterol

It is employed because of its capacity to control the fluidity of bilayer membranes. It also stabilizes the formulation by repelling space and avoiding aggregation due to electrostatic forces. The permeability of negatively charged, neutrally charged, and positively charged membranes to Cl^+, K^+, Na^+, and glucose is decreased by cholesterol. When cholesterol stabilizes the cell membrane and prevents temperature changes, the permeability of the cell membrane decreases as the temperature rises(Nkanga et al. 2019).

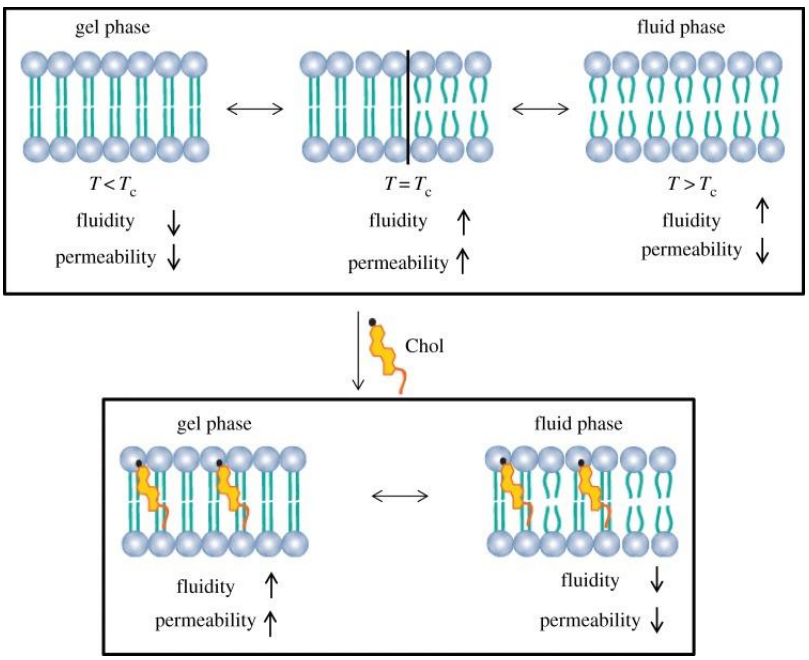

Figure 13. Presentation of “gel” to “liquid” transition (Monteiro et al., 2014b).

The liposome curvature depends on the lipid content and transition temperature (T_c). Phospholipids change from a gel to a more fluid liquid-crystalline phase at T_c. T_c is influenced by the saturation and length of the fatty acid chains (Zamani et al. 2018).

As illustrated in Figure 13, T_c drops when chain length and the number of double bonds within it decrease. Through lipid transfer to lipoproteins, disintegration, and content leakage, the presence of unsaturated lipids within the liposomes jeopardizes the integrity of the lipid bilayer. As a result, T_c predetermines the liposome bilayer's permeability and fluidity. As a result of its aromatic rings resting parallel to the fatty acid chains, cholesterol improves the fluidity of the bilayer's core. At the same time, its hydroxyl group, which is located adjacent to the phospholipid headgroups, increases the viscosity.

Liposomes' physicochemical and drug delivery properties depend on their composition, surface charge, number of lamellae, bilayer fluidity, surface modification for targeting, production method, and size Figure 14. Unilamellar vesicles are characterized by a single lipid bilayer surrounding an aqueous core with sizes between 50 and 250 nm. On the other hand, multilamellar vesicles are characterized by having dimensions between 1 and 5 micrometers. Liposomal formulations must fall under the submicron ultra filterable range, be less than 200 nm in size, be regarded as nanostructure systems, and be used therapeutically.

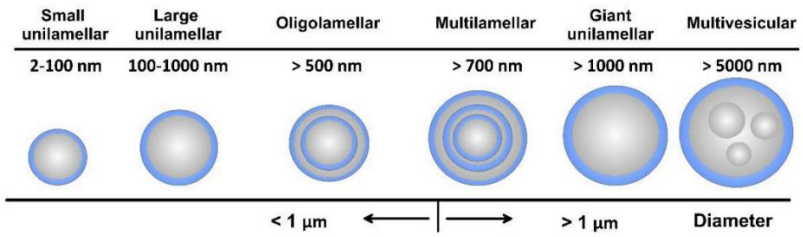

Figure 14. Liposome types together with their indicative size(Nikolova, Kumar, and Chavali 2022a)

There are numerous literature on creation of liposomes. Thin-film hydration, reverse-phase evaporation, ethanol injection, polyol dilution, freeze-thaw, double emulsions, pro-liposome method, French press extrusion, detergent removal, and high-

pressure homogenization are examples of common liposome manufacturing techniques. Depending on the approach, these procedures often result in LUVs or MLVs. Even though these techniques may be utilized to create liposomes, only the ethanol injection method, reverse-phase evaporation, and thin-film hydration are frequently employed.

Hydrophilic drugs with a log P value less than −0.3 are entrapped exclusively within the aqueous core. In contrast, strongly lipophilic drugs with a log P value greater than 5 are encapsulated almost entirely within the lipid bilayer. Drugs that are capable of partitioning between the lipid bilayer and the aqueous core possess an intermediate log P value between 1.7 and 4 (Immordino ML, Dosio F, and Cattel L. 2006). There are now many liposomal formulations on the market (Figure 15). Doxorubicine-loaded PEGylated liposomes were the first FDA-approved nanomedicine (named Doxil®) used to treat ovarian cancer and AIDS-related Kaposi's sarcoma in 1995. Since then, liposomes have been promoted for numerous diseases' therapeutic and diagnostic needs, including breast cancer, macular degeneration, leukemia, hepatitis, etc. (Silverman & Deitcher, 2013). The intriguing Medigene liposomal formulation Endotag-I, which contains neutral and cationic paclitaxel (PTX) lipid formulations, interacted with the negatively charged endothelial cells necessary for cancer angiogenesis (Rocca et al. 2004).

Active Ingredient	Liposome Composition	Size (nm)	Cancer Type Being Targeted
DOX	HSPC/DSPE/cholesterol (12.5:1:8.25 molar ratio)	130	Colorectal (in-vitro)
DOX	Cholesterol, DSPC, DSPE and DSPE-PEG2000 (10 µmol total phospholipid).	100	Prostate cancer (in-vivo/in-vitro
DOX	HSPC: cholesterol: lipid with a PEG head group (DSPE-PEG2000) (molar ratio 56.4:38.3:5.3)	100	Colorectal (in-vitro)
DOX	1-Palmitoyl-2-oleoylphosphatidylcholine: cholesterol (molar ratio 55.8:44.2)	180	Metastatic (clinical trial & in clinic)
DNR	DSPC:cholesterol (molar ratio 2:1)	50	Kaposi's sarcoma
ATRA	DPPC:cholesterol:1,2-distearoyl-sn-glycero-3-phosphoethanolamine - Methoxy PEG2000 (molar ratio 6:3:1)	200	Human Thyroid carcinoma (in-vitro)
ATRA	DOTAP, cholesterol and ATRA (molar ratio 70:20:10)	263	Lung cancer (in-vivo in animal)
MXT	HSPC: DSPE-PEG2000: cholesterol: anacardic acid (molar ratio 0.55:0.05:0.35:0.05)	112	Melanoma cell lines (in-vitro)
PCX	Egg phosphatidylcholine: cholesterol: TPGS1000-TPP (molar ratio 88:3.5:8.5)	80	Lung cancer cell lines (in-vivo & in-vitro)
Irinotecan	-	-	Pancreatic ductal adenocarcinoma

Figure 15. Liposomal formulations are used as anticancer treatments(Olusanya et al., 2018).

2.9.4 Liposomal Doxorubicin

Doxorubicin is one of the derivatives of Anthracycline glycosides (antineoplastic drugs) and remains a staple of medication combinations used in the therapy of most solid tumors. However, these chemotherapies can give rise to heart toxicity. This toxicity, especially Cardiomyopathy, is the drug's therapy-limiting toxicity, which can result in congestive heart failure (CHF) and death. This issue will affect about 2% of individuals who have received a cumulative (lifetime) doxorubicin dosage of 450–500 mg/m^2.

The primary goal of encapsulating doxorubicin in liposomes has been to reduce nonspecific organ damage. Through liposomes, doxorubicin can be directed away from locations with tight capillary connections, such as the heart muscle and the gastrointestinal system. To provide a therapeutic advantage over the free agent, doxorubicin liposomal formulations must be able to boost antitumor activity at the maximum tolerated dosage (MTD) without increasing toxicity. More significant accumulation of liposome-encapsulated doxorubicin in tumors and decreased accumulation in sensitive nontarget organs can improve the drug's therapeutic index; however, it is suggested that the principal advantages come from lower toxicity rather than increased therapeutic power (Gokhalel et al. 1996).

Doxil (approved in the United States) or Caelyx (approved in Canada and Europe) are two liposomal doxorubicin formulations that have achieved clinical approval, as well as Myocet, which got community marketing authorization from the European Commission in August 2000 for the treatment of metastatic breast cancer. The Doxil and Caelyx liposomal formulations are made up of hydrogenated soya phosphatidylcholine, cholesterol (Chol), and PEG-modified phosphatidylethanolamine (55:40:5), whereas Myocet is made up of egg phosphatidylcholine (EPC) and Chol (55:45 molar ratio). Doxil demonstrated an 8-fold increase in circulation duration and half-life compared to free doxorubicin. Furthermore, the medication exhibited fewer hazardous side effects than the free form(Abraham et al., 2005b).

Methods for encapsulating various pharmacological agents within liposomes are either passive, in which the cargo is enclosed during liposome creation, or active, in which the loading occurs after empty liposome production. Hydrophobic medications may be integrated directly into liposome forms during carrier production, and the trapping efficacy is dependent on the drug's solubility in the liposomal membrane and

can approach 100% (Gao et al. 2013). On the other hand, Doxorubicin has an amphipathic molecular structure that contains both hydrophilic and hydrophobic groups. Therefore, it can be enclosed in the phospholipid tails and liposome core. Passive loading's effectiveness is only marginally successful; encapsulation happens to a maximum of 80%(Lombardo and Kiselev 2022). Water-soluble medicines are often actively captured by mixing empty liposomes with a concentrated drug solution that spreads evenly by diffusion. "Remote loading" is the technique used to generate diffusion gradients. pH gradients across the bilayer or ion gradients can be employed to increase loading efficacy(Maria P. Nikolova 2022; Fritze et al. 2006). Transmembrane proton gradients may be created by either producing liposomes in low pH buffers or integrating ionophores that connect the outward flow of monovalent or divalent cations with the inward movement of protons, thus acidifying the liposome interior. Another method is to make liposomes with a weak base, such as ammonium sulfate. The removal of the external ammonium salt produces a pH gradient that aids in medication loading (Figure 16).

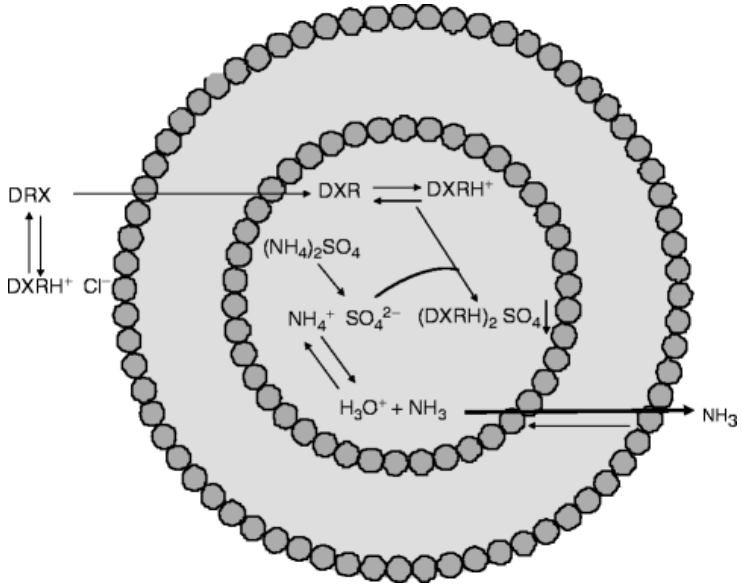

Figure 16. An ion gradient method for DOX loading(Lewrick & Süss, 2010).

The well-known remote loading mechanism for Doxil is based on the constant "escape" (efflux) of ammonia gas, which is produced by the pH-dependent breakdown of the intraliposomal NH^{4+} to neutral ammonia plus a proton, and which results in a transmembrane pH gradient ($pH_{liposome} < pH_{medium}$). This mechanism can be visualized in Figure 16. The intraliposomal-insoluble doxorubicin-sulfate (dox-sulfate) salt is created when the unionized doxorubicin diffuses from the medium to the intraliposomal aqueous phase along the gradient. The intraliposomal pH increases as a result of doxorubicin consuming more protons. To ensure that all of the doxorubicin in the medium is converted to NH_4+, it restarts the dissociation of NH_4^+ to NH_3 and H^+. The salt of dox-sulfate-insoluble doxorubicin crystallizes into nanorods when the quantities of intraliposomal doxorubicin are increased. The transmembrane ammonium gradient acts as a "driving force" in initiating the cycle in which doxorubicin is nearly entirely remotely and stably loaded into liposomes, primarily as dox-sulfate nanorod crystals (Barenholz 2012; Haran et al. 1993; Lasic et al. 1995; Sur et al. 2014). Passive and active encapsulation might be used when loading two medications into the same liposome system(Maria P. Nikolova 2022).

2.10 Fucoidan

Kylin made the initial discovery of fucoidan in 1913(Kylin 1913). A kind of polysaccharide called fucoidan is made up of sulfated fucose residues and is derived from brown algae. In basic research, it has demonstrated a wide range of biological actions, including many components that are anti-inflammatory, anti-cancer, anti-viral, anti-oxidation, anticoagulant, antithrombotic, anti-angiogenic, and anti-Helicobacter pylori, among others. Numerous studies demonstrate that fucoidan may prevent tumor cells from proliferating and from growing or metastasizing by triggering cell death and obstructing angiogenesis. Fucoidan is also widely used in functional foods, pharmaceuticals, cosmetics, and other health-related products (Wang et al. 2019).

A vast collection of marine plants known as "brown algae" includes Sargassum, Fucus, and other species. They are found in many cold-water environments. The active compounds found in brown algae include polysaccharides, terpenoids, proteins, polyphenols, sterols, multi-ring sulfurous sulfide cyclists, macrolides, trace elements, and

fucoidan (Menaa et al. 2021). Fucoidan's chemical structure is complicated, and it has two main backbones made of (1→3)-linked l-fucopyranosyl residues or of alternating (1→3)- and (1→4)-linked l-fucopyranosyl residues shown in Figure 17, but also include sulfated galactofucans with (1→6)-linked backbone. Units containing fucose or fuco-oligosaccharide may have branching and replacements for glucuronic acid, xylose, or glucose, as well as -d-galactose and (1→2)-d-mannopyranosyl units(Ale, Mikkelsen, and Meyer 2011). Fucoidan is insoluble in ethanol, acetone, chloroform, and other organic solvents but soluble in water. Its aqueous solution has a pH of 6.46, which is slightly acidic (Shen et al. 2018).

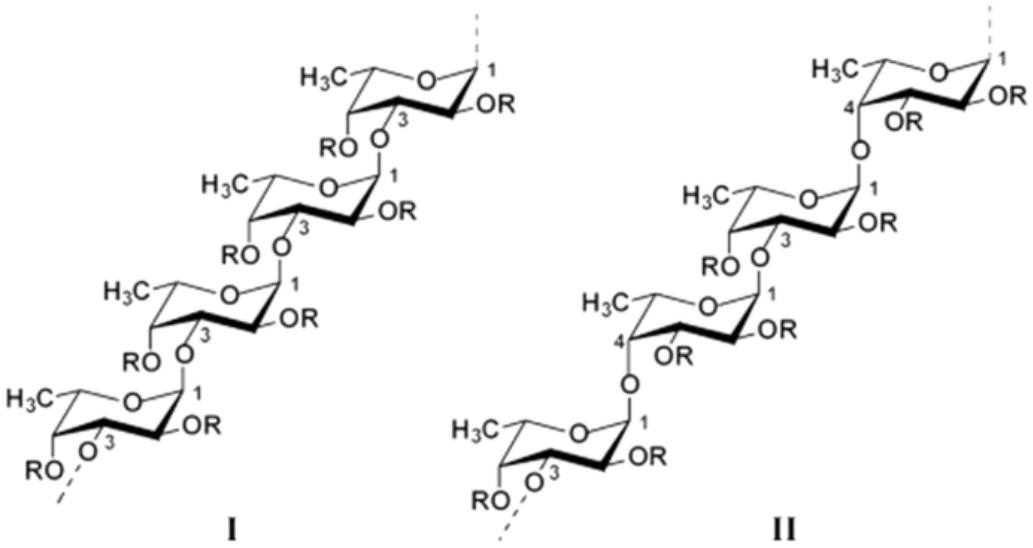

Figure 17. Two sorts of homofucose backbone chains of fucoidan (Cumashi et al. 2007).

Many studies have been carried out to assess the relationship between the chemical structure and bioactivities of fucoidan (FUC). In particular, the sulfate content of fucoidan is attracting many research efforts due to sulfation being a crucial factor in improving fucoidan bioactivity. The degree of branching, in addition to sulfation, has a substantial impact on the bioactivities of fucoidan, with greater degrees of branching correlating to more significant cytotoxicity in the antitumor effects of fucoidan (Oliveira et al., 2017). Another important aspect of fucoidan as a bioactive agent is its molecular weight. According to Cho et al. (2010), although having a lower sulfate concentration than the F5 kDa and F30 kDa fractions, the F5-30 kDa fraction of fucoidan had the

greatest tumor growth inhibitory activity. It is well known that fucoidan has antitumor and anticancer properties. Previous research has shown that fucoidan's anticancer mechanism primarily consists of four elements. Those elements are Cell cycle arrest, apoptosis induction, antiangiogenesis, and anti-inflammatory actions. In a study for cell cycle arrest, Fucoidan was administered to C57 mice bearing transplanted Lewis lung adenocarcinoma. They found that fucoidan successfully suppressed the metastasis and proliferation of the tumor cells *in vivo* since the tumor mass and the number of lung metastases were much lower than those lacking FUC (Alekseyenko et al. 2007).

Fucoidan can activate cancer cells' apoptosis signals, induce apoptosis through related pathways, and thus produce an anti-cancer effect. Eun et al. co-cultured HT-29 and HCT116, human colon cancer cells, with fucoidan extracted from Fucus vesiculosus. From the results of apoptosis detection, fucoidan induced activation of caspase-3, -7, -8, -9, chromatin condensation, and cleavage of poly (ADP-ribose) polymerase (PARP). These data indicate that fucoidan can induce HT-29 and HVT116 cells apoptosis through caspase-8 and -9 dependent pathways (E. J. Kim et al. 2010). In MCF-7 cells, fucoidan extract enhanced mitochondrial depolarization by upregulating proapoptotic proteins Bax and Bad and downregulating antiapoptotic proteins Bcl-2 and Bcl-xl expression(Teruya et al. 2007). The hallmarks of apoptosis, such as PARP breakage and caspase-3/7 activation, are also brought on by fucoidan administration in MCF-7 cells. Interestingly, Miyamoto et al. (2009) observed that activation of caspase-3 is not required for fucoidan-induced apoptosis in MCF-7 cells, but the latter requires caspase-7(Yamasaki-Miyamoto et al. 2009).

In inhibition of angiogenesis, fucoidan can stop the production of Vascular endothelial growth factor (VEGF), which prevents angiogenesis, stops the flow of nutrients and oxygen to the tumor, reduces its size, and prevents the spread and transfer of cancer cells. When Lewis lung cancer cells were transplanted into mice, Tse-Hung et al. administered fucoidan to the animals. As a result, the levels of VEGF in the blood and lung tissue were much lower than in the control group(Huang et al. 2015). A large number of studies have shown that oversulfated fucoidan in brown seaweeds exhibits antiproliferative activity by inhibiting the angiogenesis around the tumor cells and blocking the infiltration and metastasis of the tumor cells (Matou et al., 2002; Koyanagi et al., 2003).

Fucoidan can boost the body's immunological response, improving the capacity of T cells and natural killer cells (NK cells) to destroy tumor cells. According to research

by Farzaneh et al. on mice that had NB4 acute promyelocytic leukemia cells implanted into them, fucoidan might successfully boost the killing activity of Natural killer cells (NK cells) (W. Zhang et al. 2015).

2.11 P-selectin and Fucoidan Relationship

P-selectin (SELP) is an inflammatory cell adhesion protein that attracts leukocytes and binds platelets. It is produced constitutively in ECs and stored in Weibel-Palade bodies, which are intracellular granules. P-selectin translocates to the cell membrane and into the lumen of blood vessels in response to endothelial activation by endogenous cytokines or external stimuli like ionizing radiation. Human lung, breast, and kidney malignancies have been linked to increased P-selectin expression in the vascular system. In addition, P-selectin encourages the adherence of circulating cancer cells to activated platelets and endothelium in distant organs, causing initiation of the metastatic process. These connections to tumors and micrometastases, together with their activation by radiation, point to P-selectin as a potential target for the administration of cancer drugs and radiation-guided drug delivery.

Selectins, expressed in leukocytes, endothelial cells (ECs), and platelets, are known to bind to oligosaccharide ligands containing fucose. Thus, fucoidan serves as an excellent tool for blocking the action of selectins.

The paper by Jafari et al. illustrates the creation of a fucoidan-based drug delivery system for Doxorubicin (Dox) adverse effects reduction by active targeting toward P-selectin. By directly conjugating doxorubicin to the fucoidan backbone, fucoidan-doxorubicin nanoparticles (FU-Dox NPs) demonstrated a well-controlled size distribution and sustained release. In comparison to the MDA-MB-468 cell line with low P-selectin expression, the dynamic targeting capabilities of FU-Dox NPs toward P-selectin resulted in improved cellular uptake and cytotoxicity against the MDA-MB-231 cell line with high P-selectin expression (Jafari et al. 2020).

CHAPTER 3

MATERIALS AND METHODS

3.1 Materials

Chemicals used in this study; DSTAP 1,2-stearoyl-3-trimethylammonium-propane (chloride salt), DSPC (1,2- distearoyl-sn-glycero-3-phosphocholine) lipids were purchased from Avanti Polar Lipids (Alabaster, AL, United States). Cholesterol and Chloroform, Tariquidar, Doxorubicin (DOX.HCL, European Pharmacopoeia Reference Standard), and TritonX-100 were all purchased from Sigma Aldrich (St. Louis, MO, United States). The dialysis membrane (RC tubing Spectra/Por 6 Dialysis Membranes with MWCO: 10 kD) was obtained from Repligen (Waltham, Massachusetts, United States).

3.2 Methods

3.2.1 Plain Liposome Preparation

The first and essential stage in the production of liposomes was the development of a thin lipid film. The liposomes were prepared from the DSPC, Cholesterol, and DSTAP mixture, keeping the lipid content constant at 15 (mol) and cholesterol content at 30 mol% unless otherwise stated. Liposomes with varying percentages of DSTAP (0-5-10-15-20%) were prepared to determine the most stable liposomes. As mentioned above, in all liposome formulations, DSPC+DSTAP content was kept constant at 15 μmol and cholesterol percentage at 30 mol% out of hundred percent. Plain Liposomes

were prepared by weighing all components in a 20 ml vial and adding 2 ml chloroform to dissolve and make a homogenous mixture. A stream of nitrogen gas was used to remove most of the chloroform while agitating on a spinning table (Yellowline OS10 Basic) at a rate of 200 rpm. After the chloroform's evaporation and the thin film's formation, the vial was put into the vacuum oven overnight to ensure the complete removal of the chloroform within the thin film. If the film was stored at -20°C if not used immediately for further experiment. For Tariquidar-loaded liposomes, a predetermined amount of Tariquidar was added to the cholesterol and lipid mixture, and the thin film was prepared, as explained above.

Table 3. Composition of Liposomes

	DSPC (mg)	Cholestrol(mg)	DSTAP (mg)
%0 DSTAP	11.85	2.48	-
%5 DSTAP	11.00	2.48	0.75
%10 DSTAP	10.15	2.48	1.50
%15 DSTAP	9.31	2.48	2.25
%20 DSTAP	8.46	2.48	3.00

The hydration of the thin lipid film was the second stage in the preparation of liposomes. Because the DOX was to be loaded actively to the liposomes using pH gradient in the further steps, the lipid film was hydrated with 1 ml of ammonium sulfate [$(NH_4)_2SO_4$] (250 mM, pH= 5.4.) buffer solution. It incubated for about 1 hour at 65°C in an agitating water bath at 150 rpm.

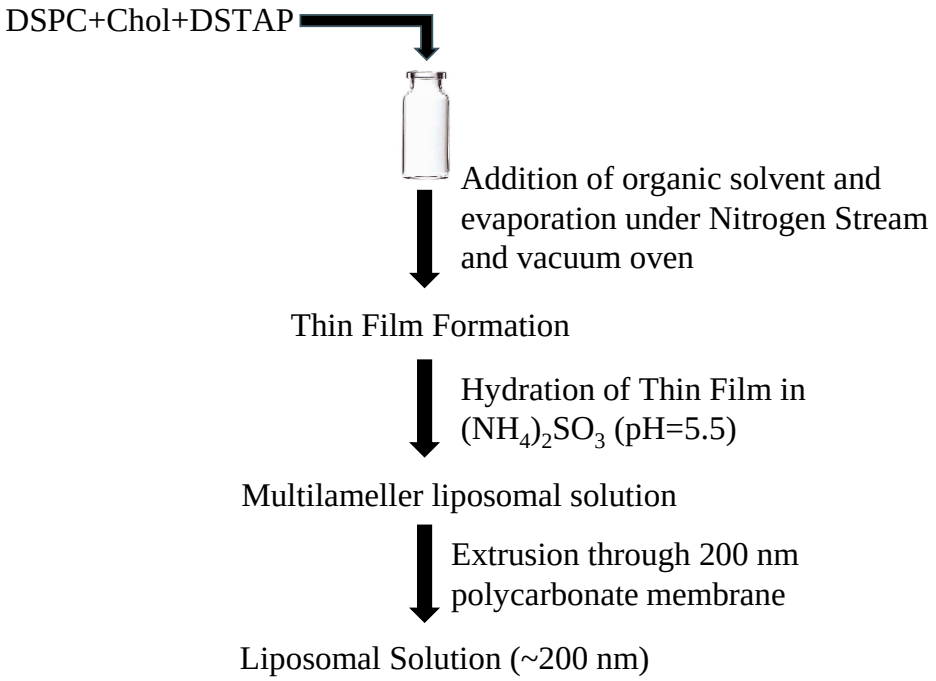

Figure 18. Liposome preparation steps.

The thin lipid film extrusion was the third stage in the production of liposomes. The extruder used in this study (mini-extruder obtained from Avanti Polar Lipids, Inc., Alabaster, AL, United States) has composed of the following components: polycarbonate membrane (Whatman Nucleopore Track-Etch filtering product), PTFE filter supports, O-rings, and a Swagelok connector assembly for retaining the filter system. Extrusion was done at 65 °C on a hot plate to maintain the lipid solution above the phase transition temperature of the lipids. To set up the mini-extrusion device seen in Figure 19, the longer extruder outer casing was used to house the second internal membrane support after inserting white spherical PTFE into the retainer nut. Then, two filter supports and one polycarbonate membrane were wetted in the buffer, especially in [$(NH_4)_2SO_4$] buffer for DOX loading. The polycarbonate membrane with a pore size of 200 nm was positioned between the filter supports and then placed on a membrane support equipped with a white spherical O-ring. Another O-ring was used to seal the retainer nut after it had been fitted correctly. Before being discarded for lipid extrusion, the Hamilton syringe was filled with buffer and repeatedly passed through the filter to replace air and fill holes. This step was crucial for preventing liposome solution loss. The filtration assembly was filled with the lipid solution using a Hamilton syringe. A mini extruder containing lipids was placed on

the hot plate and warmed to 65°C for 10 minutes. Lipid solution was passed 11 times through the polycarbonate membrane to reduce the size of the multilamellar vesicles formed during the hydration step. The final liposome solution was transferred into a vial and stored at 4 °C to cool down and stabilize. In Figure 18, all stages were explained.

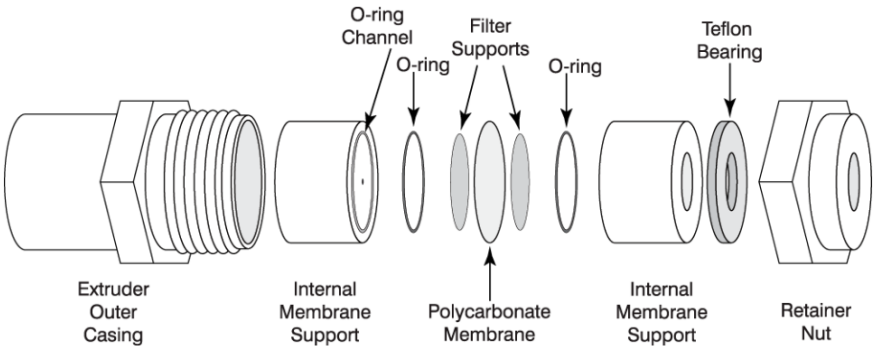

Figure 19. Assembly of Mini-Extruder Parts (Source: Avanti Polar Lipids Inc., Alabaster, AL, United States).

3.2.2 Loading Procedure of Tariquidar

The number of studies for Tariquidar-loaded liposomes is very limited in the literature. Yuqiong Xia et al. used a TRQ/lipid molar ratio of 0.012. Tariquidar-containing liposomes were prepared after determining the optimum DSTAP % for stable liposomes (15% DSTAP in this study). To the lipid mixture composed of DSPC/Cholesterol/DSTAP at a molar ratio of 55/30/15, Tariquidar at varying amounts was added (tariquidar/lipid molar ratio = 0.003, 0.006, 0.012, 0.018, 0.024 where total lipid content was 0.015 μmol). Tariquidar was added to the lipid mixture after it was dissolved in Acetonitrile. After removing Acetonitrile with the stream of nitrogen, the lipid mixture chloroform was added, and lipids were homogenized. Bulky chloroform was removed by a stream of nitrogen while agitating on a spinning table at a rate of 200 rpm. After the chloroform's evaporation and the thin film's formation, the vial was put into the vacuum oven (Nuve EV 018 Vacuum Oven) overnight to remove the trace

amounts of solvents remaining within the thin film. Tariquidar-containing liposomes were prepared like the plain liposomes in 3.2.1, as seen in Figure 20.

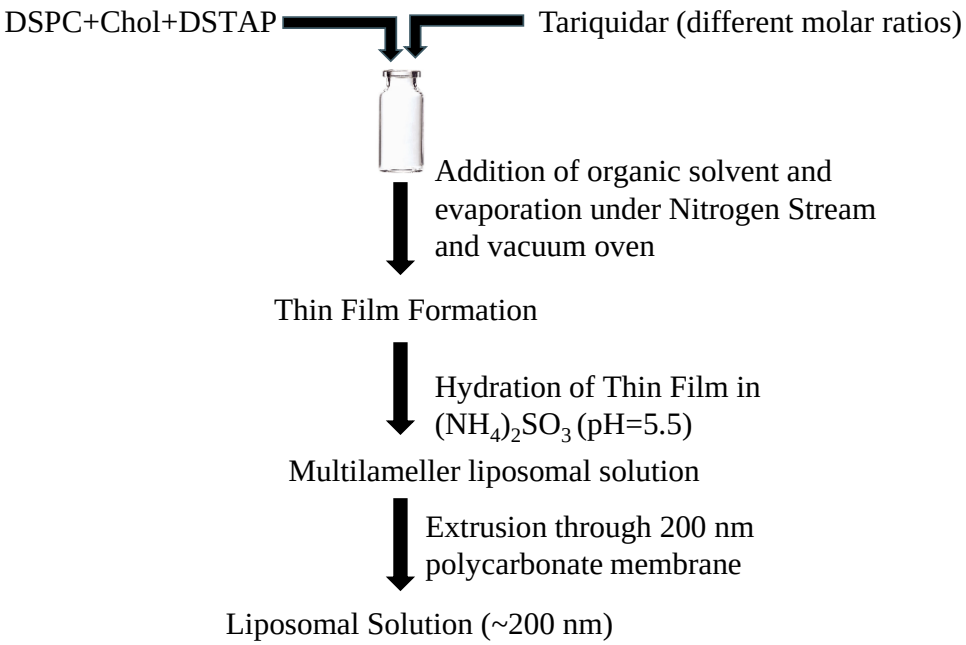

Figure 20. Tariquidar loaded liposomes preparation steps.

Taking DOX loading into account to be done in the next step, hydration of the thin lipid film was done with 1 ml of ammonium sulfate [$(NH_4)_2SO_4$] (250 mM, pH=5,4) buffer solution (to create pH gradient for DOX loading) and heated for about 1 hour at 65°C in an agitating water bath at 150 rpm. After incubation, the liposome mixture was extruded through a polycarbonate membrane with a pore size of 200 nm 11 times. Size and zeta potential measurements of Tariquidar loaded liposomes were made by taking 20 µl of liposomal solution and adding 980 µl of 10 mM NaCl solution.

3.2.3 Loading of Doxorubicin into Liposomes

Before incubation with doxorubicin solution, the liposomal solution was put into a dialysis membrane with 10 kDa pore size and dialyzed against 2 L of %0.9 NaCl solution overnight for external buffer exchange. After being taken from the dialysis bag, 500 µl of the liposomal solution was incubated with 500 µl of 1 mg/ml doxorubicin solution at 65°C for 3 hours at 200 rpm agitation. Liposomal doxorubicin was put into a dialysis membrane with 10 kDa pore size and dialyzed against 2 L of %0.9 NaCl solution overnight to remove the nonencapsulated doxorubicin, as explained in Figure 21.

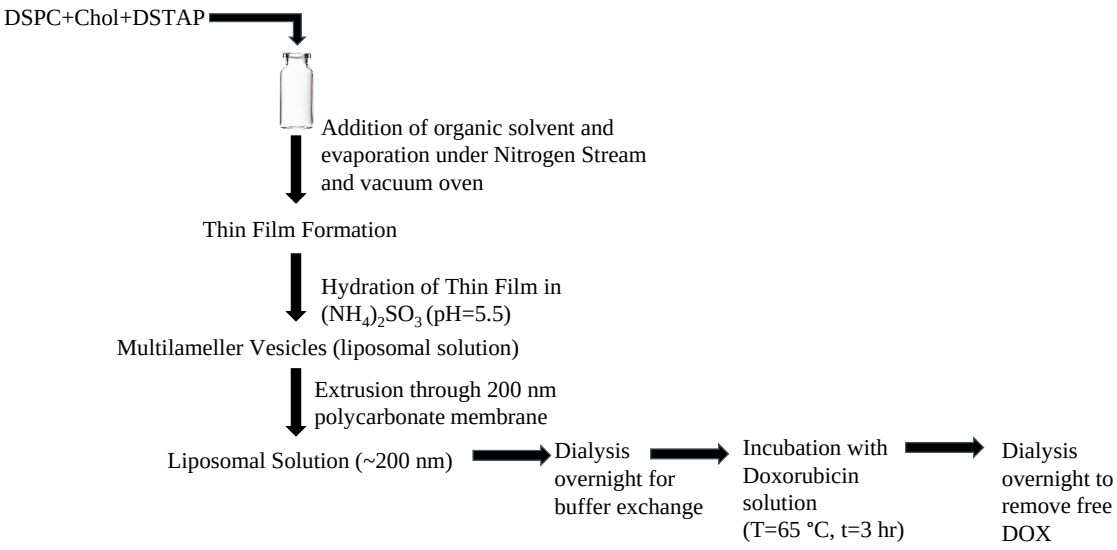

Figure 21. Doxorubicin loaded liposomes preparation steps.

3.2.3.1 Loading of Doxorubicin into Liposomes Containing Different Amounts of Tariquidar

Hydrophilic Doxorubicin (DOX.HCL) is expected to locate in the core of liposomes. Being hydrophobic and situated in the bilayer of the liposomes, Tariquidar may affect the loading of DOX into the liposomes by active mode via pH gradient. , Liposomes with %15 DSTAP and containing different amounts of Tariquidar at tariquidar/lipid molar ratios of 0.003, 0.006, 0.012, 0.018, 0.024 were prepared. After dialysis of the liposomes against 0.9% NaCl solution overnight, to the 500 uL of each liposome solution containing already, tariquidar was added 500 uL of Doxorubicin solution at the concentration of 1 mg/ml and incubated at 65°C for 3 hours, resulting in 0.5 mg/ml of Doxorubicin concentration. 290 µl of UPW and 10 µl of liposomal Doxorubicin were added to the well and diluted five times (5 wells) at a 1:1 volume ratio. Fluorescence values were read with and without Triton-X before and after dialysis to calculate the encapsulation efficiency, as explained in materials and methods in 3.3.8.

3.2.4 Coating of Liposomes

3.2.4.1 Conformation of Fucoidan in Different Solutions

Fucoidan is a long-chain polysaccharide that may present different conformations in different solutions. To identify this, Fucoidan stock solutions were prepared in ultrapure water and 10 mM NaCl solutions at a concentration of 3.4 mg/ml and diluted at an 80% volume ratio for the first five dilutions, and after that, 50% volume ratio. The size and Zeta Potential of stock solutions were measured by Malvern ZetaSizer, by mixing 20 µl of fucoidan solution with 980 µl of 10 mM NaCl solution in the Size Cuvette. Then, the mixture was transferred to the Zeta Cell for zeta potential measurements.

3.2.4.2 Coating Liposomes by Fucoidan

In the literature, generally, coating materials are added by drop-by-drop method. Nevertheless, fucoidan solutions were added to the liposomal solution in our study. %15 DSTAP liposomal solution (total of 15 µmol lipid) was diluted with ultrapure water at a 1:1 volume ratio, resulting in a final lipid concentration of 7.5 mM (initial lipid concentration was 15 mM). Fucoidan stock solutions were prepared by serial dilution (at 80% volume ratio) of the initial Fucoidan solution (3.4 mg/ml in 10 mM NaCl). 20 µl of Fucoidan stock solutions were added to 200 µl of diluted liposomal solutions, then mixed for 10 mins at 170 rpm. Each mixture's size and zeta potential measurements were made by mixing 20 µl of fucoidan-liposome solution with 980 µl of 10 mM NaCl solution.

3.2.4.3 Dilution of Fucoidan Solutions and its Effect on Liposome Sizes

In the above experiment setup, fucoidan-liposome incubations were carried out at a total volume of 220 uL. Considering that the total volume of fucoidan-liposome solution during incubation may be an issue with the size and zeta potential of the coated liposomes, incubation was carried out at different volumes. For this, the fucoidan stock solution prepared from the fucoidan solution at 3.4 mg/ml was further diluted with 10 mM NaCl solutions. Dilutions were made by taking 20 µl of fucoidan stock solutions and mixing them with 30 µl, 80 µl and 180 µl of Ultra Pure Water, resulting in fucoidan stock solutions with volumes of 50 uL, 100 uL, and 200 uL. These fucoidan stock solutions were mixed with diluted 200 µl liposomal solutions and mixed for 10 mins at 170 rpm as before. In this experiment, the fucoidan/lipid molar ratio was kept constant, but the total incubation volume was varied as 250 uL, 300 uL, and 400 uL. Size and Zeta Potential measurements were done by taking 20 µl of fucoidan-liposome solutions and mixing them with 980 µl of 10 mM NaCl solutions.

3.3 Characterization Methods

3.3.1 Size and Zeta Potential Measurements of Plain and Drug-Loaded Liposomes

Malvern Zetasizer Nano is used for equipment. The procedure was chosen for general purpose, done at room temperature. Size and zeta potential measurements were done by taking 20 ul of liposomal solution and mixing in 980 ul of medium (10 mM NaCl or 1 mM NaCl was selected for a medium (conductivity less than 5 mS/cm) for using SFR mode.

3.3.2 Determination of the Optimum Centrifugation Time for Liposomes

Tariquidar was encapsulated in a liposome bilayer because of its hydrophobic behavior. Centrifugation is a general method for hydrophobic drugs to determine drug encapsulation. However, two different methods are proposed in the literature. The first one is the centrifugation of liposomal solution in much smaller centrifugal forces (rpm's), assuming that unencapsulated drug molecules are precipitated as pellets(Patel et al. 2011b). In the second method, the liposomal solution is centrifuged at a much higher rpm to pelletize the liposomes with the loaded drug, assuming the unencapsulated drug molecules remain in a supernatant (C. H. Kim et al. 2022). The second method was employed in this study because sedimentation of the tariquidar molecules is unlikely according to Stoke's law.

To determine the optimum liposome centrifugation time, liposomes were diluted with [$(NH_4)_2SO_4$]at a ratio of 1:3 (200 µl of liposome solution with 400 µl [$(NH_4)_2SO_4$]. Diluted liposomes were subjected to different centrifugal forces, and DLS monitored the change in liposome properties by measuring the liposome size and derived count rate. 120 µl of the diluted liposomes was aliquoted into Eppendorf tubes for each period of

centrifugation for each centrifugal force (3000 rpm, 10000 rpm, and 17500 rpm). Before centrifugation, taking 20 µl of the solution and transferring it into 980 µl medium of 10 mM NaCl, the derived count rate, as well as the size of the liposome solution in each Eppendorf tube, was measured and noted as the derived count rate at t=0. The remaining 100 µl Sample was put in the centrifuge with refrigeration (Hettich Zentrifugen Mikro 220R) and centrifuged at predetermined centrifugal force (3000 rpm, 10000 rpm, or 17500 rpm) at four °C for the predetermined period. Every sample's supernatant part was transferred into a new Eppendorf tube with the help of a pipetter. The supernatant was homogenized by up-and-down mixing of the Eppendorf, and 20 µl was taken for derived count rate measurements and size. By taking the ratio of the derived count rate at a particular time point to the one at t=0, a change in the number of liposomes was determined.

3.3.3 Quantification of Tariquidar by UV-Vis Spectroscopy

UV-Vis spectroscopy was employed to determine the loaded amount of Tariquidar into the liposomes. UV-Vis spectroscopy is an analytical technique that measures the number of discrete wavelengths of UV or visible light absorbed by or transmitted through a sample compared to a reference or blank sample. In an absorption experiment, as seen in Figure 22, light passes through a cuvette filled with a sample solution. The intensity of the light passing through the cuvette is compared to the light passing through a reference cell.

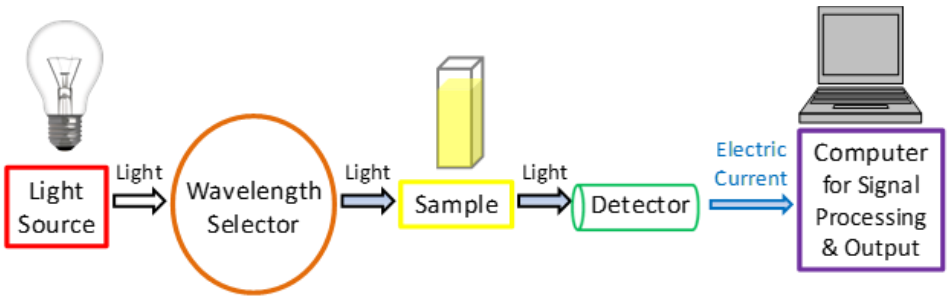

Figure 22. UV-Vis spectrometer illustration

The Beer-Lambert law is commonly used in absorption and transmission measurements on samples. It can be used to determine the concentration of a substance if a linear relationship exists between a measured set of standard solutions with known concentrations and their absorbances. The Equation below shows the mathematical relationships between absorbance, Beer–Lambert's law, the light intensities measured in the instrument, and transmittance.

$$A = \varepsilon\, L\, c = \log_{10}\left(\frac{I_0}{I}\right) = \log_{10}\left(\frac{1}{T}\right) = -\log_{10}(T)$$

Equation 1. Beer–Lambert's law

ε= molar decadic extinction coefficient,

I_0= the sample's entering light intensity,

I =the strength of the approaching light,

c = The concentration of the light-absorbing sample,

d= length of the route

ε is affected by the wavenumber (v) or wavelength (λ).

According to the manufacturers, Tariquidar is soluble in DMSO and has solubility >10 mM or ≥ 16.168 mg/mL (Sigma-Aldrich, P.N: SML1790). In this study, we used Acetonitrile as a solvent because cholesterol and lipids are not soluble, so they can be easily separated from the Tariquidar. Firstly, to determine the wavelength at which Tariquidar exhibits the maximum absorbance, the Full Spectrum of Tariquidar in Acetonitrile was taken using UV-Vis Spectrometer (PerkinElmer Lambda 25). The calibration curve of Tariquidar in Acetonitrile at that maximum wavelength was generated using its solution at the concentration of 48.75 µg/ml (0.45 mg tariquidar dissolved in 9.32 ml Acetonitrile) and employing serial dilution at a 70/30 ratio. In the experiment, a quartz cuvette (Hellma Micro Cuvette, QS Quartz, 1000 µl) was used to measure the UV region. The same dilutions were also used in the HPLC calibration curve.

To determine the loaded amount of Tariquidar, liposomes were dialyzed first against water containing 0.9% NaCl to remove the unloaded Tariquidar. This dialyzes step also helps doxorubicin to be loaded by pH gradient.

To determine the amount of Tariquidar loaded into the liposomes, the procedure seen in Figure 23 was employed. 100 µl of the tariquidar loaded-liposome solution was put into the Eppendorf tube and centrifuged for 60 min at 17500 rpm. Phase separation was observed. A supernatant solution (around 100 µl) was transferred to another Eppendorf tube, and 500 µl of Acetonitrile was added to dissolve the unencapsulated Tariquidar (supernatant-1). 600 µl of Acetonitrile was added to the pellet that remained at the bottom of the first Eppendorf tube. The latter tube was subjected to sonication and vortex to dissolve Tariquidar and then centrifuged again at 17500 rpm for 60 mins to pelletize the lipids (lipids are insoluble in Acetonitrile) and take Tariquidar to the acetonitrile phase. After centrifugation, the supernatant (600 µl) of the pellet (which contains Tariquidar in Acetonitrile) was taken to a new Eppendorf tube (supernatant-2), and 600 µl acetonitrile was again added to the pellet. This solution was centrifuged as before to separate the pellet and the supernatant (supernatant-3). All three supernatants were analyzed in UV-Vis spectrophotometry between 200-600 nm wavelength, but absorbance at 240 nm was recorded since it is the unique peak for Tariquidar. The absorbance of the supernatant-1 was usually high. It was considered that this absorbance might have been resulting from scattered signal due to the liposomes, which may have remained in the supernatant as well as tariquidar aggregates in the water-acetonitrile mixture (supernatant containing 1 part water + 5 parts acetonitrile). As a result, this absorbance was not counted in calculating the tariquidar amount loaded into the liposomes.

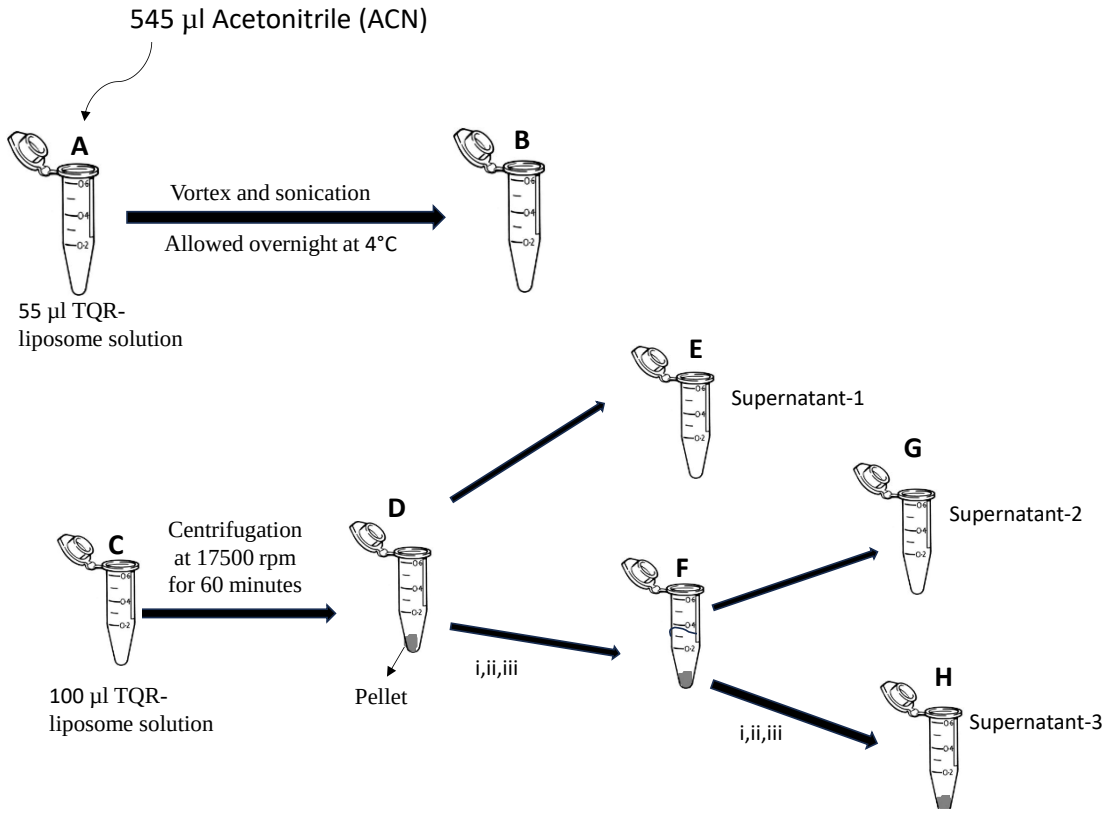

Figure 23. Procedure for the determination of Tariquidar by centrifugation process.

A) 55 ul Tariquidar-loaded liposome was lysed by 545 ul of ACN.

B) After vortexing and sonication of Tube A, the supernatant (600 ul) was transferred to Tube B. UV measurements were taken after keeping the sample overnight at 4°C.

C) 100 ul Tariquidar-loaded liposomes.

D) Phase separation of liposomal solution as pellet and supernatant.

E) Supernatant-1 contains free (unencapsulated) Tariquidar dissolved in Acetonitrile and a non-precipitated lipid mixture. UV measurement was taken after keeping the sample overnight at 4°C.

F) Pellet remained in the Eppendorf tube after the removal of süpernatant-1.

G) Supernatant-2 contains liposomal Tariquidar from the lysis of liposomes by Acetonitrile. UV measurement was taken after keeping the sample overnight at 4°C to allow the Tariqudar entirely dissolve in ACN.

H) Supernatant-3 contains Tariquidar obtained from 2nd wash of lipid mixture by Acetonitrile. UV measurement was taken after keeping the sample overnight at 4°C to allow the Tariqudar entirely dissolve in ACN.

i. 600 µl Acetonitrile was added to the pellet.
ii. Vortex and sonication.
iii. Centrifugation @17500 rpm for 60 mins.

Encapsulation efficiency and Loading efficiency were calculated as follows :

$$EE(\%) = \frac{W_{ST}}{W_T}$$

Equation 2. Encapsulation efficiency equation

W_{ST}= Total weight of Supernatant-2 and Supernatant-3 calculated from absorbance measurements.

W_T= Total weight of Tariquidar founds in 100 µl Tariquidar loaded liposomes.

$$DL(\%) = \frac{W_{ST}}{W_{MT}}$$

Equation 3. Loading efficiency equation

W_{ST}= Total weight of Supernatant-2 and Supernatant-3 calculated from absorbance measurements.

W_T= Total weight of Tariquidar incubated with a liposomal solution.

3.3.4 Quantification of Loaded Amount of Tariquidar by HPLC

Tariquidar is encapsulated in a liposome bilayer because of its hydrophobic behavior. We also used the HPLC technique to quantify the loaded Tariquidar and compare the results with UV spectroscopy. In the literature, the Researchers used the

reversed-phase HPLC (Agilent 1100) technique using the Xbridge C18 (4.6 mm × 250 mm) column (Waters Corporation, Milford, MA). Ammonium acetate buffer (pH 4): Acetonitrile mixture (40:60 wt ratio) was used as a mobile phase, and UV detection was performed at 240 nm(Patel et al., 2011a). 100 µl of the tariquidar loaded-liposome solution was put into the Eppendorf tube and centrifuged for 60 min at 17500 rpm. Phase separation was observed. All the supernatant solution was transferred to another Eppendorf tube, and 500 µl of Acetonitrile was added to dissolve the unencapsulated Tariquidar (supernatant-1). 600 µl of Acetonitrile was added to the pellet that remained at the bottom of the first Eppendorf tube. The latter tube was subjected to sonication and vortex to dissolve Tariquidar and then centrifuged again at 17500 rpm for 60 mins to pelletize the lipids (lipids are insoluble in Acetonitrile) and take Tariquidar to the acetonitrile phase. After centrifugation, the supernatant of the pellet (which contains Tariquidar in Acetonitrile) was taken to a new Eppendorf tube (supernatant-2), and 600 µl acetonitrile was again added to the pellet. This solution was centrifuged as before to separate the pellet and the supernatant (supernatant-3). All three supernatants were analyzed in HPLC.

3.3.5 Cholesterol Effect on Tariquidar Loading

Tariquidar has a hydrophobic structure, and it is located in the liposomal bilayer. We hypothesize that decreasing the cholesterol amount will affect the tariquidar encapsulation efficiency. For this purpose, we made different liposomal formulations. Each liposome.

Table 4. Compositions of liposomes used to investigate cholesterol effect on Tariquidar loading total lipid content (DSPC+DSTAP) was kept constant at 0.015 mmol lipid.

Mole %	**1**	**2**	**3**	**4**	**5**	**6**
DSPC	55	55	55	65	75	85
Cholesterol	42	35	30	20	10	0
DSTAP	15	15	15	15	15	15

3.3.6 Temperature Stability of Tariquidar

As explained above, tariquidar was loaded into liposomes in passive mode. Doxorubicin was loaded in active mode at 65 °C for 3 hours. The temperature stability of tariquidar-loaded liposomes was tested at this temperature to ensure whether tariquidar was not affected during the DOX loading process due to any reason, such as degradation or release. Liposomes composed of DSPC/Chol/DSTAP at 55/30/15 and containing tariquidar at drug/lipid mol ratio =0.012 were prepared as before. The solution was aliquoted into Eppendorf tubes as 145 µl for each time point (0,30,45,60,90,180 minutes), and all tubes were placed in a water bath at 65 °C. At predetermined time intervals, 55 µl of this solution was withdrawn and mixed with 545 µl Acetonitrile to determine the total amount of Tariquidar. The remaining 90 µl of the solution was used to determine the encapsulated amount of Tariquidar. This 90 µl of the solution was centrifuged at 17500 rpm for 1 hour, and the supernatant part (supernatant-1) was transferred to another Eppendorf tube and added acetonitrile up to a total volume of 600 µL. The remaining pellet after centrifugation was dissolved in 600 µl Acetonitrile and sonicated before the next centrifugation. After being sure the pellet was fully dissolved, the solution was centrifuged again at 17500 rpm for 1 hour. Again, this solution was separated as a pellet and supernatant (supernatant-2). Pellet was washed with 600 µL Acetonitrile, vortexed, and centrifuged. The supernatant part (supernatant-3) was removed for analysis. All

supernatants were quantified regarding Tariquidar at UV-Vis spectrophotometry, as explained in Figure 23.

3.3.7 Determination of Doxorubicin Amount Loaded into Liposomes

There are several methods for determining the encapsulation efficiency of liposomal Doxorubicin. In this research, two ways were used HPLC and fluorescence spectrophotometry.

3.3.8 Doxorubicin Quantification by Fluorescence Spectrophotometry

Fluorescence spectrophotometry is a set of techniques that deals with the measurement of fluorescence emitted by substances when exposed to ultraviolet, visible, or other electromagnetic radiation. Fluorophores are molecules that absorb light at one wavelength (excitation wavelength) and emit light at another (emission wavelength). Fluorescence is mainly used to measure substances in solution. Most spectrofluorometers can record both excitation and emission spectra. They primarily consist of four parts: light sources, monochromators, optical filters, and detector Figure 24.

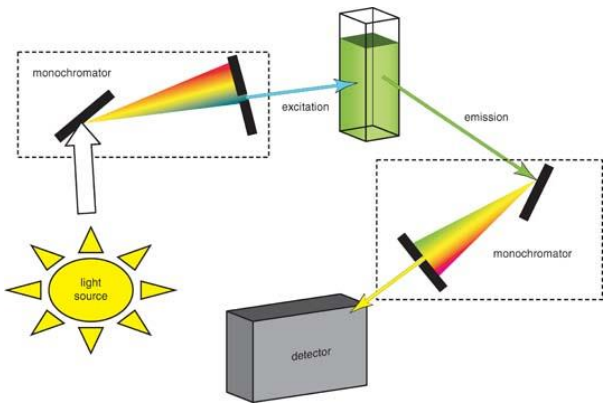

Figure 24. Fluorescence spectroscopy principle(Delfino et al., 2021).

Doxorubicin has a fluorescence property. It has an excitation/emission at 495 /590 nm wavelength. The amount of drug loaded into liposomes was measured via fluorescence spectrophotometer (BioTek, Synergy HTX Multi-Mode Reader).

Doxorubicin quantification was performed using 96 wells plate with 350 µl well volume. Before measurements, the calibration curve of the DOX solution in ultrapure water was generated by serial dilution (80/100) to the DOX solution at 0.2 mg/ml (0.2 mg Doxorubicin dissolved in 1 ml ultrapure water). During the measurements, 290 µl of ultrapure water and 10 µl of liposomal Doxorubicin were added to the well, and the resulting solution was diluted 5 times by serial dilution of 1:1. To each well containing diluted liposomes, 10 µl of Triton-X (20 wt%) was added. Liposomes were lysed by take-and-release method of the solution by pipetter. Air bubbles were burst by using a small needle if there were any. Using the linear relationship between fluorescence and concentration, the loaded amount of DOX was determined, as shown below. For this purpose, the fluorescence of DOX-loaded liposomes at different dilutions was read both before and after dialysis to calculate the encapsulation efficiency.

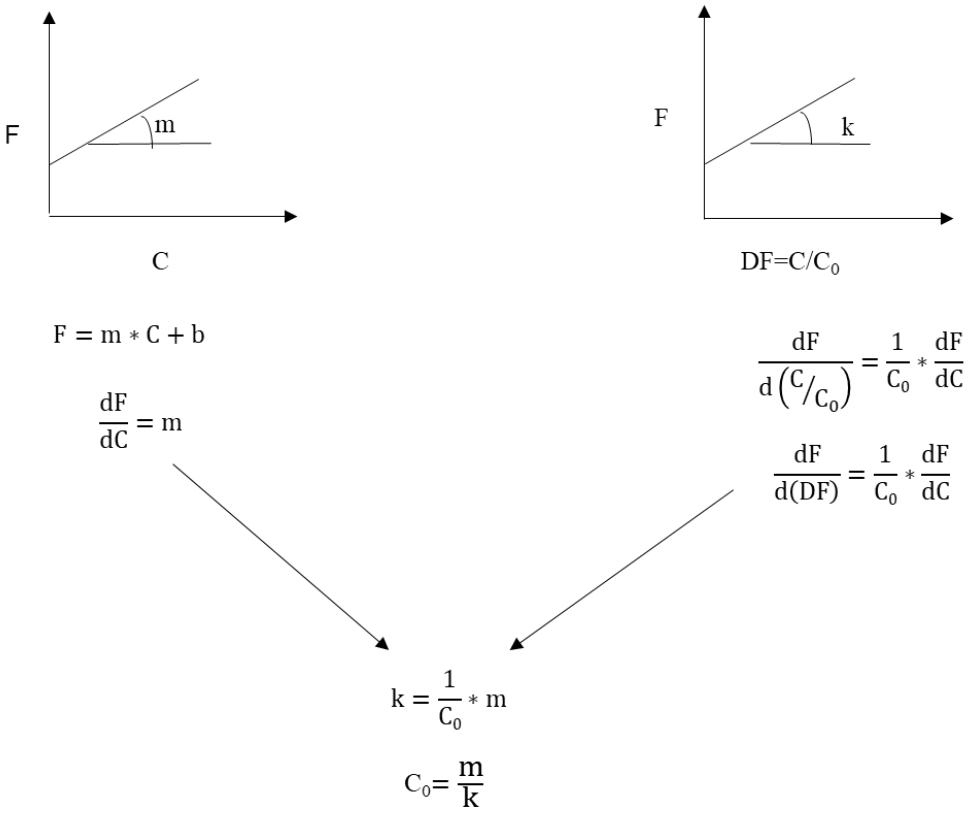

$$\text{Encapsulation efficiency} = \frac{(C_0)_{after}}{(C_0)_{before}} = \frac{\left(\frac{m}{k_{after}}\right)}{\left(\frac{m}{k_{before}}\right)}$$

$$\text{Encapsulation efficiency \%} = \frac{(k_{before})}{(k_{after})}$$

Equation 4. Determination of Doxorubicin concentration from fluorescence measurements.

Where,

F: measured fluorescence value,

C: concentration of the sample,

m: the slope of the calibration curve produced with the known concentration of DOX,

k: the slope of the curve of the measured fluorescence of the unknown sample at different dilution factors,

DF: dilution factor (=C/Co),

Co: concentration of DOX in the main stock solution,

C: concentration of DOX at the given dilution.

3.3.9 Doxorubicin Quantification by HPLC Method

HPLC (Agilent 1100) method is the second most used method for determining liposomal Doxorubicin. Firstly, both lipid (DSPC, DSTAP, and Cholesterol) and doxorubicin HPLC unique peaks were determined by using the mobile phase gradient method with MeOH (w/%0.1 TFA (Trifluoroacetic acid)) and water (w/0.1% TFA) at a flow rate of 1.6 ml/min in method with HPLC column Inertsil ODS3 (5µm, 4.6 x 250mm), at room temperature. Four main components (DSPC, Cholesterol, DSTAP, and DOX) had clear and well-separated peaks.HPLC's calibration curve was produced by diluting 1 mg/ml Doxorubicin in 1 ml Methanol and making serial dilutions by 70/100.

For further experiments, lipids calibration curves were also obtained by dissolving 3 mg of each DSPC, DSTAP, and Cholesterol in 1 ml of Methanol for each of them. Methanol was used as a solvent because lipids, Cholesterol, and Doxorubicin are all soluble in MeOH.

3.3.10 Analysis of Lipid-Doxorubicin Interaction by HPLC

This study also aimed to understand the lipid (DSTAP, DSPC, Cholesterol) interaction with Doxorubicin. For this purpose, two different sets of experiments were designed. In the first experiment set, lipid amounts were kept constant, and DOX amounts were varied. For this reason, DSPC, Cholesterol, and DSTAP were weighed as 9.33 mg, 2.31 mg, and 2.25 mg, respectively, resulting in a 56.3/28.5/15.3 molar ratio. The lipid mixture (13.89 mg) was dissolved in 1 ml MeOH. Doxorubicin (1.11 mg) was dissolved in 1 ml MeOH. Four vials with 100 µl of this lipid solution were taken, and doxorubicin solution was added into these vials as 50 µl,100 µl,150 µl, and 200 µl.

In the second experiment set, a constant amount of DOX was added to the varying amounts of the lipid mixture. For this reason, lipids and Doxorubicin solution were prepared as above. 50 µl of doxorubicin solution was added to each vial containing 50 µl, 100 µl, and 200 µl of lipid solution at a molar ratio of DSPC/Cholesterol/DSTAP: 56.3/28.5/15.3. HPLC analysis was done using the method above (column Inertsil ODS3 (5µm, 4.6 x 250mm), mobile phase gradient method with MeOH (w/%0.1 TFA) and water (w/0.1% TFA) at a flow rate of 1.6 ml/min and at room temperature).

3.3.11 Tariquidar Quantification After Loading of Doxorubicin

Doxorubicin was loaded into already Tariquidar-containing liposomes by the active method by incubating the mixture for 3 hours at 65 °C in an agitating water bath at 150 rpm. 65 °C is the phase transition temperature for lipids; however, Tariquidar is located in the bilayer. Considering the Tariquidar could be affected by extended time

incubation measurements for Traiquidar was reperformed, using the same procedure explained above (Figure 23). Briefly, to characterize the tariquidar amount, %15 DSTAP liposomes which contain Tariquidar with 0.003,0.006,0.012,0.024 drug/ lipid ratio prepared each liposome incubated with 500 µ1 of 1 mg/ml doxorubicin incubated at 65°C for 3 hours, and the final concentration of Doxorubicin was 0.5 mg/ml. Tariquidar quantification was done by taking 55 µl of each solution by dissolving it in 600 µl Acetonitrile; 100 µl of the solution was used to determine the encapsulated amount of Tariquidar. 100 µl of solution was centrifuged at 17500 rpm for 1 hour and divided into supernatant and pellet. After centrifugation of supernatant, 100 µl completed to 600 µl with Acetonitrile. Pellet dissolved in 600 µl Acetonitrile and was sonicated before centrifugation. After being sure the pellet fully dissolved, the solution was centrifuged at 17500 rpm for 1 hour. Again, this solution is divided into a pellet and supernatant. Pellet was washed with 600 µl Acetonitrile. To increase the dissolution, the pellet vortexed and centrifuged. Both supernatants were quantified in terms of Tariquidar at UV-Vis spectrophotometry.

3.3.12 Interference of Tariquidar and Doxorubicin in Uv-Vis Spectrofotometry Measurements

To understand the self-interactions between Tariquidar and Doxorubicin, they were mixed in the same amounts as in the liposomes. Samples were prepared without lipids. For this experiment, 126 µl of Tariquidar (0.048 mg/ml as dissolved in Acetonitrile) was taken from the stock solution, and 474 µl of Acetonitrile was added. Seven vials were prepared. Additionally, 55 µl of Dox solution (1 mg/ml) was taken and diluted seven times at a 1:1 ratio. These diluted DOX solutions were added to each tariquidar solution. The mixture was mixed, resulting in a total volume of 655 uL. Absorbance values were read by transferring 600 uL of this solution to the quartz cuvette of the UV-spectroscopy.

CHAPTER 4

RESULTS AND DISCUSSION

4.1 Liposomes and Their Characterizations

Liposomes composed of DSPC, cholesterol, and DSTAP were prepared by the thin-film hydration method. Positively charged lipid DSTAP was added to the liposome formulation in order to coat the liposomes with negatively charged fucoidan for targeting. Because the repulsive forces between the liposomes determine the colloidal stability of the liposomes, liposomes containing various amounts of DSTAP were formulated, and their stability was assessed by zeta potential and size measurements with ZetaSizer. As shown in Figure 25, the zeta potential of the liposomes increases with increasing DSTAP and reaches around +35 mV at 20% DSTAP in the medium of 10 mM NaCl. The zeta potential is a measure of the electrical potential difference between the primary fluid in which a particle is dispersed and the layer of fluid containing oppositely charged ions associated with the particle surface; hence, its value varies with the ionic strength of the medium. Typically, zeta potential is inversely related to the medium ionic strength, i.e., a lower ionic strength medium results in higher zeta potential values for the same particles. Indeed, zeta potentials measured in 1 mM NaCl solution were much higher than in 10 mM NaCl, reaching roughly +50 mV at 20% DSTAP concentration (Figure 26). Zeta potential provides information about the stability of colloidal particles, as particles with higher zeta potential generally repel each other more strongly due to electrostatic forces, preventing aggregation. Generally, colloids with zeta potential values in the range of ±30 mV are typically considered stable colloids. Therefore, 15% DSTAP was selected as the optimum concentration for further experiments. 15% DSTAP containing liposomes exhibited a zeta potential of 32 mV in 10 mM NaCl solution while 43.6 mV in 1 mM NaCl solution when the hydration process was done in an ammonium sulfate solution.

The formulation resulted in a zeta potential value of 17 mV when hydrated in 1 mM NaCl prior to liposome making and then measured in 1 mM NaCl.

As can be seen from both figures, the size of the liposomes did not show a significant change with increasing DSTAP% in both mediums, exhibiting a monomodal size distribution around 200±10 nm and 180±10 nm in the medium of 10 mM NaCl and 1 mM NaCl, respectively. These sizes suggest that the size of the liposomes is determined by the pore size of the polycarbonate membrane used in the extrusion. Because the intervals between endothelial cells range from 100 to 800 nm, these sizes are excellent for liposome accumulation in tumor sites. Previous works found that accumulation was greater when the sizes were between 400-200 nm (Sawant & Torchilin, 2012).

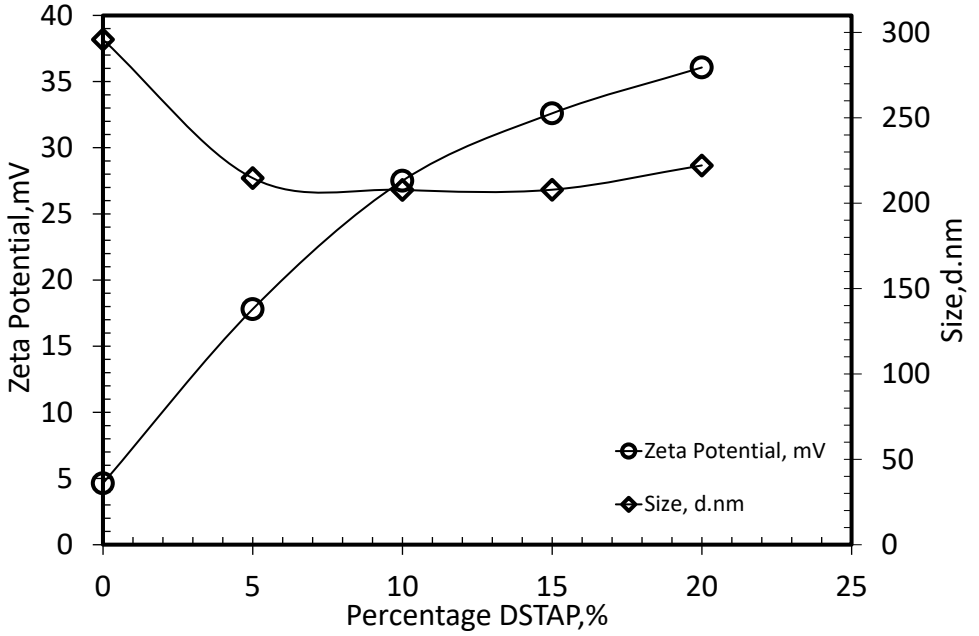

Figure 25. Average size and zeta potential of different DSTAP mole percentages liposomes made in $(NH_4)_2SO_3$ buffer and measurements made in 10 mM NaCl.

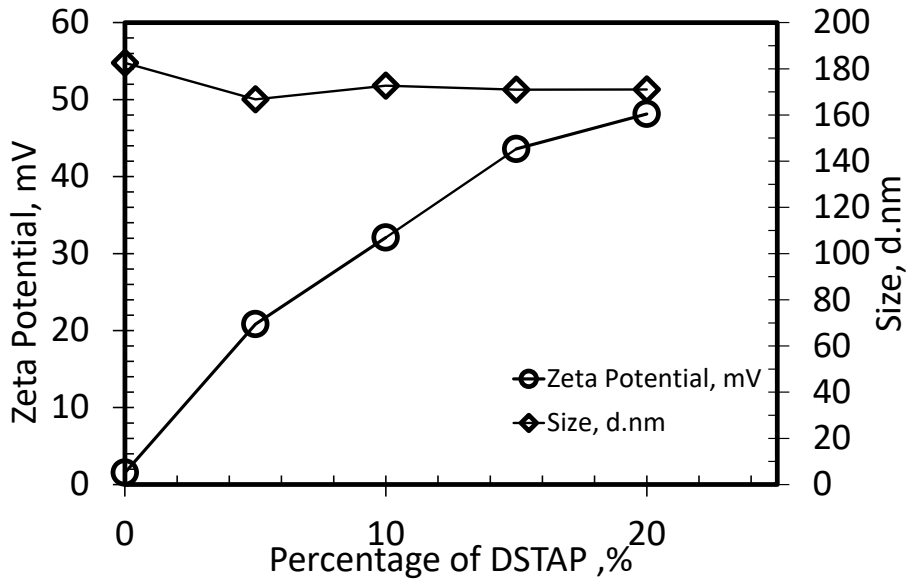

Figure 26. Average size and zeta potential of different DSTAP mole percentages liposomes made in $(NH_4)_2SO_3$ buffer and measurements made in 1 mM NaCl.

In the above liposome formulations, $(NH_4)_2SO_3$ buffer was used for hydration, considering doxorubicin loading by pH gradient method in the subsequent experiments. To understand if the hydration medium also affects the liposome's zeta potential, a thin film was hydrated in 1 mM NaCl solution, and zeta potential and size measurements were also performed in 1 mM NaCl solution. As seen in Figure 27, the hydration medium did not significantly change in size, but much lower zeta potentials were observed. This result implies that the ions of the hydration medium are adsorbed on the liposome surface, altering the double layer thickness and, thus, zeta potential.

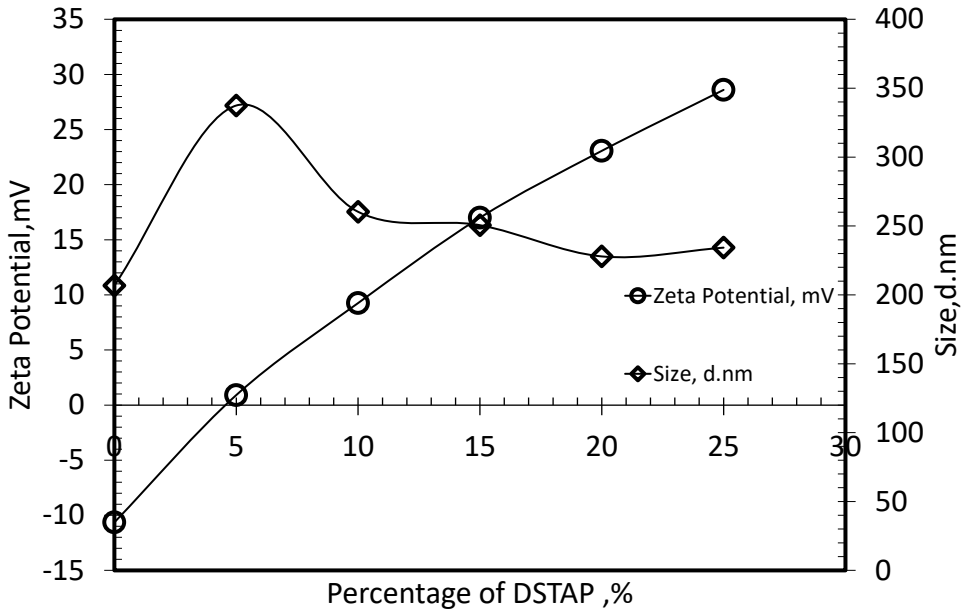

Figure 27. Average size and zeta potential of different DSTAP mole percentages liposomes hydrated in 1 mM NaCl and measurements made in 1 mM NaCl.

The effect of different Mediums on Zeta Potential and Size measurements was also evaluated (Figure 28). First, salt solutions were prepared in the concentration range from 1 mM to 62.5 mM to compare the effect of both the concentration and type of the medium. Measurements were done by mixing 980 µl salt solution with 20 µl of %10 DSTAP containing liposomal solution. As seen in Figure 28, when the salt concentration increases, the liposomal solution's zeta potential decreases, in agreement with DLVO theory. On the other hand, the medium does not affect liposome size; as mentioned before, size is related to polycarbonate membrane pore size.

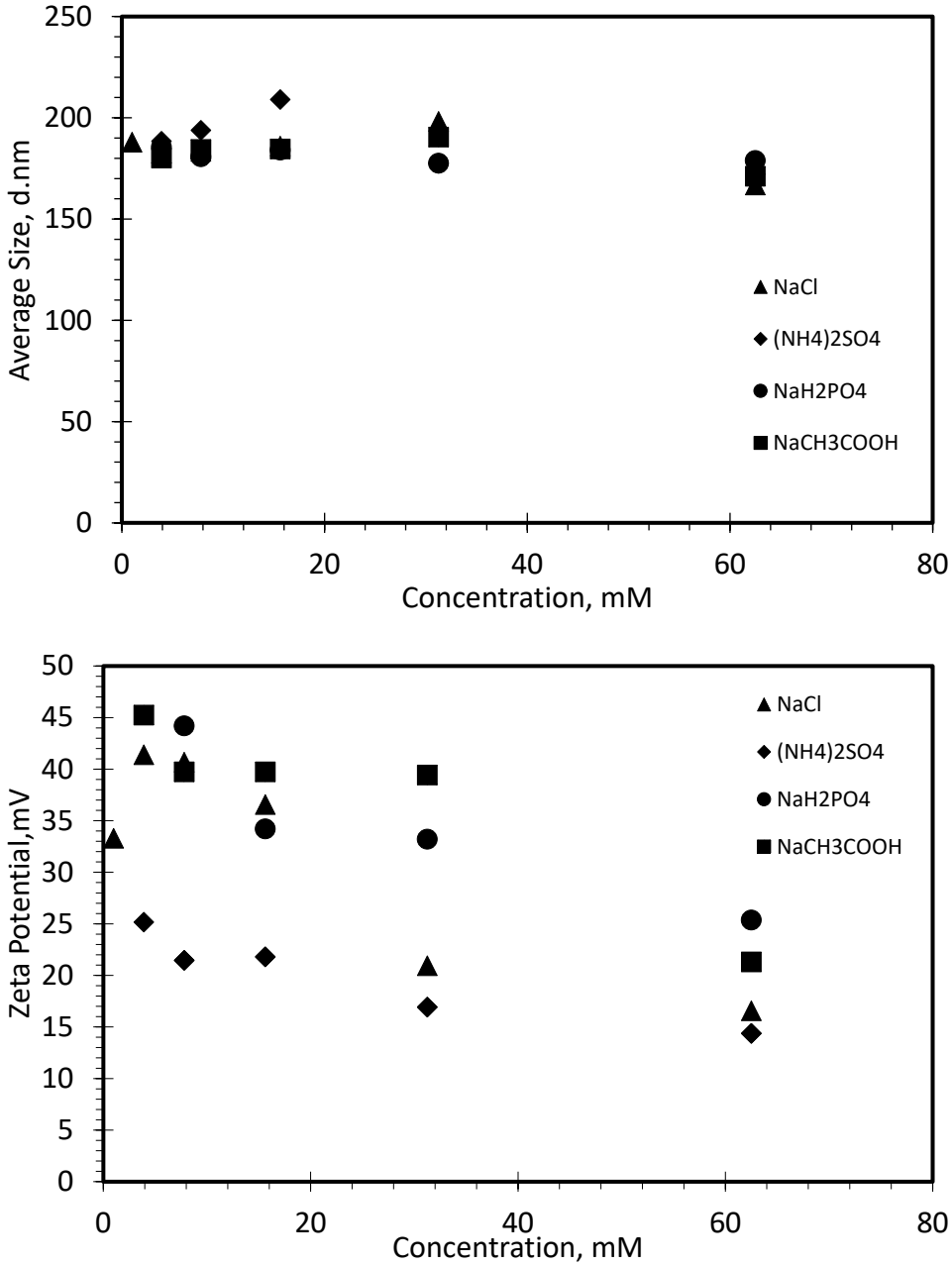

Figure 28. Size and Zeta potential measurements of %10 DSTAP liposomes in different salt mediums (NaCl, $(NH_4)_2SO_3$, NaH_2PO_4, $NaCH_3COOH$ concentration varying from 1 mM to 62.5 mM).

4.1.1 Determining the Optimum Centrifugation Time for Liposomes

The centrifugation method is generally used to determine hydrophobic drug encapsulation efficiency. In literature, Hydrophobic drugs such as Curcumin, Tariquidar, Calcein, etc., were encapsulated into liposomes, and the centrifugation method was employed to separate the unloaded drug from the liposomes (Hardiansyah et al., 2017; Mourtas et al., 2008; Patel et al., 2011b). However, limited research has been done on optimizing liposome centrifugation time and rpm. This study aimed to determine the optimum centrifugation force and duration in which liposomes are unaffected and entirely precipitated.

Patel et al. reported using centrifugation at 10,000 rpm for 10 minutes to precipitate non-entrapped Tariquidar (Patel et al., 2011) . In a subsequent study by Montesinos, unloaded elacridar and Tariquidar were separated from the liposomes by precipitating under centrifugation at 10.000 g for 5 minutes. Mourtas et al. determined unencapsulated Calcein by centrifugation at 15.000 rpm for 40 mins. These studies assumed that non-encapsulated free drugs precipitated as pellets upon centrifugation(Mourtas et al. 2008). Contrary to those studies, Gomez et al. separated the unencapsulated drug by centrifugation at 30k relative centrifugal force for 2 hours, assuming the free drug remained in the supernatant phase (Gonzalez Gomez et al. 2019). Indeed, drug molecules are very small compared to liposomes; therefore, according to Stoke's Law, they remain in the supernatant phase, as suggested by Gomez et al. There are contradictory results in the literature for the separation of hydrophobic drugs by centrifugation method. Moreover, none of these studies investigated the fates of liposomes after centrifugation. In our study, firstly, we tried to understand the effect of centrifugation on liposomes in terms of size and number using an indirect method. Unfortunately, no method is available to measure liposome concentration directly. In this study, we indirectly observed the change in size and number of liposomes upon centrifugation using the derived count rate in dynamic light scattering measurements.

According to Stokes' law Equation 5, a particle will sink in a fluid medium under the action of gravity when a force is applied to it. The velocity, fluid viscosity, and sphere radius all directly relate to the force.

$$V = \frac{2(\rho_s - \rho_l) * r^2 * g}{9\mu}$$

Equation 5.Stokes' law equation

V= rate of sedimentation

ρ_s= density of the particles

ρ_l= density of the liquid

r= radius of the particle

g= acceleration due to the gravity

μ= viscosity of the liquid

When the equation is analyzed, precipitation due to density difference seems very unlikely in our system, considering that our liposomes are stable colloidal systems. One should keep in mind that this colloidal stability results from the high zeta potentials, not necessarily similar densities of the liposomes and the medium. On the other hand, spontaneous precipitation of liposomes with low zeta potential may suggest that precipitation occurs due to flocculation and coagulation of liposomes under centrifugation. The sedimentation rate is proportional to the square of the particle's radius and the acceleration of gravity. Therefore, during the centrifuge process, tariquidar precipitation is very unlikely due to their small size compared to liposomes, as opposed to the assumption by Patel, Mourtas and Montesinos (Patel et al. 2011b; Mourtas et al. 2008; Nieto Montesinos et al. 2015).

To understand the fate of liposomes upon centrifugation, liposomes were exposed to centrifugation at different centrifugal forces (3000 rpm, 10000 rpm, and 17500 rpm) for different durations (Figure 29). As mentioned in the materials and method chapter, 100 µl of the liposomal solution was put in the Eppendorf tube for each time point and centrifuged for a predetermined period. Changes in the number and size of the liposomes in the supernatant phase were monitored by the derived count rate. The derived count rate is a calculated parameter in the ZetaSizer nano software. It is representative of the scattering intensity that would be measured at the APD detector in the absence of the laser attenuation filter. Whereas, in the mean count rate, the attenuator is varied by the

software to maintain the count rate between 200–500 kcps. In 3.000 rpm, derived count rates do not significantly change with the centrifugation period, as presented in Figure 29, indicating that liposomes are still in suspended form. At 10.000 rpm, however, after 30 mins, the derived count rate decreased by around 30% compared to the initial. Centrifugation of the liposomes at 17.500 rpm caused a significant decrease in the derived count rate even at 20 minutes. About in 60 minutes, 70% of the liposomes seemed to pelletize. Precipitation of liposomes was also observed visually, resulting in a clear supernatant phase. The derived count rate varies with size and number of the particles in the solution. A higher number of particles and/or greater size result in higher values of the derived count rate. Similarly, a lower number of particles and/or smaller sizes result in lower values of the derived count rate. The derived count rate of the supernatant not going to lower values when centrifuged further might be explained by breaking down of the liposomes into smaller ones at the expense of an increase in number and/or not reaching the liposome clusters to a critical size to precipitate as a result of flocculation and coagulation (Figure 29). It is important to note that the derived count rate of Ultra-Pure Water was not close to zero either.

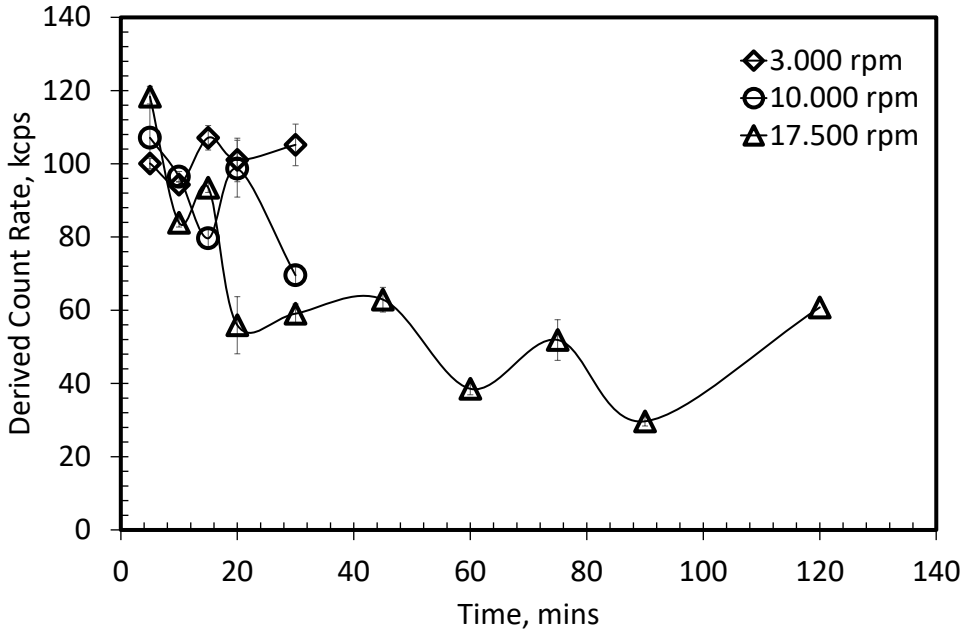

Figure 29. Derived Count Rate changes during periods at different Revolutions per Minute (3.000,10.000,17.500 rpm).

4.2 Tariquidar Loading Liposomes Characterization

4.2.1 Size and Zeta Potential Measurement of Tariquidar Loaded Liposome

As explained in materials and methods section 3.2.2, lipids were weighed then TRQ dissolved in ACN solution was added to lipids. Not a good thin film formation was not obtained when the chloroform was added to Lipid-TRQ- ACN solution because lipids are not soluble in ACN. On the other hand, when ACN was removed from the mixture under the Nitrogen gas stream first, and then chloroform was added to the lipid-TRQ mixture to homogenize. Completely dried film was obtained after keeping the film in a vacuum oven overnight.

As seen in Figure 30, the size of the liposomes did not change again with the loading of TRQ, indicating almost similar sizes with plain liposomes. The Zeta potential of the Tariquidar loaded liposomal did not show a trend. Fluctuations of the zeta potential might be explained by the adsorption of TRQ on the liposome surface and, thus, a change in the double layer thickness (TRQ encapsulation efficiency did not show any trend either, as will be explained later).

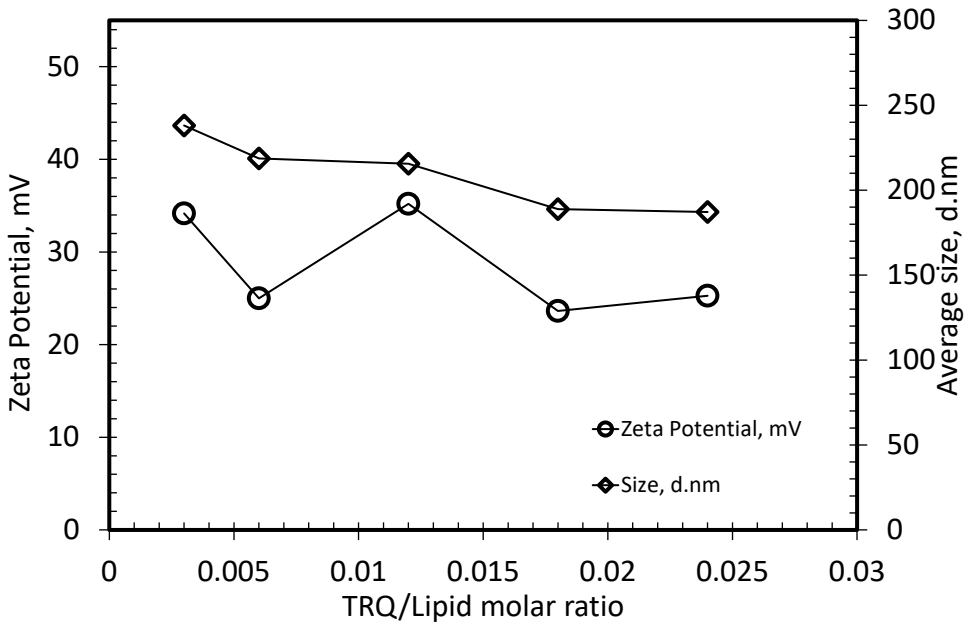

Figure 30. Tariquidar loaded liposome size and zeta potential measurements.

4.2.2 Quantification of Tariquidar loaded Liposomes

Tariquidar is encapsulated in a liposome bilayer because of its hydrophobic nature. UV-Vis Spectrophotometry and HPLC methods were employed for quantification. For UV-Vis Spectrophotometry measurements, a full scan of TRQ dissolved in ACN was taken to determine the maximum absorbance wavelength. As seen in Figure 31, TRQ exhibits a maximum peak at 240 nm. The calibration curve at 240 nm was generated by 80% serial dilution of TRQ solution in ACN at a concentration of 48.75µg/ml (Figure 32).

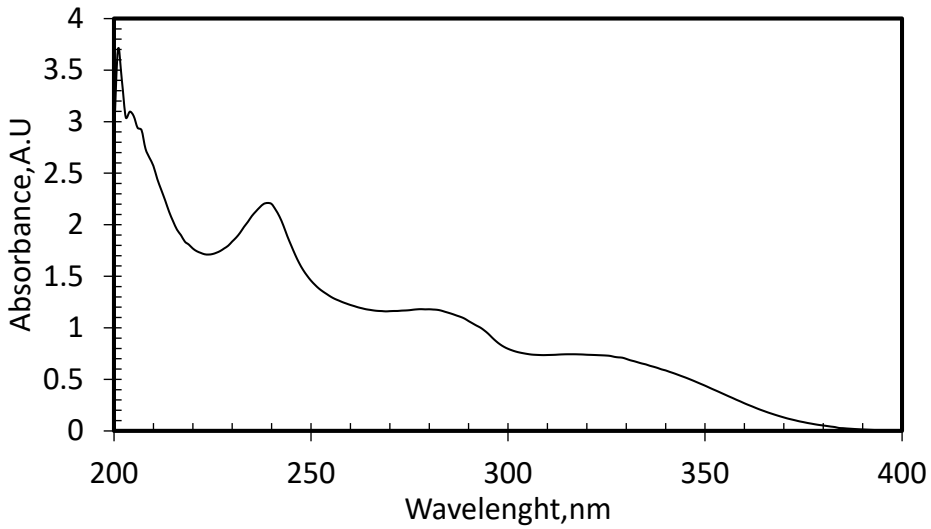

Figure 31. Full absorbance spectrum of Tariquidar.

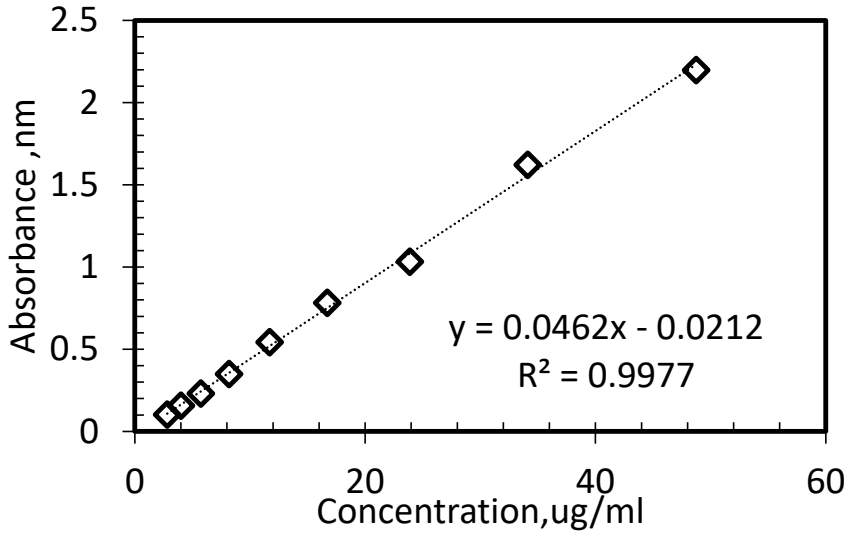

Figure 32. Calibration curve of Tariquidar in UV-Vis Spectrophotometry at 240 nm.

The reversed-phase HPLC technique was used in the literature with the Xbridge C18 (4.6 cm × 250 cm) column (Waters Corporation, Milford, MA). Ammonium acetate buffer (pH 4): Acetonitrile mixture (40:60 wt. ratio) was used as a mobile phase, and a UV detector was used at 240 nm. The authors generated the calibration curve of Tariquidar in HPLC using concentrations varying from 0 ug/ml to 20 ug /ml (Patel et al., 2011a). However, they did not mention the solvent they used to dissolve the Tariquidar.

The calibration curve of the TRQ was produced using the same solution in UV-Vis Spectrophotometry.

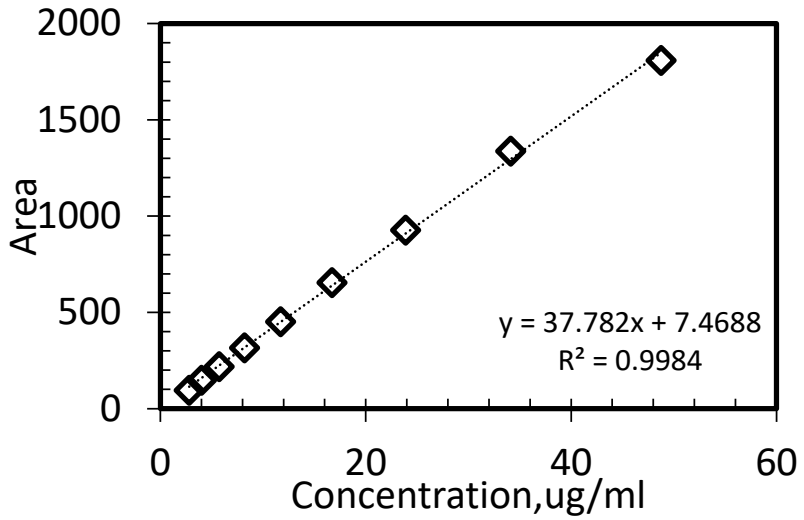

Figure 33. Calibration curve of Tariquidar in HPLC at 240 nm.

Tariquidar's encapsulation and loading efficiency was determined by HPLC and UV-Vis absorbance after centrifugation of the samples. Liposomes were prepared with different amounts of Tariquidar and subjected to a centrifugation process summarized In Figure 23. To determine the total amount of Tariquidar present in the liposomal solution, first, 55 µl of the tariquidar-loaded liposomal solution was withdrawn from the original solution and mixed with 545 µl of ACN. The resulting solution was sonicated and vortexed to disrupt the liposomes, and the total Tariquidar amount was determined by both UV-Vis and HPLC. To determine the encapsulated Tariquidar, 100 µl of Tariquidar-liposomal solution was transferred into an Eppendorf tube from the original solution and then was centrifuged at 17500 rpm for 1 hour. All of the supernatant phase (supernatant-1) was transferred to another Eppendorf tube, and it was completed to 600 µl with ACN. The remaining pellet was dissolved in 600 µl ACN. The solution was sonicated and vortexed for a few minutes to lyse the liposomes and allow the Tariquidar to dissolve in the ACN phase. This solution was centrifuged again at 17500 rpm for 1 hour to accelerate the precipitation of the liposome components (DSPC, Chol, and DSTAP are all insoluble in ACN). The supernatant of this centrifugation process (supernatant-2) was measured for Tariquidar content. The pellet of this step was washed one more time with ACN to

take the remaining TRQ (if there is any) to the ACN phase. The resulting solution was centrifuged again at 17500 rpm for 1 hour to accelerate the precipitation of the liposome components. The supernatant phase was taken to a new Eppendorf tube (supernatant-3). All supernatants (supernatant-1, supernatant-2, supernatant -3) were analyzed by HPLC and UV-Vis spectrophotometry.

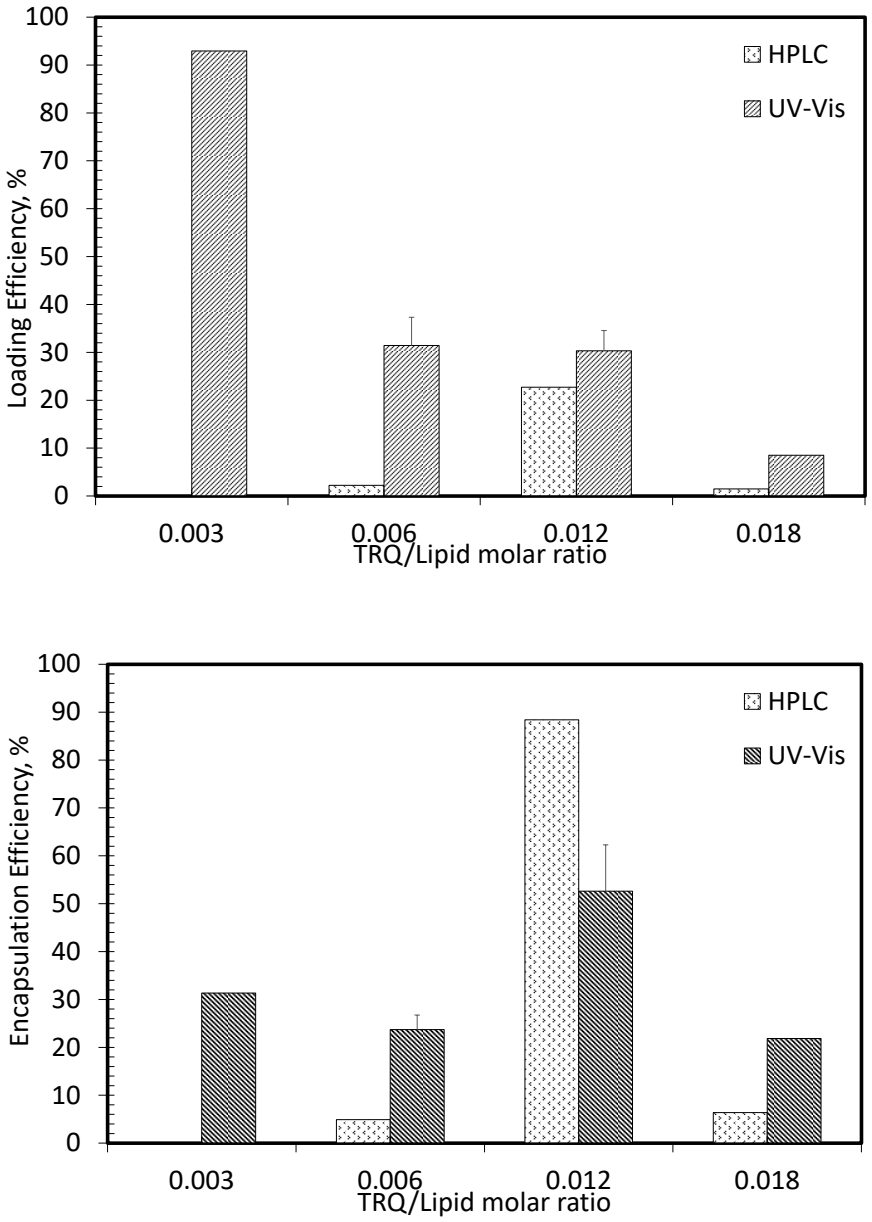

Figure 34. Comparison of Encapsulation and Loading efficiencies of Tariquidar loaded liposomes (DSPC/Chol/DSTAP:55/30/15, Total lipid content: 0.015 mmol) analyzed by HPLC and UV-Vis Spectrophotometry (in the standard deviations n=2 for 0.006, n=3 for 0.012).

Both the Loading and encapsulation efficiency of Triquidar were reported in Figure 34. Loading efficiency indicates the encapsulated amount of TRQ with respect to the TRQ amount initially added to the lipid mixture. Whereas encapsulation efficiency indicates the encapsulated amount of TRQ with respect to the total amount in the liposomal solution determined by UV-vis or HPLC measurement. Loading efficiency dramatically decreased with increasing TRQ/Lipid molar ratios from 0.003 to 0.006 in UV-Vis measurements. The change was insignificant at the TRQ/Lipid molar ratio of 0.006 and 0.012 but decreased considerably at the 0.018 molar ratios. Because of the water-insoluble nature of TRQ, there could be some circumstances in which some of the TRQ might be lost during the preparation of the liposomal form. For instance, TRQ may aggregate during the hydration process and settle down at the bottom of the vial, resulting in some of the TRQ not being withdrawn to a syringe for the extrusion process. Additionally, the TRQ-lipid mixture withdrawn from the syringe might have caused clogging in the pores of the polycarbonate membrane. Indeed, the polycarbonate membrane used during the extrusion process for 0.018 TRQ/Lipid molar ratio was more yellowish in color than the one used for 0.006 TRQ/Lipid molar ratio, suggesting that some of the TRQ were remained on the polycarbonate membrane during the extrusion process (Figure 35). Additionally, as seen from the DLS measurement in Figure 36, although there is a slight decrease in the size of liposomes, there was a dramatic decrease in the derived count rate of liposomes with increasing Tariquidar content, also suggesting a decrease in the number of liposomes passing through the polycarbonate membrane as a result of this pore-clogging issue. In conclusion, these issues might have caused the low loading efficiency of TRQ into liposomes.

Figure 35. Polycarbonate membrane color changes after the extrusion process (left polycarbonate membrane: 0.018 TRQ/Lipid molar ratio, right polycarbonate membrane: 0.006 TRQ/Lipid molar ratio).

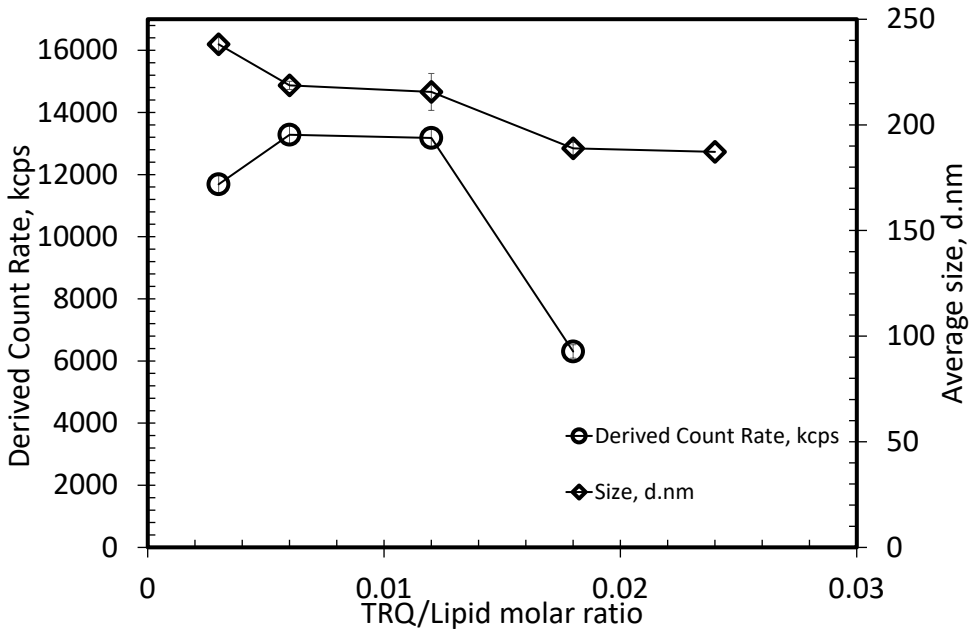

Figure 36. Derived Count Rate and Average size of liposomes loaded with different amounts of Tariquidar (DSPC/Chol/DSTAP:55/30/15, Total lipid content: 0.015 mmol).

In all TRQ/Lipid molar ratios, HPLC measurements indicated lower loading efficiencies than UV-Vis measurements. From these results, HPLC analysis might be misleading for the same amount of sample used in both methods if the loaded amount of Tariquidar is low because of the reasons discussed above. As a result, measurements may have fallen below the instrument's detection limit. Furthermore, as seen from the chromatograms in Figure 37 and Figure 38, tariquidar peaks consist of shoulders, resulting in an incorrect reading of the HPLC area. This could be because of unsuitable column selection, mobile phase properties, and solvent selection. Because of all these reasons, HPLC results were evaluated as unreliable.

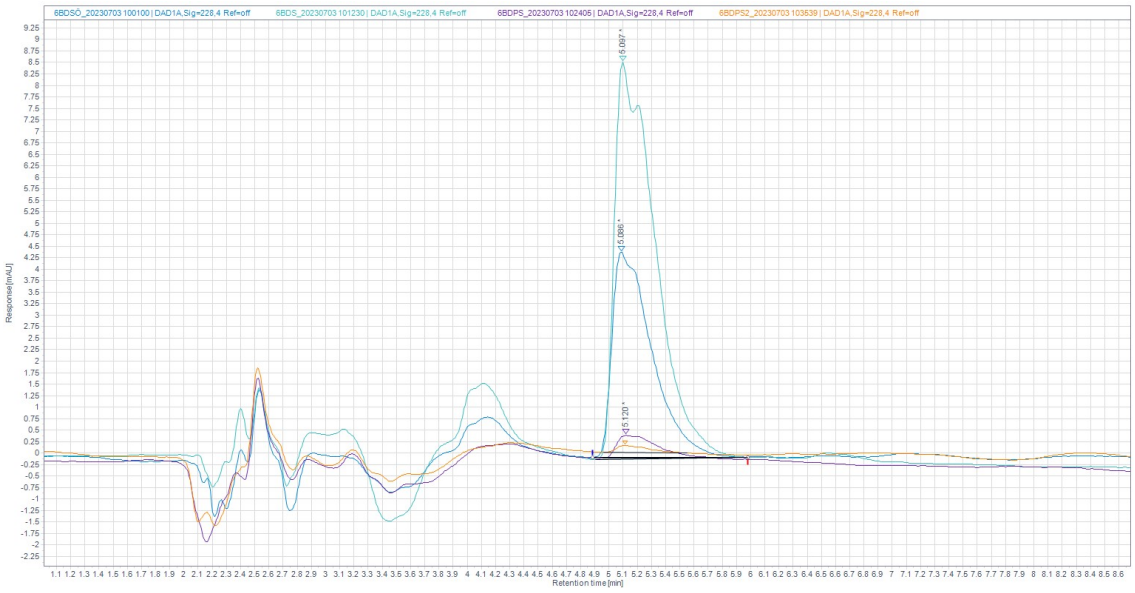

Figure 37. HPLC chromatogram of %15 DSTAP liposomes loaded with Tariquidar at TRQ/Lipid ratio of 0.006 (after dialysis of liposomes) (SO: before centrifuge, S: Supernatant-1, PS: Supernatant-2, PS2: Supernatant-3).

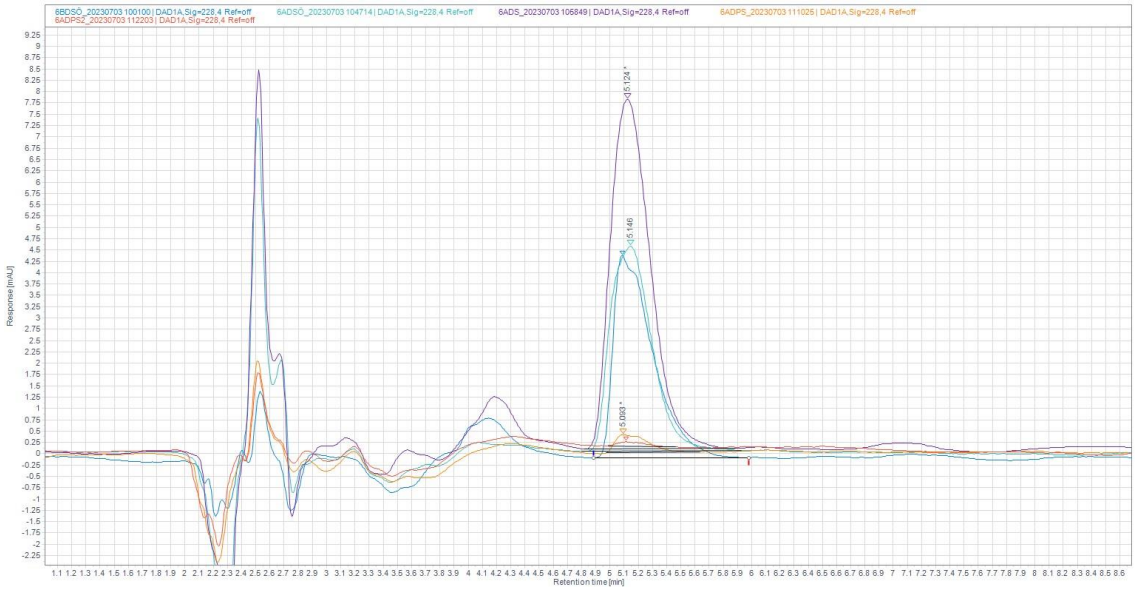

Figure 38. HPLC chromatogram of %15 DSTAP liposomes loaded with Tariquidar at TRQ/Lipid ratio of 0.018 (after dialysis of liposomes) (SO: before centrifuge, S: Supernatant-1, PS: Supernatant-2, PS2: Supernatant-3).

Encapsulation efficiency (EE%) indicates the percent of the liposomal TRQ in the solution. Encapsulation efficiency did not show a trend but showed maximum encapsulation efficiency at 0.012 TRQ/Lipid molar ratio in both UV-Vis and HPLC measurements.

Interestingly, this molar ratio used by Patel's study and loading efficiency was reported as around 70% (Patel et al., 2011b). Montesinos et al. studied the co-loading of Elacridar and Triquiadar into liposomes. Liposomes were produced by sonication method and centrifuged at 10.000 g for 10 mins, assuming nonencapsulated drugs were pelletized. They reported the loading efficiency as 63.4±2.4%. Montesinos et al. used a method similar to the one used by Patel et al. (Nieto Montesinos et al., 2015). In these studies, loading efficiencies were reported higher than ours because they assumed they removed the unencapsulated Tariquidar by centrifugation. Authors claimed that unencapsulated Tariquidar precipitated as a pellet, contrary to our assumption. As we stated before, Tariquidar cannot get precipitated because of its molecular size, according to Stoke's Law. In other words, it is very likely that nonencapsulated Tariquidar has not been removed from their liposomal solution and counted as encapsulated, resulting in

these high loading efficiencies. However, in our study, liposomes were dialyzed and centrifugated to remove the nonencapsulated (free) Tariquidar (present in supernatant-1). Low encapsulation efficiency can be attributed to again insoluble nature of TRQ. TRQ might have been aggregated in the buffer solution during the hydration,n forming clusters that can not migrate to the bilayer of liposomes. It is also possible that some of the clusters that have achieved to go to the bilayer of liposomes causing disorder in the bilayer may have migrated out from the bilayer during the centrifugation process, leading to the quantification of low encapsulation efficiencies. In calculating encapsulation efficiencies, a separate 100 µl was taken from the original solution, and the total amount (free+ encapsulated TRQ) was analyzed. If there is an inhomogeneity in sampling, this could be another reason for low encapsulation efficiencies.

4.2.3 Cholesterol Effect On Tariquidar Loading

In the literature, researchers proposed that cholesterol resides in bilayers of liposomes as hydrophobic drugs. We aimed to investigate if the cholesterol content affects the tariquidar loading.

We designed two sets of experiments. In the first set, the DSTAP mole percent was kept constant at %15 and the total lipid content at 0.015 mmol while increasing the Cholesterol content in the formulation (formulations 3 to 6). In the other set, DSPC/DSTAP mole percents were kept constant at 55/15, and Cholesterol content was increased (formulations 1 to 3). In all formulations (Table 5), TRQ/Lipid molar ratio was constant at 0.012.

Table 5. Compositions of liposomes used for investigation of cholesterol effect on Tariquidar loading. Total lipid content (DSPC+DSTAP) was kept constant at 0.015 mmol lipid.

Mole %	**1**	**2**	**3**	**4**	**5**	**6**
DSPC	55	55	55	65	75	85
Cholesterol	42	35	30	20	10	0
DSTAP	15	15	15	15	15	15

Tariquidar was added to the lipid mixture as a solution dissolved in ACN. However, lipids are insoluble in ACN. Therefore, in the thin film preparation step, first, ACN was removed under a nitrogen stream, and then chloroform was added to the mixture. When chloroform was added to ACN, removal of the organic solvents' mixture took longer, and an even thin film could not have been obtained due to the insolubility of lipids in ACN. Liposomes were prepared as before and then dialyzed to remove the free Tariquidar. Tariquidar content was determined by UV-Vis spectrophotometry after centrifugation, as explained in Figure 23. Liposome films with 0% and 10% cholesterol were prepared; however, in the extrusion step for both formulations, the hydrated solution could not get passed through the polycarbonate membrane. In the liposomal solution with 20% Cholesterol content, the extrusion process required more force to push to solution through the membrane, and therefore only 0.8 ml of liposomal solution was obtained instead of 1 ml due to the leakage of solution during the extrusion.

There was no problem with the liposomes containing 30% and 35% cholesterol, producing 1 ml liposomal solution completely. However, liposomes with 35% cholesterol could not have been reproducibly obtained even though there was no problem with the thin film. Liposome preparation was unsuccessful when cholesterol content was increased to 42%. Interestingly, liposomes containing 30% cholesterol were reproducible, while others were not.

Both Cholesterol and Tariquidar load into the bilayer of liposomes. In the absence and lower cholesterol content (10%), Tariquidar could not have been loaded in the bilayer of liposomes. Indeed, it interfered with liposome formation due to its aggregation in the aqueous solution and clogging the pores of the polycarbonate membrane. When the Cholesterol content was increased to 20%, liposome production became possible, but

with some solution leakage (0.2 ml leakage) during the extrusion, perhaps again because of the Tariquidar aggregation and clogging of the pores of the polycarbonate membrane. Encapsulation and loading efficiencies increased when cholesterol was increased from 30 to 35% (Figure 39). Nevertheless, with the increase in cholesterol content (42%), liposome production was unsuccessful again, perhaps due to competition between cholesterol and Tariquidar migrating to the bilayer. There was visible aggregation in the solution during the extrusion, as seen in Figure 40.

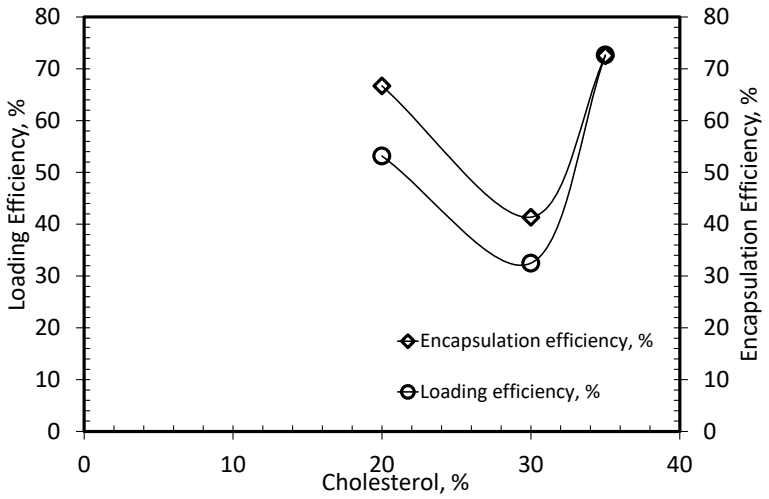

Figure 39. Effect of Cholesterol content on Tariquidar loading (TRQ/Lipid molar ratio =0.012)

Figure 40. Image of the liposomal solution with 42% cholesterol content during the extrusion process.

4.2.4 Release Studies Of Tariquidar At Elevated Temperature

The eventual goal of this study was to load both Tariquidar and Doxorubicin into the same liposomes. Therefore, Tariquidar containing liposomes was prepared in an Ammonium Sulfate buffer solution (250 mM, pH: 5.5) to be able to load Doxorubicin by pH gradient. Doxorubicin loading was performed by incubating the mixture of Doxorubicin solution (1 mg/ml) and Tariquidar-loaded liposomes at equal volumes at 65°C for 3 hours. Therefore, release studies were performed firstly performed at 65°C. This temperature is even higher than the phase transition temperature of the lipids. Above the phase transition temperature, lipid molecules become fluidity, causing the release of Tariquidar molecules from the bilayer. To assess the stability of encapsulated Tariquidar, Tariquidar loaded liposomes prepared as before (DSPC/Chol/DSTAP:55/30/15, Total lipid content: 0.015 mmol, TRQ/Lipid molar ratio: 0.012) and dialyzed before UV-Vis measurements. Tariquidar-loaded liposomal stock solution was aliquoted into glass vials (6 vials containing 145 µl of stock solution in each vial), and all vials were incubated in a water bath at 65°C.

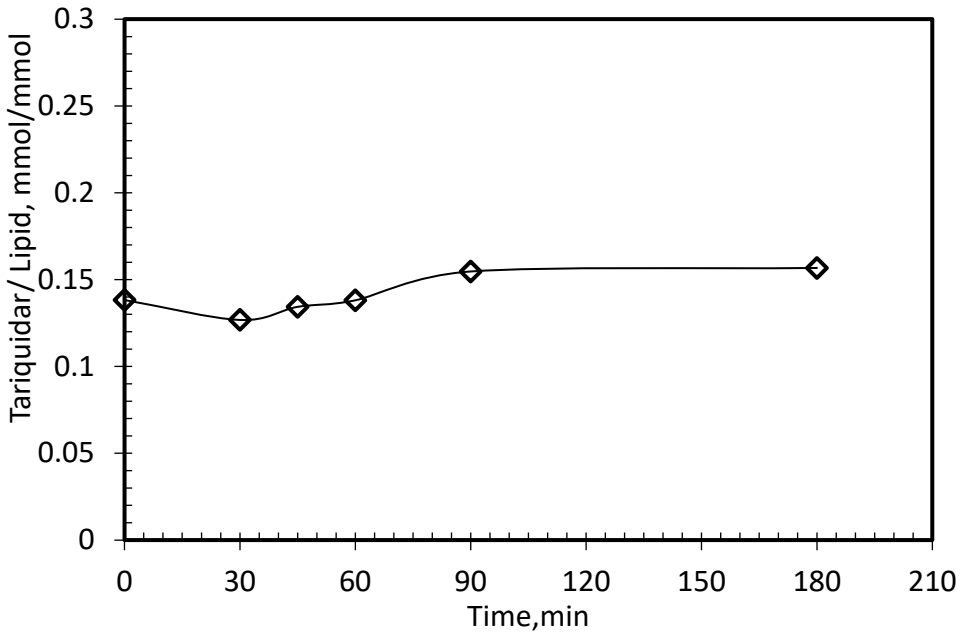

Figure 41. Change of Tariquidar in the liposomal solution after incubation at 65°C (measurements were performed by withdrawing 55 µl solution).

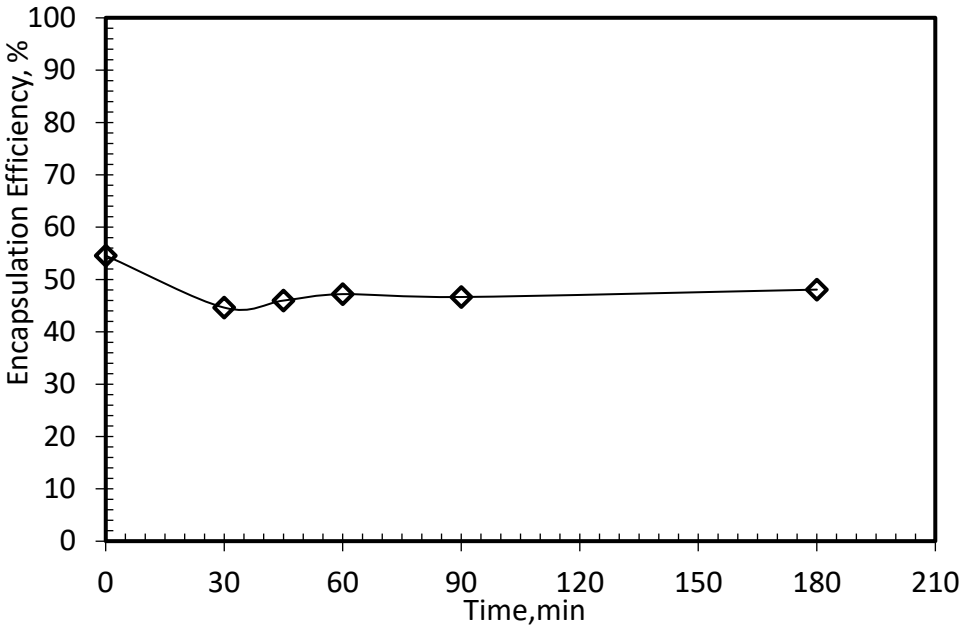

Figure 42. Encapsulation efficiencies of Tariquidar in the liposomal solution after incubation at 65°C (measurements were performed by applying the centrifugation method).

At indicated times, one of the vials was removed from the water bath and analyzed by UV-Vis spectrophotometry according to the procedure shown in Figure 23.

As seen in Figure 41, there was no change in the detected amount of Tariquidar, which shows the temperature stability of the Tariquidar at 65°C. This result shows that Tariquidar would not be affected by incubation during Doxorubicin loading. The tariquidar lipid ratio remained constant at around 0.13-0.15 molar ratio. There was a burst release of Tariquidar in the first 30 mins, and the encapsulation efficiencies decreased from 54% to 44% and remained almost the same in the rest of the experiment (Figure 42). Since the release is not very significant at this temperature, the study of release at body temperature was not needed to be performed.

4.2.5 Tariquidar Quantification After Doxorubicin Loading

Figure 43 shows the absorbance of the liposomes with different TRQ/Lipid molar ratios, and Figure 44 shows the absorbance of the same liposomes after DOX loading. Absorbances of the TRQ-loaded liposomes and TRQ-DOX-loaded liposomes were measured after the disruption of liposomes (55 µl) in 545 ul ACN.

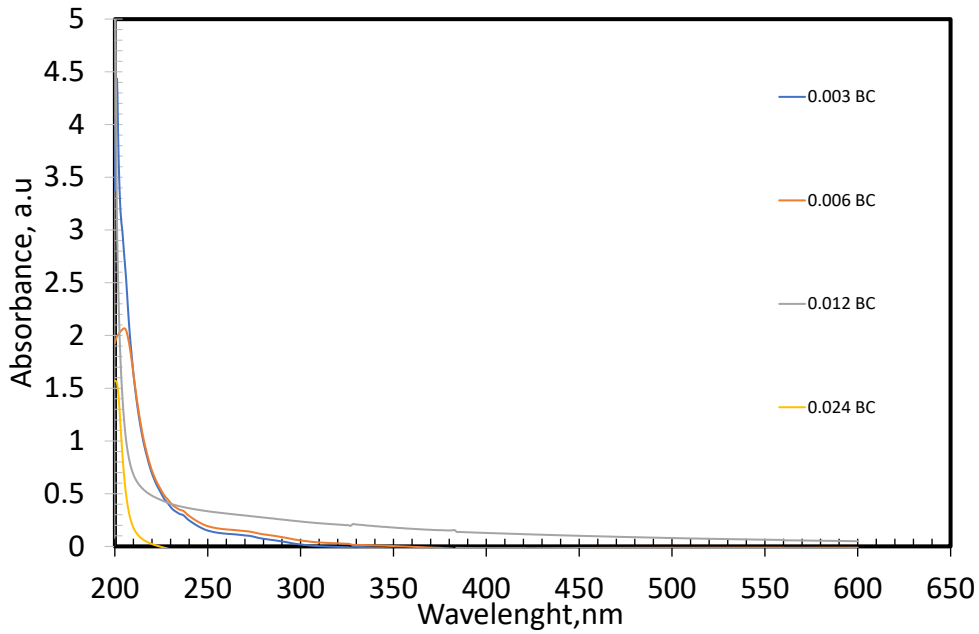

Figure 43. 0.003,0.006,0.012,0.024 TRQ/Lipid ratio liposomes UV absorbance spectrophotometry (BC: before centrifuge).

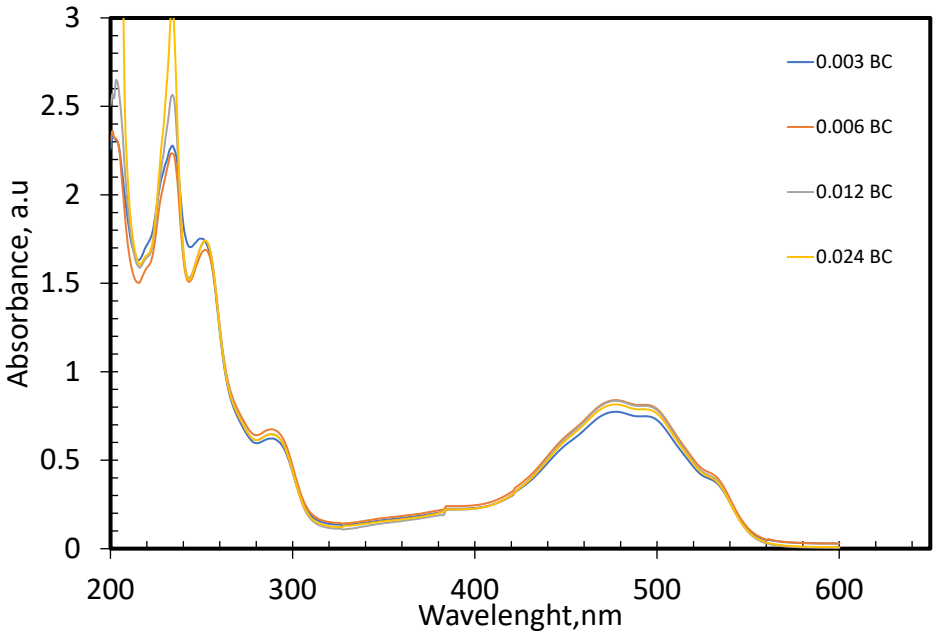

Figure 44. 0.003,0.006,0.012,0.024 TRQ/Lipid ratio doxorubicin-loaded liposomes UV absorbance spectrophotometry (BC: before centrifuge).

From the comparison of both figures, it can be seen that TRQ-DOX-loaded liposomes had much higher absorbance values compared to TRQ-loaded liposomes. These results suggest that doxorubicin interfered with the absorbance of TRQ at 240 nm, making impossible TRQ measurement after the doxorubicin loading.

4.3 Doxorubicin Loading And Characterization

The Fluorescence spectrophotometry and HPLC method were used in the literature to quantify Doxorubicin in the liposomes. In this study, both methods were used for quantification purposes. A calibration curve for Fluorescence measurements (BioTek, Synergy HTX Multi-Mode Reader) was obtained by 80% serial dilution of 0.2 mg/ml Doxorubicin solution in Ultra Pure Water (UPW) (Figure 45).

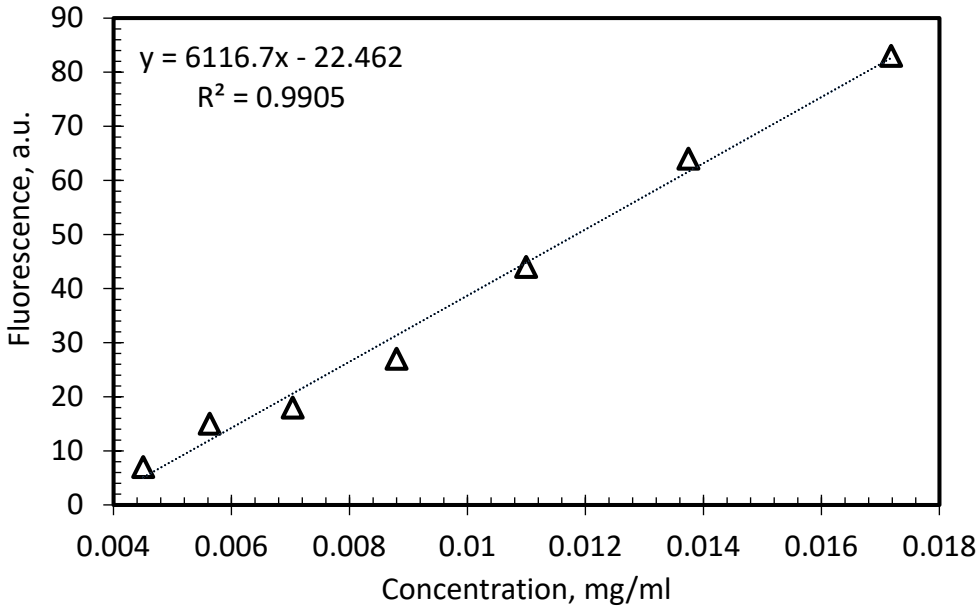

Figure 45. Calibration curve in Fluorescence Spectrophotometer.

To understand if there is an effect of DSTAP on DOX loading, plain liposomes with different DSTAP percent were prepared. 500 µl of liposomal solution and 500 µl of 1 mg/ml doxorubicin solution were incubated for 3 hours at 65°C in a hot water bath at 150 rpm. After incubation, liposomal doxorubicin (Lipo-Dox) fluorescence was determined before and after dialysis. For before dialysis, 290 µl of UPW and 10 µl of Lipo-Dox were added to the well, and the mixture was diluted 1:1 (v/v) 5 times. Fluorescence reading of the wells was done at excitation/emission: 480/590 nm. For disruption of liposomes, 10 µl of Triton-X (10%) was added to each well, and the fluorescence values of the solutions were read again.

After the Lipo-Dox solution (around 2 ml) was dialyzed against 2 L %0.9 NaCl solution overnight. Fluorescent reading was done, as explained above. Encapsulation efficiency was determined from the ratio of concentrations measured after dialysis to before dialysis according to Equation 4. Loading efficiencies were calculated from the ratio of concentrations measured after dialysis to the initial amount (0.5 mg/ml) added to incubation.

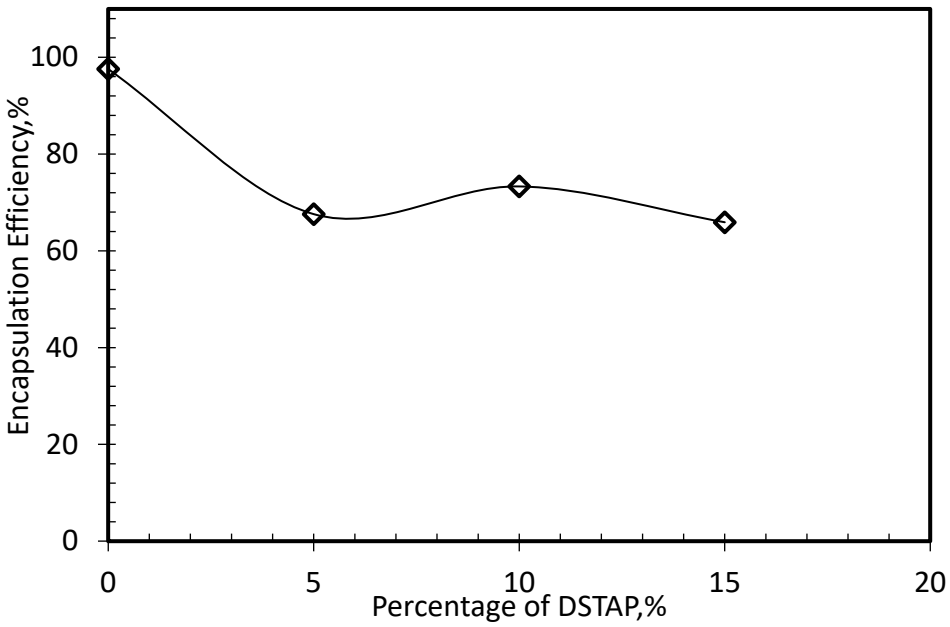

Figure 46. Encapsulation efficiency vs. Percentage of DSTAP.

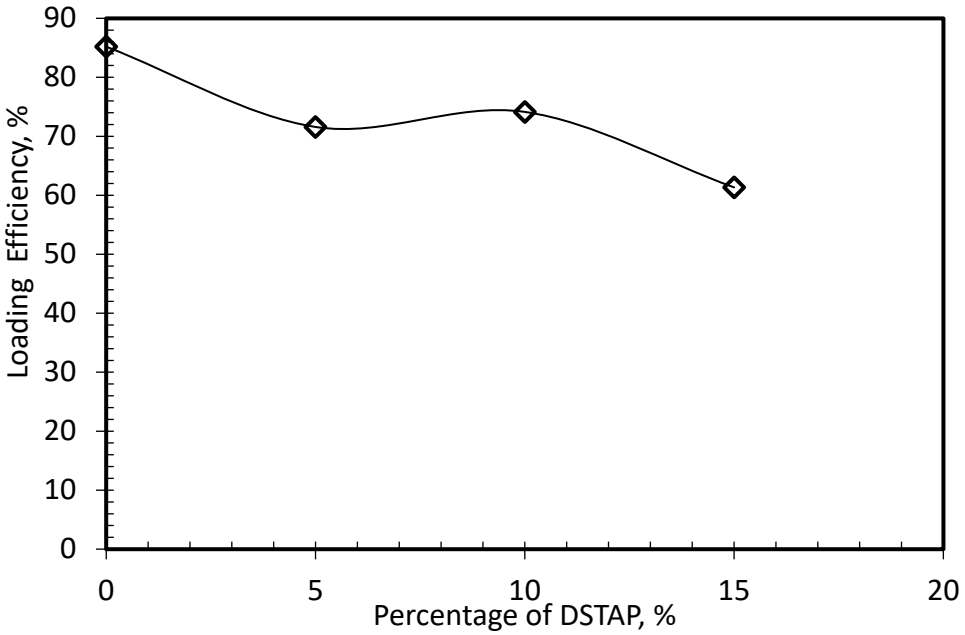

Figure 47. Loading efficiency vs. Percentage of DSTAP.

Figure 46 and Figure 47 show that both loading and encapsulation efficiencies were highest in the absence of DSTAP. Encapsulation efficiency decreases from 99% to

around 70%; loading efficiency decreases from 85% to 70% with the addition of DSTAP. Further, increased DSTAP content in the liposome did not cause a significant change in encapsulation and loading efficiencies.

Because of its hydrophobic nature, TRQ must be loaded into liposomes by passive loading. However, Doxorubicin is loaded into the core of liposomes by pH gradient by active mode. To investigate if the presence of TRQ in the bilayer affects the encapsulation of doxorubicin, %15 DSTAP liposomes which contain varying amounts of tariquidar (0.003,0.006,0.012,0.024 TRQ/ lipid ratio) were prepared and mixed with the doxorubicin at 1 mg/ml at equal volumes. Fluorescence readings of DOX were done, as explained above.

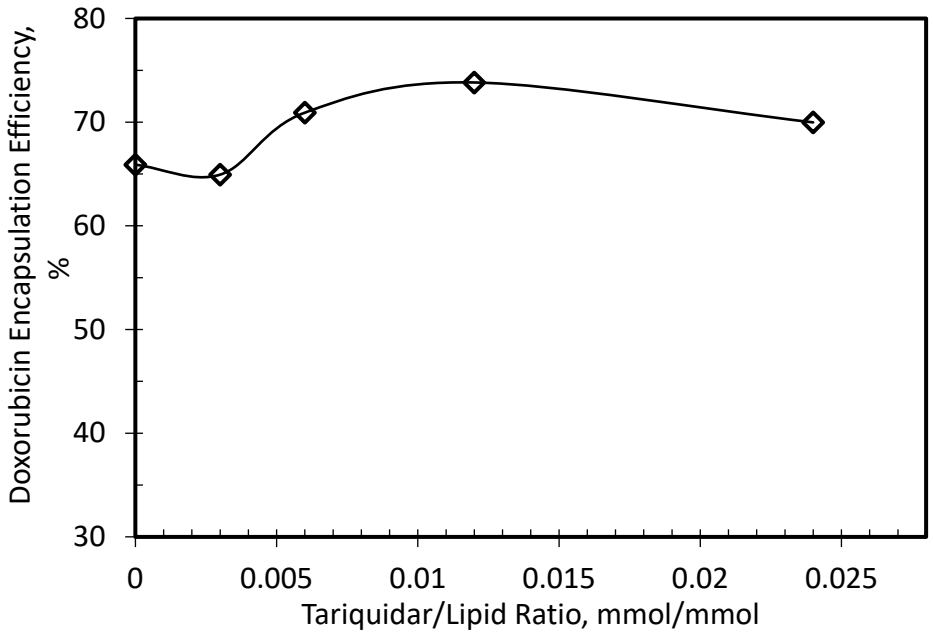

Figure 48. Doxorubicin encapsulation efficiency at various Tariquidar/lipid ratios.

Interestingly, the presence of TRQ in the bilayer enhanced the DOX loading, causing encapsulation efficiency to increase from 65% to around 70% when TRQ/lipid molar ratio was increased from 0 to 0.006. This may mean that TRQ created interstitial pores in the bilayer, allowing DOX to pass through. Further, an increase in the TRQ/Lipid molar ratio did not significantly affect encapsulation efficiency.

DOX quantification was also done by the HPLC method. HPLC's calibration curve (Figure 49) was made by serial dilution (70%) of 1 mg/ml Doxorubicin in Methanol (solvent: MeOH).

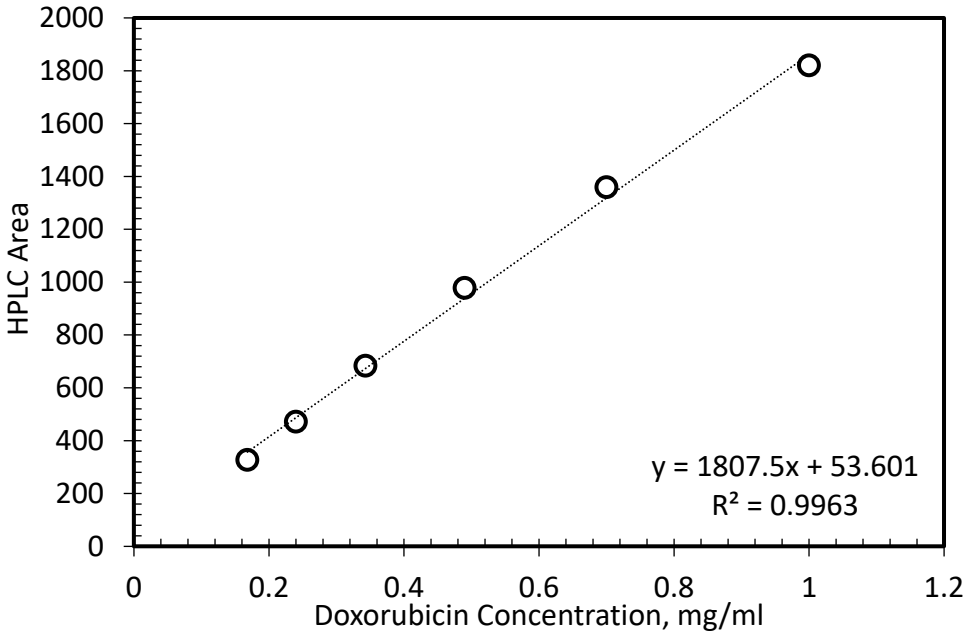

Figure 49. Calibration curve of DOX in Methanol in HPLC.

To determine if there is an interaction between DOX with liposome components (DSPC, Cholesterol, and DSTAP), calibration curves of the liposome components were also generated. Each component (3 mg) was added to the same vial, and the mixture was dissolved in 3 ml Methanol, resulting in a 3 mg/ml solution at a molar ratio of DSPC/cholesterol/DSTAP: 24/49/27. As seen in Figure 50, elution times of DSPC, Cholesterol, and DSTAP were 15 mins,13 mins, and 8 mins, respectively. The final solution was diluted serially by 70% (v/v). As seen, the Elution times of components did not change with concentration. Calibration curves for each component were generated from a reading of the areas in Figure 52. Figure 52 and Figure 52 indicates that each component shows linear behavior in the concentration range studied.

-

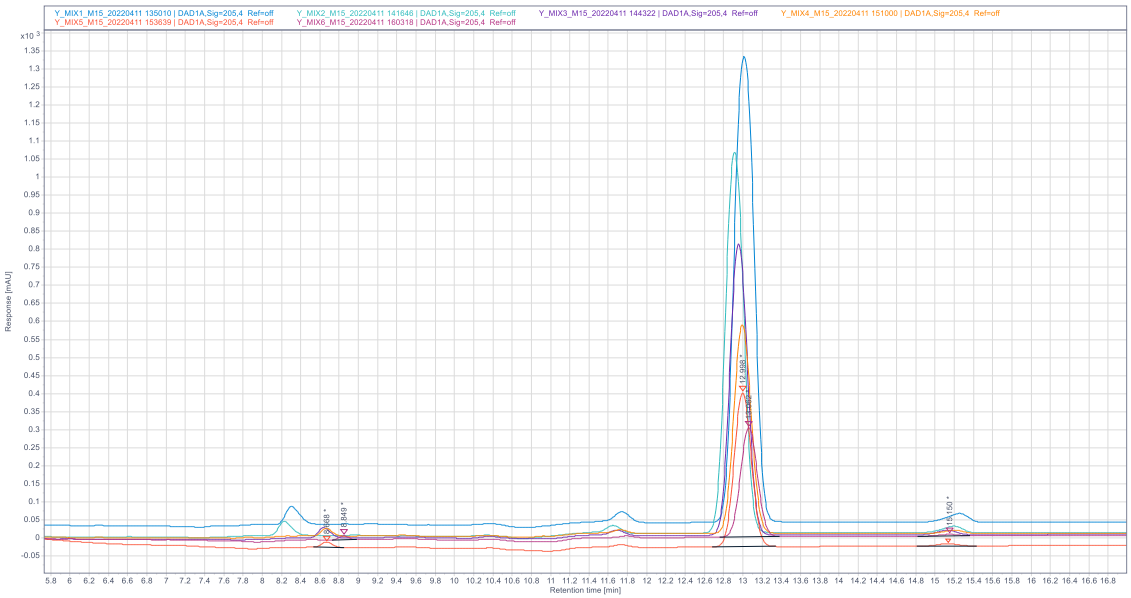

Figure 50. HPLC chromatogram of lipid mixture at different concentrations.

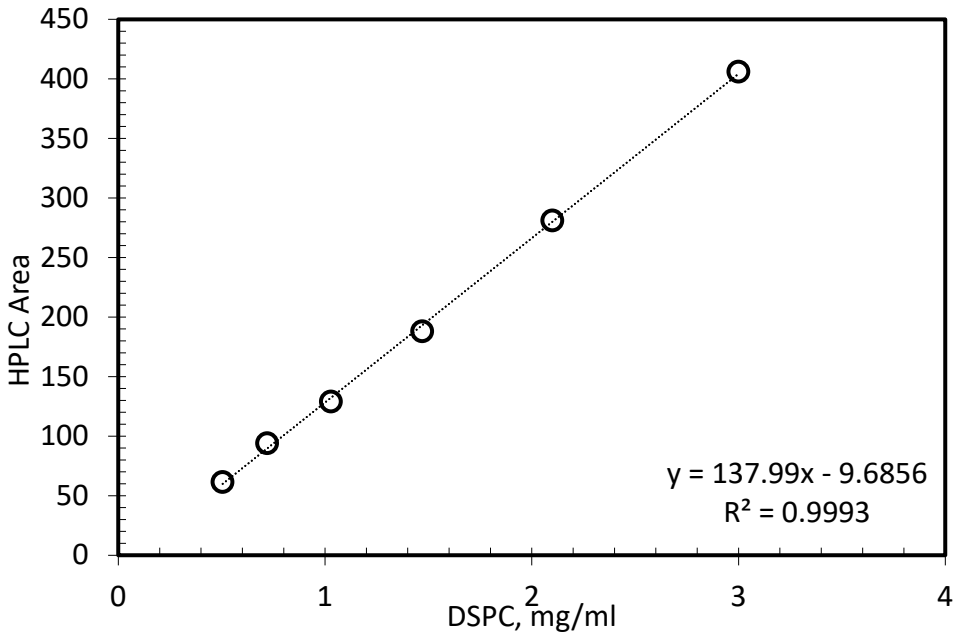

Figure 51. DSTAP calibration curves in MeOH for HPLC analysis.

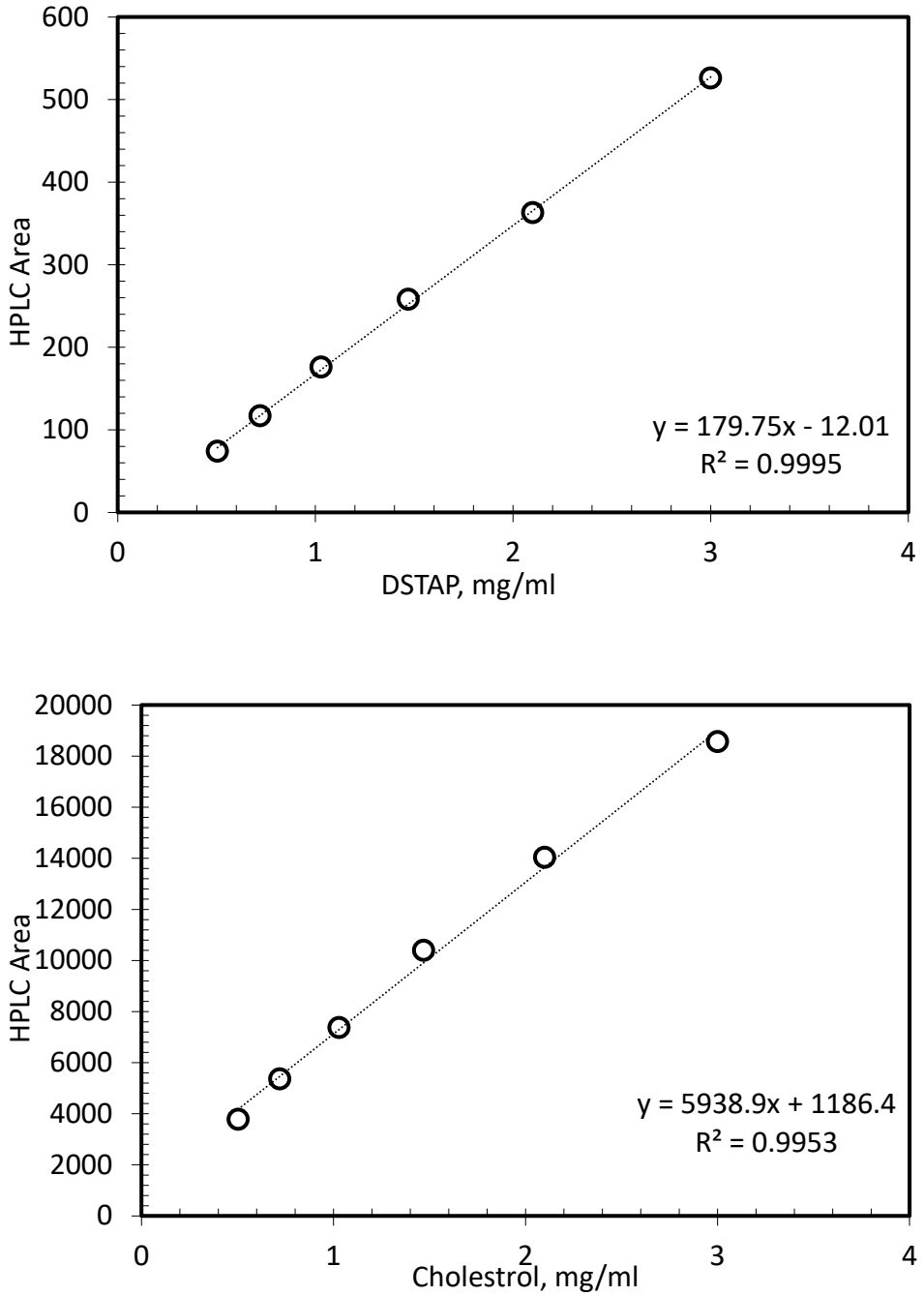

Figure 52. DSPC, and Cholesterol calibration curves in MeOH for HPLC analysis.

Using these calibration curves, we attempted to analyze the composition of plain liposomes; however, when standard 100 µl of liposomal solution was employed, the peak of DSTAP was very small, causing our efforts to determine the liposome composition to fail.

4.3.1 Lipid- Doxorubicin interaction

Two separate studies were conducted to understand whether any interaction between DOX and liposome components interferes with the measurements. In the first study, lipid composition was kept the same, and the DOX amount was varied. In other words, varying DOX amounts were added to the lipid mixture at constant composition. For this purpose, DSPC/Chol/DSTAP was mixed at a molar ratio of 56/28/15 at a total concentration of 13.89 mg/ml in methanol. A varying amount of DOX solution (at 1.11 mg/ml in methanol) was added to the 100 µl of this mixture (

Doxorubicin (µL)	Lipid mix (µL)	Added MeOH (µL)	Total Volume (µL)
50	100	100	250
100	100	50	250
150	100	0	250
200	100	0	300

). Indicated amounts of methanol in Table 6 were added to the solution to prepare a solution at a total volume of 250 µl. HPLC results of the mixtures are summarized in Table 7.

Table 6. The volumes used to prepare samples are in Figure 55 (a).

Doxorubicin (µL)	Lipid mix (µL)	Added MeOH (µL)	Total Volume (µL)
50	100	100	250
100	100	50	250
150	100	0	250
200	100	0	300

Table 7. HPLC results of the samples are prepared in Table 6.

		HPLC Area				
DOX/Lipid (µL/µL)	**DOX (mg/ml)**	**DOX**	**DSTAP**	**Cholesterol**	**DSPC**	**Unkown peak**
50/100	0.22	4007	119	5584	412	1322
100/100	0.44	6557	128	5415	400	1955
150/100	0.66	7725	132	5454	395	2666
200/100	0.74	8075	93	4440	325	2776

As seen in Figure 55 (a), lipid molar ratios were not significantly different from primary liposomal lipid molar ratios. Small differences are thought to be due to the very small HPLC area of the DSTAP peak. However, Figure 55 (b) shows that the Doxorubicin HPLC concentration was higher than the theoretical concentration. As seen from Table 7, although DOX amounts used in this study are within the DOX calibration curve (Figure 49), HPLC areas obtained are outside the range of the calibration curve. In the chromatogram, DSPC was observed at 15 min, Cholesterol at 13 min, DSTAP at 8 min, DOX at 1.30 min, and an unidentified peak at 2.92 minutes. (Figure 53). It was thought that the interaction of DOX and lipids caused the unidentified peak that appeared in the HPLC and thus affected the DOX HPLC areas (Mady et al., 2012). To identify this peak, a second study was planned. This time, the same amount of DOX was mixed with varying amounts of the lipid mixture. Table 8 shows the volumes of the DOX, lipid mixture, and Methanol volumes used in sample preparation. HPLC results of the mixtures are summarized in Table 9. Although the DOX concentration was 0.222 mg/ml in all mixtures, the concentrations obtained from HPLC results were much higher than the one had to be (Figure 56(b)). Therefore, in this study, DOX was preferred to be quantified using Fluorescence Spectrophotometry.

Table 8. The volumes used to prepare samples are in Figure 56 (a).

Doxorubicin (µL)	Lipid mix (µL)	Added MeOH (µL)	Total volume (µL)
50	50	150	250
50	100	100	250
50	200	0	250

Table 9. HPLC results of the samples are in Table 8.

		HPLC Area			
DOX/Lipid (µL/µL)	DOX (mg/ml)	DOX (µL)	DSTAP (µL)	Choleterol (µL)	DSPC (µL)
50/50	0.22	1154	64	2363	173
50/100	0.22	985	141	4543	346
50/200	0.22	1092	233	10188	773

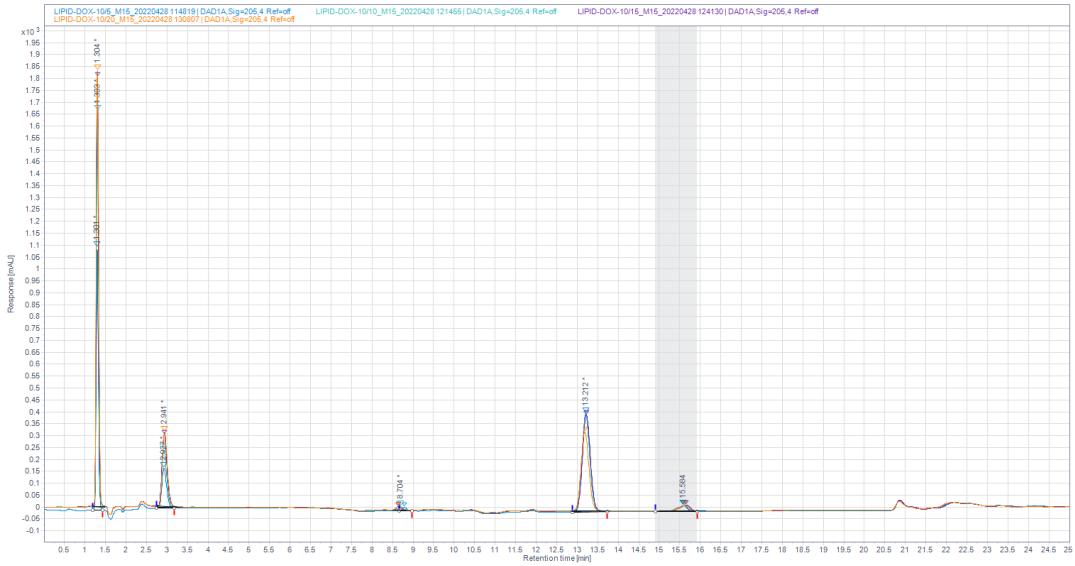

Figure 53. HPLC chromatogram of lipids and Doxorubicin.

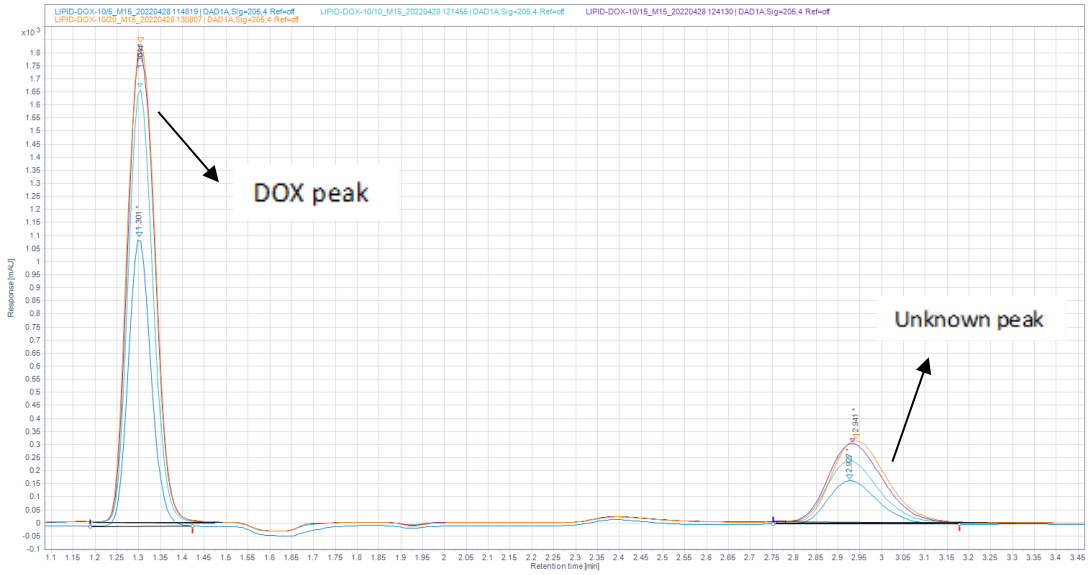

Figure 54. HPLC chromatogram of UNnkown peak and Doxorubicin.

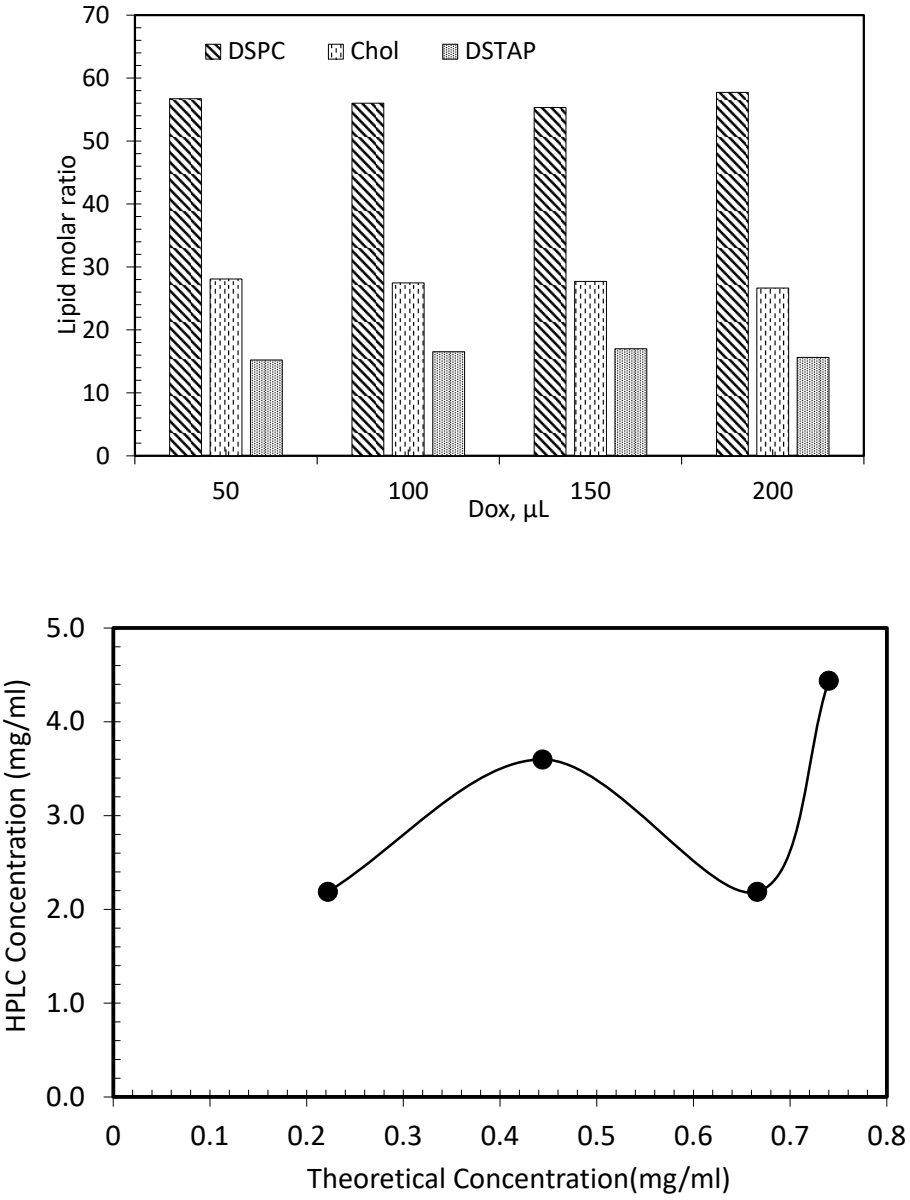

Figure 55. a) Effect of Doxorubicin concentration on the composition of liposomes, b) Doxorubicin HPLC concentration versus Theoretical Concentration.

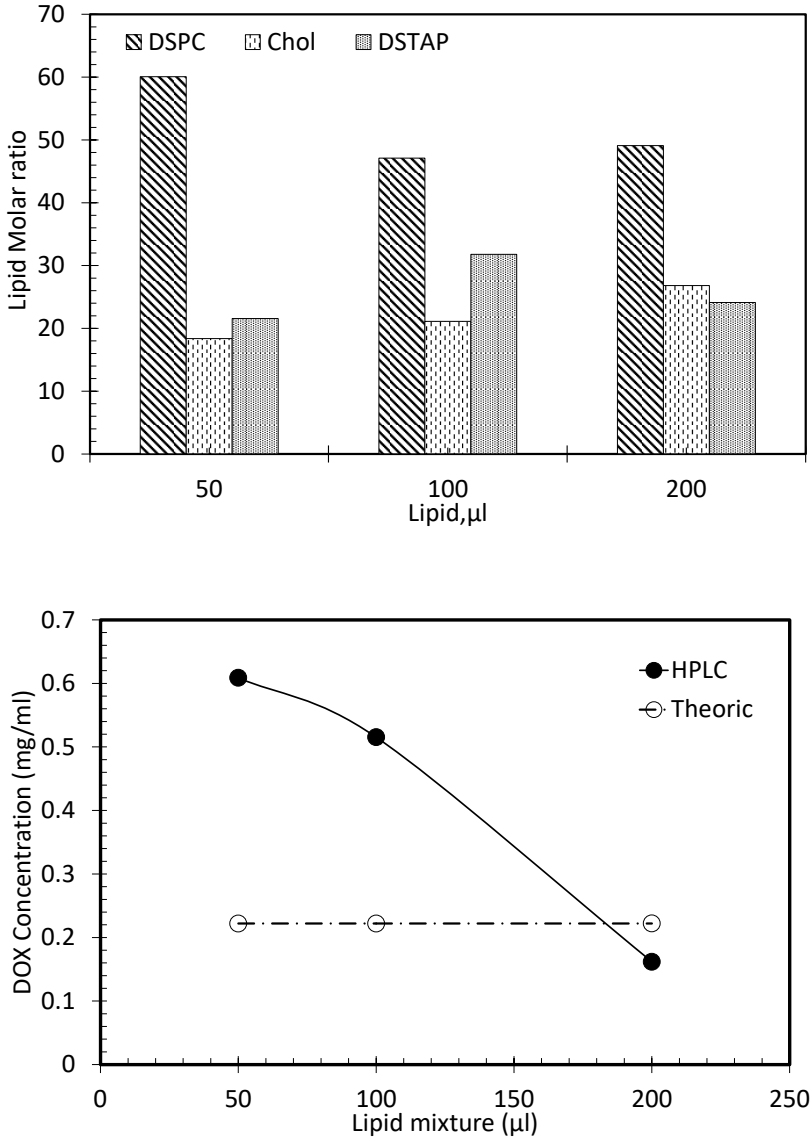

Figure 56. a) Effect of constant DOX amount on lipid composition at varying volumes but at the same composition. b) Doxorubicin HPLC concentration vs. Theoretical Concentration (----: Doxorubicin theoretical concentration)

4.4 Fucoidan Coating Studies

Decoration of Liposomes polysaccharides is a widely used method for active targeting. Chitosan, Alginate, Hyaluronic acid and Xantham Gum are examples of those polysaccharides. Coating of liposomes is still not a well-studied topic. It contains several key features such as adding method (at one time or dropwise), chain conformation, medium, and polysaccharide concentration effect on liposome size and zeta potential. Mady & Darwish coated DPPC liposomes with 0.5% (w/v) Chitosan (Mw: 15kDa) ratio added by the drop-wise method under magnetic stirring at room temperature, and the mixture was kept under stirring for 1 hour. On the other hand, Manca et al. slowly added Chitosan dispersion and then the Xantham Gum solution under magnetic stirring. Fucoidan coating onto liposomes is a new study, and few studies are available in the literature. A similar study was done by Li et al., who coated pH-sensitive liposomes with fucoidan. However, their paper did not report the details of the coating procedure and concentration of Fucoidan. Therefore, In our study, we attempted to understand the conformation of fucoidan in different mediums.

4.4.1 Conformation of Fucoidan in Different Solutions

Fucoidan is a long polymer chain that can acquire different conformations in different solutions. To identify this, Fucoidan stock solutions were prepared in ultrapure water and 10 mM NaCl solutions at a concentration of 3.4 mg/ml and diluted by 80% (v/v) for the first five dilutions. After that, other dilutions were made by 50% (v/v). Size and Zeta Potential measurements of the solutions were done by Malvern ZetaSizer. 980 µl of 10 mM NaCl solution was put into Size Cuvette, and 20 µl of stock solution was added. For zeta potential measurements, the same solution was transferred to the zeta cell (Figure 57, Figure 58)

When the results in ultrapure water are examined (Figure 57), fucoidan exhibited a size of 800 nm-1200 nm. The Zeta potential of the solution showed a decrease in negativity with increasing concentration of fucoidan in the ultrapure water. Negative zeta

potential results from the sulfate groups (OSO_3^-) in the fucoidan chain. However, when fucoidan was dissolved in 10 mM NaCl, smaller sizes of the fucoidan chain were detected (around 500 nm – 800 nm). Zeta potential values also exhibited a decrease in NaCl solution (Figure 58). The reduction in size and zeta potential can be related to the screening of the negative charges by the sodium ions, which results in more compact fucoidan chains.

4.4.2 Coating Liposomes with Fucoidan Dilutions

To coat liposomes with fucoidan, the liposomal solution containing %15 DSTAP was diluted in half with ultrapure water, yielding a 7.5 uM lipid solution). Fucoidan solution prepared at 3.4 mg/ml in ultrapure water was also diluted serially. 200 µl of the liposomal solution was added to these diluted fucoidan solutions dropwise. The resulting 220 ul fucoidan-liposome solution was shaken at 170 rpm for 10 minutes. Each combination's zeta potential and size were determined by combining 20 µl of fucoidan-liposome solution with 980 µl 10 mM NaCl solution. As seen in Figure 59, the size of the liposomes increased first with increasing concentration of fucoidan and decreased with further increasing concentration. The zeta potential of the liposomes declined and became more negative values as the Fucoidan/Lipid molar ratio increased, suggesting that the liposomes were coated with fucoidan chains. The liposomes ' size changes dramatically when the Fucoidan/Lipid molar ratio is low. This can be attributed to bridging flocculation. Larger sizes at higher Fucoidan/Lipid molar ratios can be attributed to depletion flocculation of the liposomes. It is important to note that each sampling of the fucoidan-coated liposomal solution produced varied findings, showing that the coating is not homogeneous.

4.4.3 Dilution of Fucoidan Solutions and its Effect on Liposome Sizes

We attempted to carry out the coating technique at varied volumes to see if the final fucoidan-liposome solution volume influences the flocculation of the liposomes. Fucoidan solutions were further diluted with ultrapure water for this purpose. Fucoidan dilutions were made by adding an additional 30 µl, 80 µl, and 180 µl of ultrapure water to 20 µl of fucoidan solutions already prepared by serial dilution of stock solution. 200 µl of the liposomal solution was added dropwise to these diluted fucoidan solutions that had already been diluted in half and then agitated for 10 minutes at 170 rpm. As explained above, size and Zeta potential measurements were performed (20 µl of fucoidan-liposome solutions and 980 µl 10 mM NaCl solutions).

In general, there was a decrease in the size of the coated liposomes, confirming our hypothesis. We believe that the odds of flocculation is lower at diluted volumes. According to the size results, the amount of fucoidan per lipid amount should be more than a certain threshold to avoid bridging flocculation. Different samples of fucoidan-coated liposomes from the same vial yielded a variety of results, indicating that the solution was not homogeneous. As seen in SEM images in Figure 61, the solution may potentially include large clusters. The Zeta potential of the coated liposomes, in general, decreased by an increase in the fucoidan/lipid molar ratio. The change in zeta potential from positive to negative and the continual reduction in zeta potential demonstrates that the liposomes were coated with fucoidan.

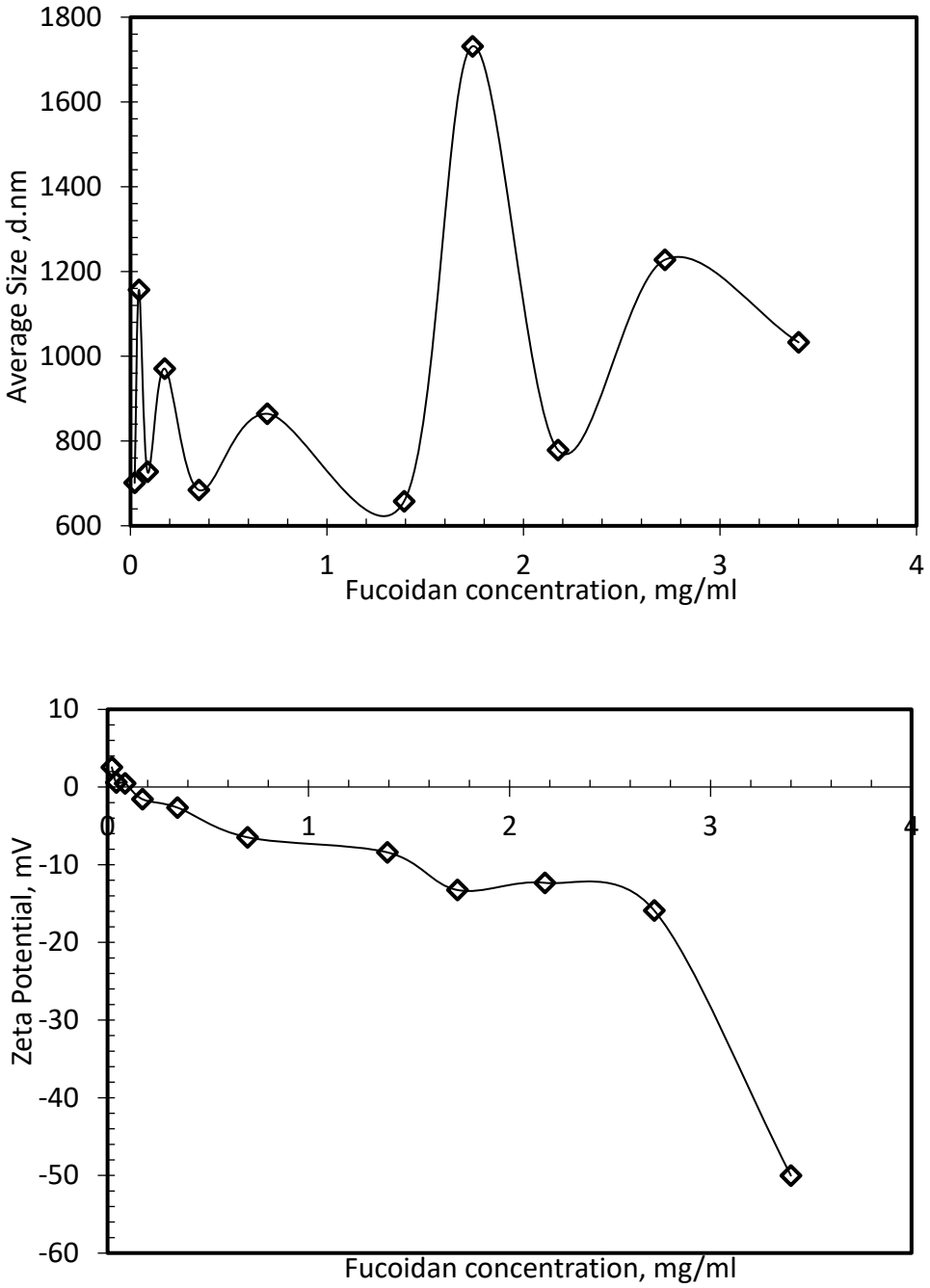

Figure 57. Size and zeta potential measurement of Fucoidan solutions at different concentrations in ultrapure water.

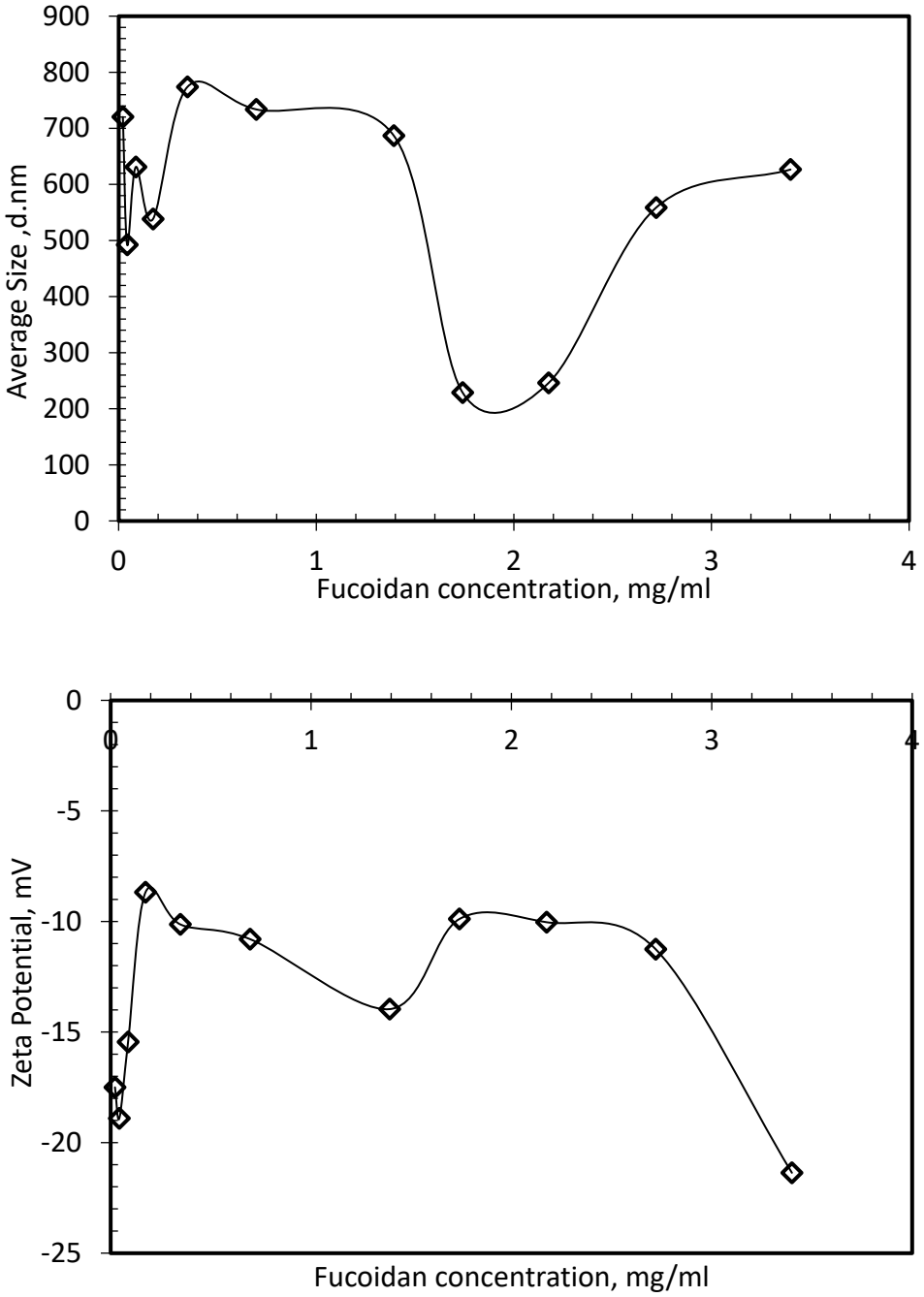

Figure 58. Size and zeta potential measurement of Fucoidan solutions at different concentrations in 10 mM NaCl.

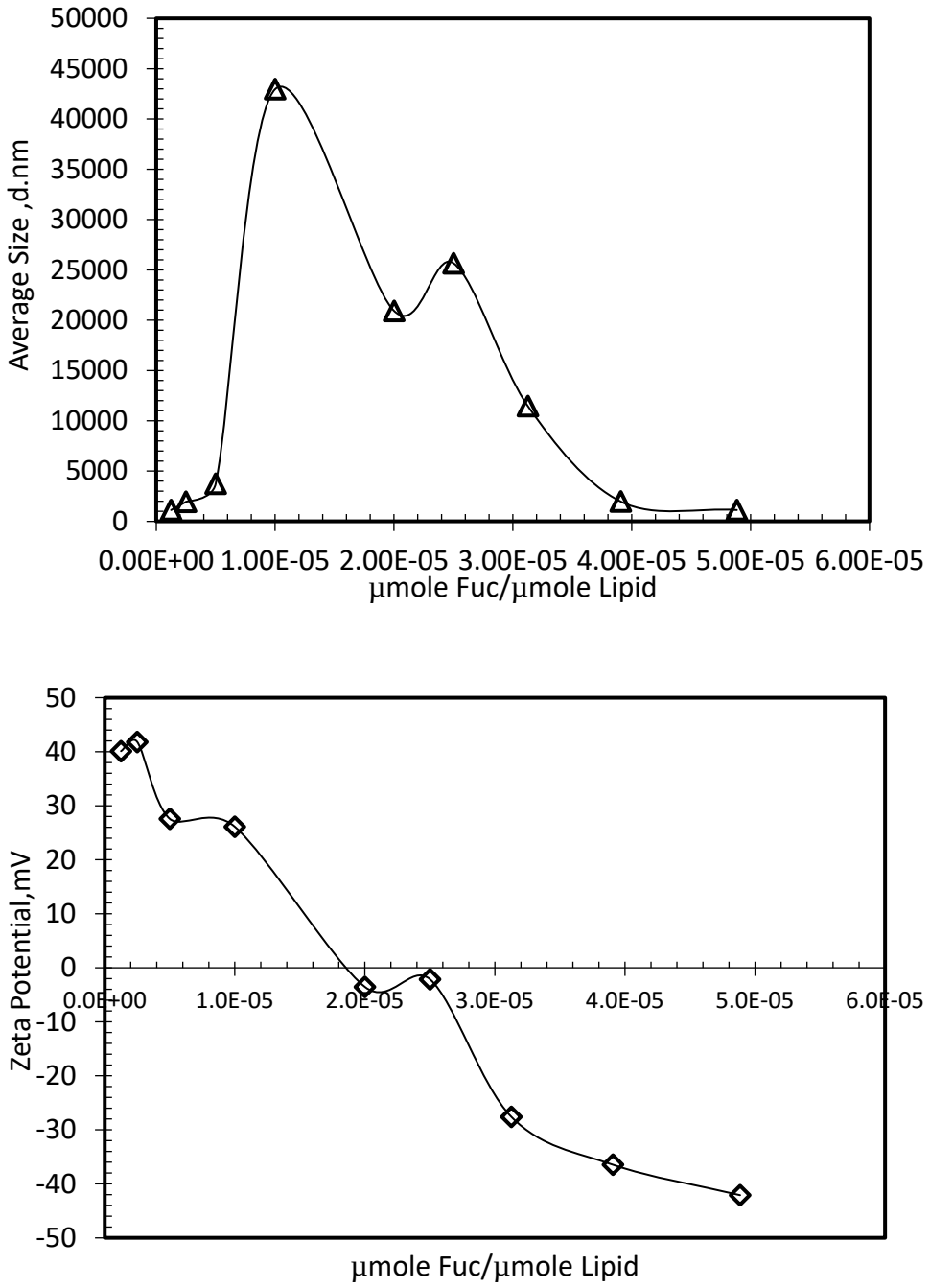

Figure 59. Size and Zeta Potential measurements of 200 µl %15 DSTAP liposomes (7.5 µM) coated with 20 µl of fucoidan solution at different concentrations

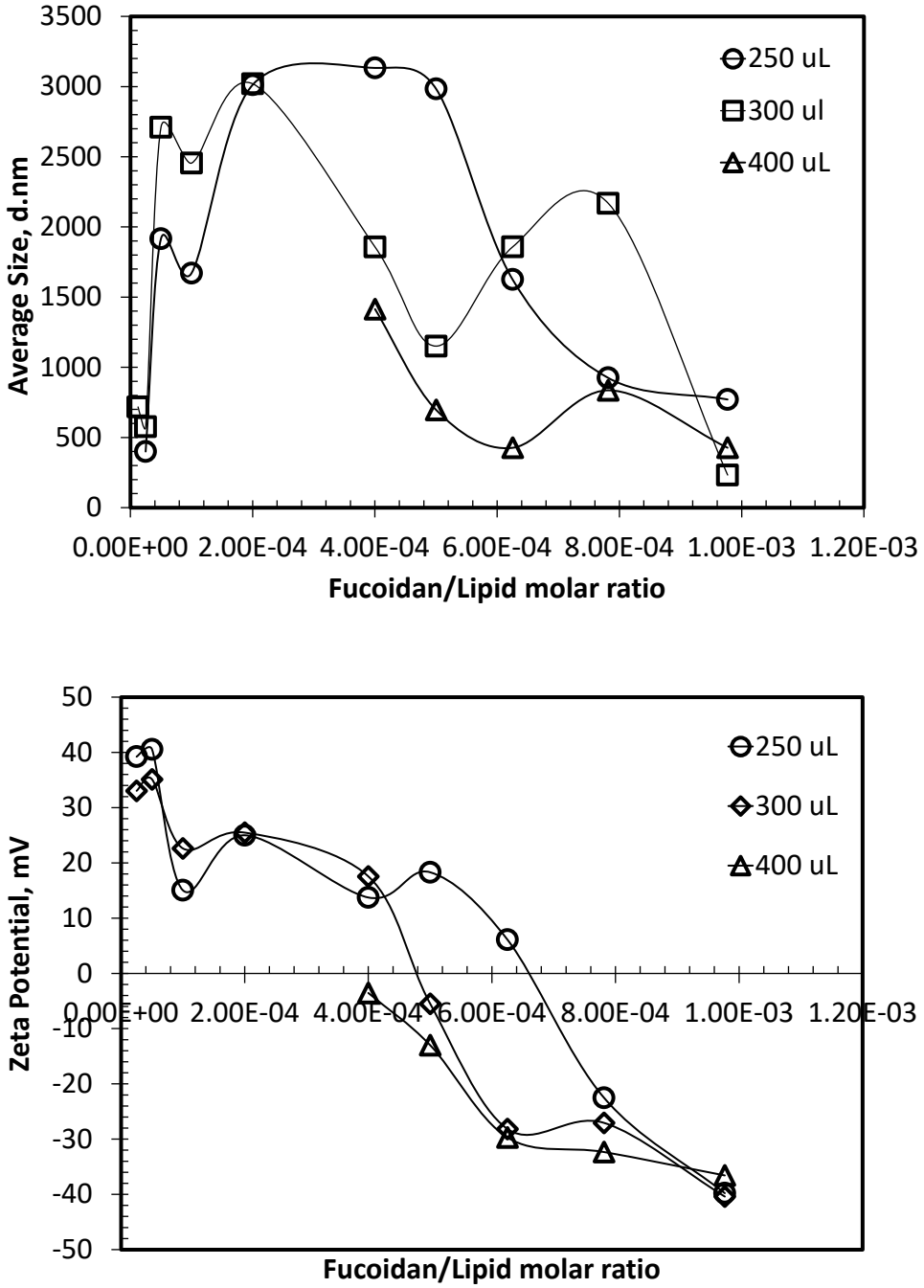

Figure 60. Total volume effect on size and zeta potential of liposomes coated with fucoidan diluted to different volumes. (220 µl volume data was not shown because of high size of liposomes).

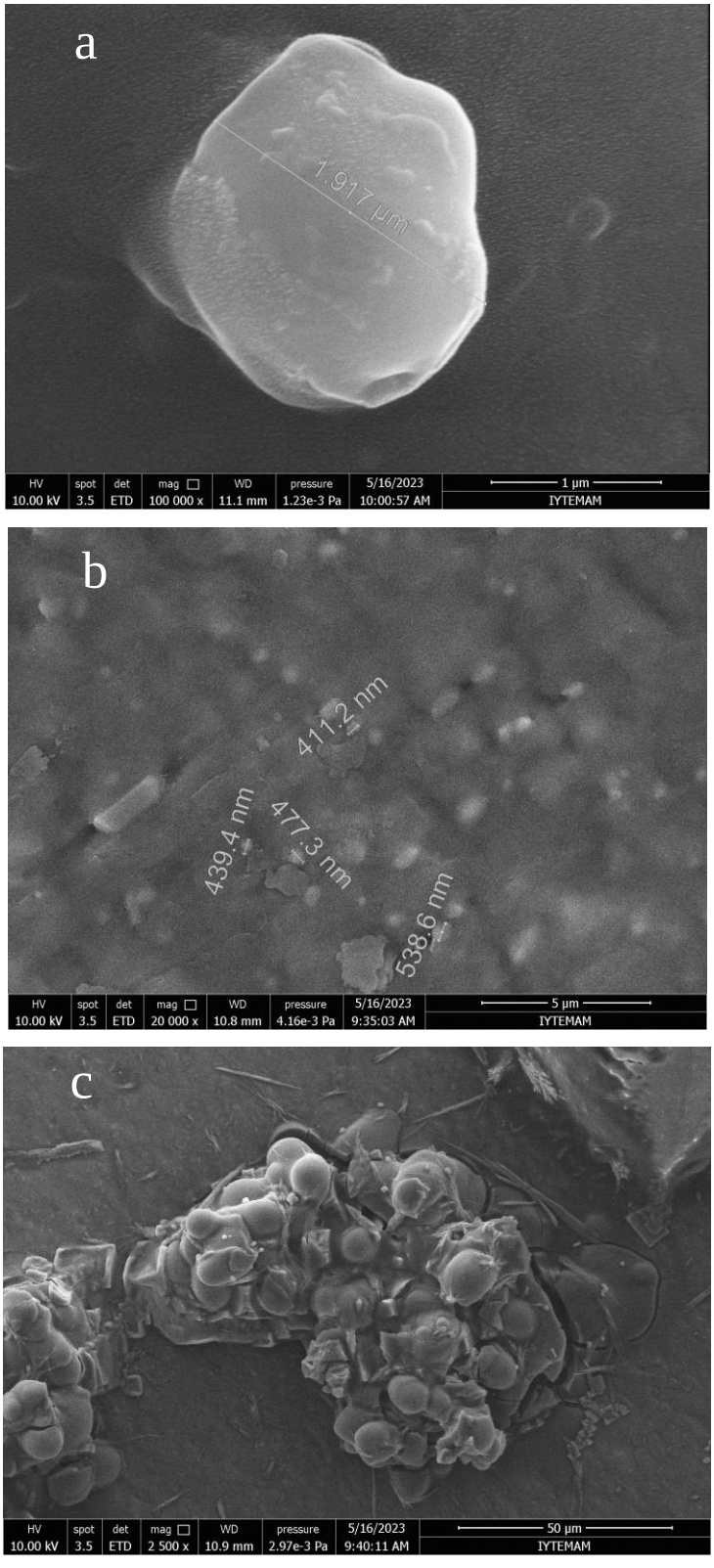

Figure 61. SEM Analysis pictures of 20 µl fucoidan solution diluted with 80 µl solution and coated onto 200 µl Liposomal solution (Picture (a), partially covered liposome with higher size scale, (b) liposome with much smaller sizes', (c) agglomerated liposomes).

4.5 In-Vitro Studies

In-vitro studies were carried out using MDA-MB-231 cells. Cytotoxicity of the free form of Fucoidan was studied for 24-, 48- and 72 hours in 96 well plates (Figure 62). As seen in Figure 63, cell viability decreased with increasing Fucoidan concentration.

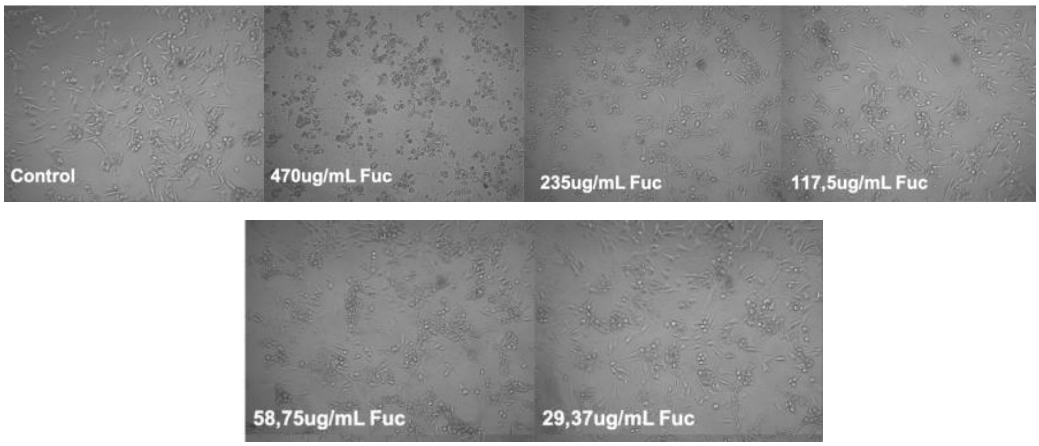

Figure 62. Microscopic images of MDA-MB-231 cells after treatment with free Fucoidan at various concentrations.

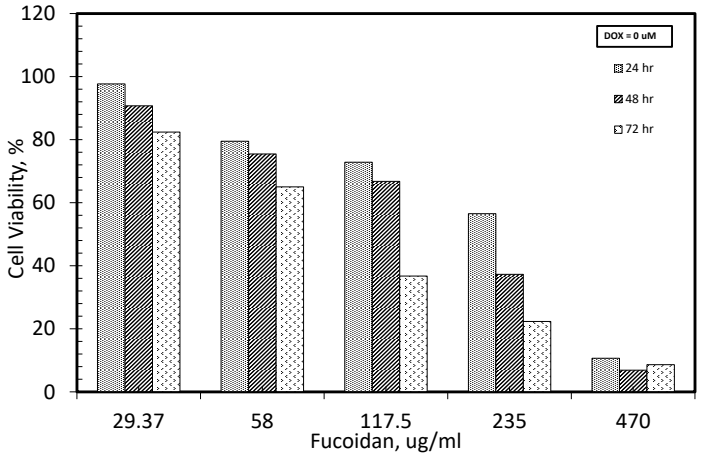

Figure 63.MTT results of the free form of Fucoidan.

Doxorubicin, being an anti-cancer agent, also affects cell viability (Figure 64). As seen from the MTT results, DOX did not affect the cell viability up to 1 µM at low concentrations. But at 10 µM, in 24 h and 48 h, around 40% cell viability was observed. Cell viability increased to about 70% in 72h, suggesting that DOX acts as nutrition for the cells at longer incubations. With the further increase in DOX concentration, cell viability decreased in 24 hours but remained almost unchanged in 48 and 72 hours.

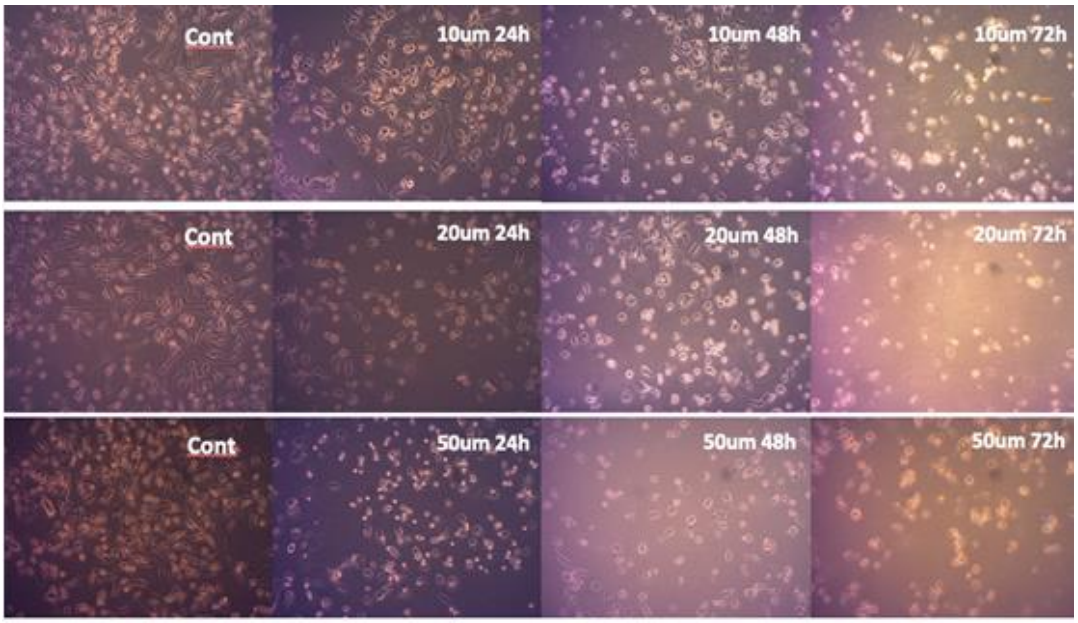

Figure 64. Microscope images of MDA-MB 231 cells treated with 10 µM, 20 µM, and 50 µM DOX at 24h, 48h, and 72h (hour).

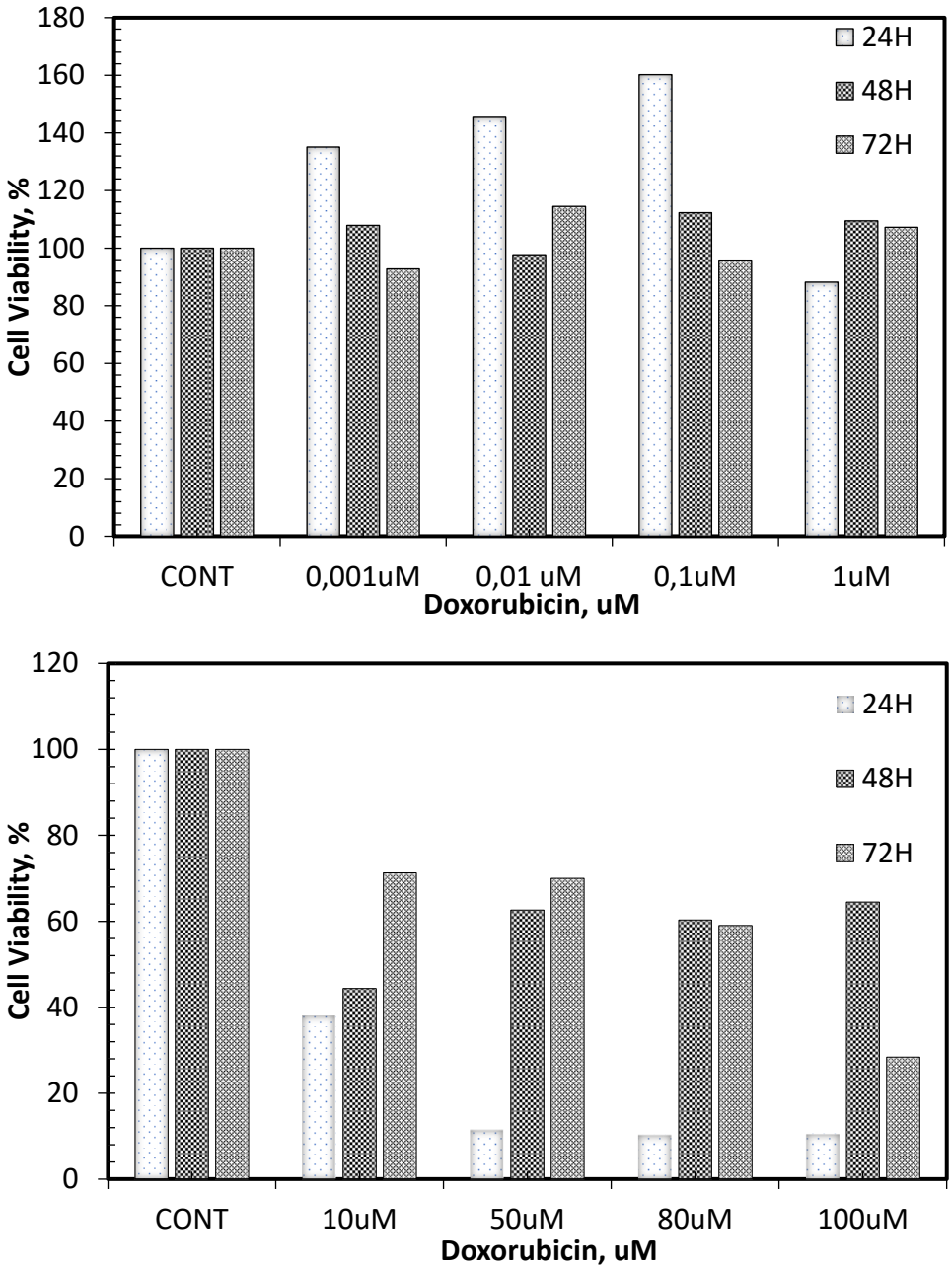

Figure 65. MTT results of the free form of Doxorubicin.

Tariquidar as a p-glycoprotein inhibitor was also tested on the cell viability of MDA-MB-231 cells. As seen in Figure 66 and Figure 67, free Traquidar does not have a detrimental effect on cell viability, in agreement with Xia et al. study (Xia et al. 2018). Indeed, there was a dose-dependent increase in cell viability with the administration of Tariquidar, especially in the first 24 hours.

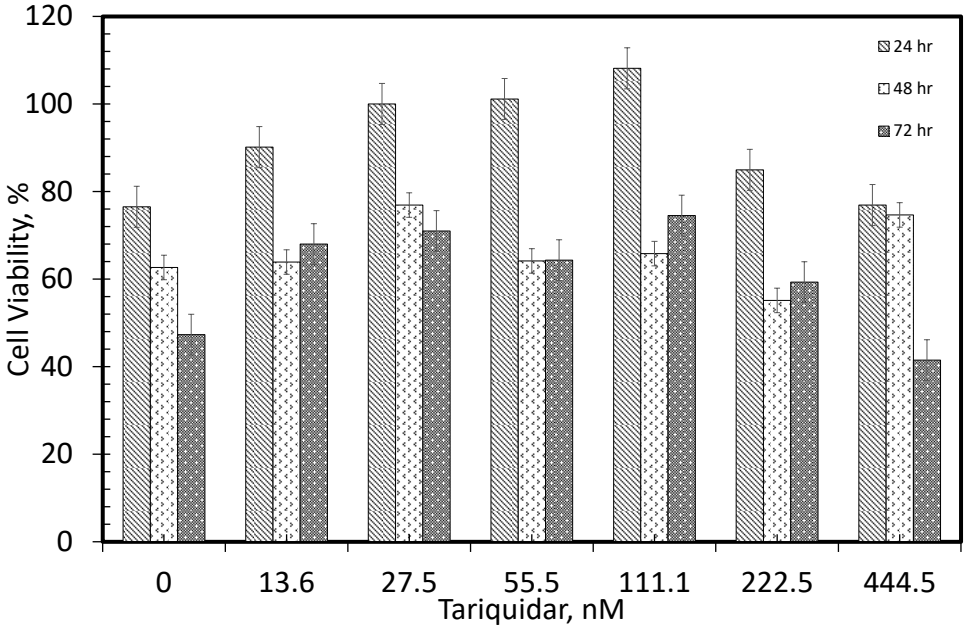

Figure 66. MTT results of the free form of Tariquidar.

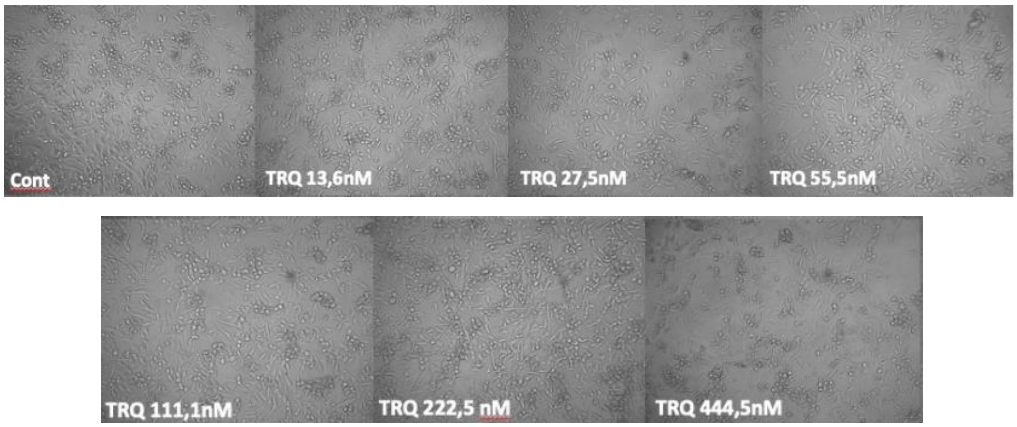

Figure 67. Cell viability of MDA-MB 231 cells treated with tariquidar (444.5 nM, 222.5 nM, 111.1 nM, 55.5 nM, 27.5 nM, 13.6 nM) at 24 hours

On MDA-MB-231 cells, the effects of combinations of Doxorubicin with Tariquidar and Fucoidan were examined. As shown in Figure 68, when a constant dose of DOX (10 µM) was combined with different doses of TRQ, there was essentially no difference in the viability of the cells up to around 110 nM TRQ concentration in the first

24 hours. Cell viability decreased when TRQ was further increased. However, in 48 and 72 hours, cell viability was approximately 60% for almost all TRQ doses examined. It was observed a further decline in cell viability after around 220 nM.

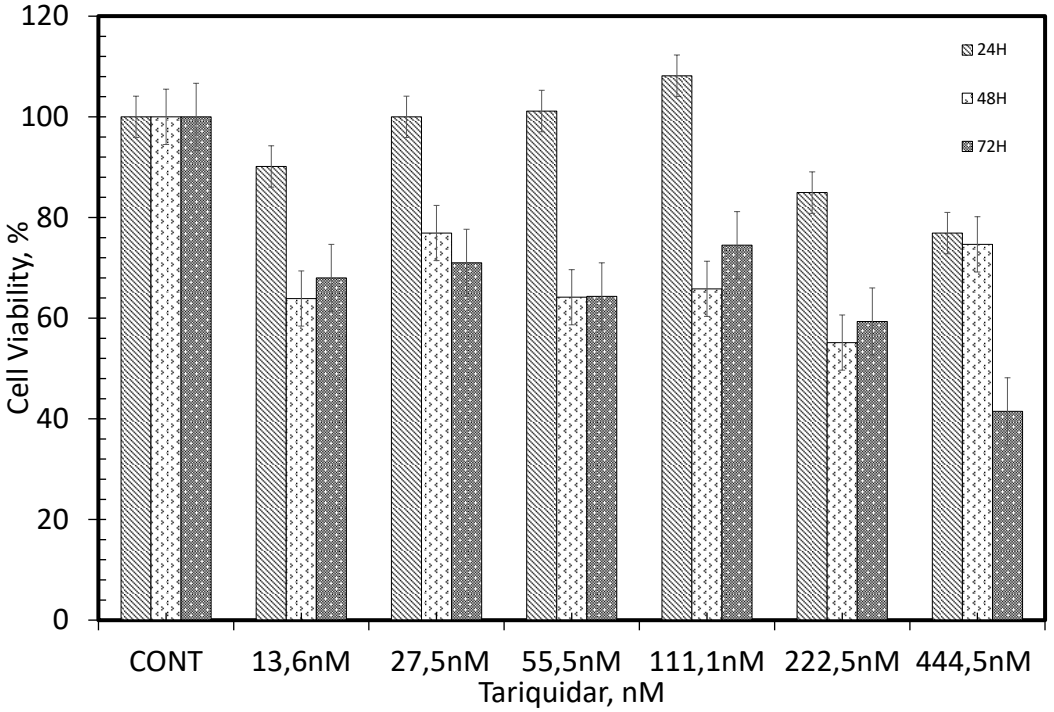

Figure 68. The combined effect of Doxorubicin (10 µM) with Tariquidar on cell viability.

Fucoidan is regarded as an anticancer agent in the literature, but we anticipated it would work synergically with DOX. According to our findings, DOX and fucoidan together promoted cell proliferation at nearly all fucoidan doses (Figure 69, Figure 70). It was found that there was a time-dependent decline in cell viability when each dosage was evaluated separately.

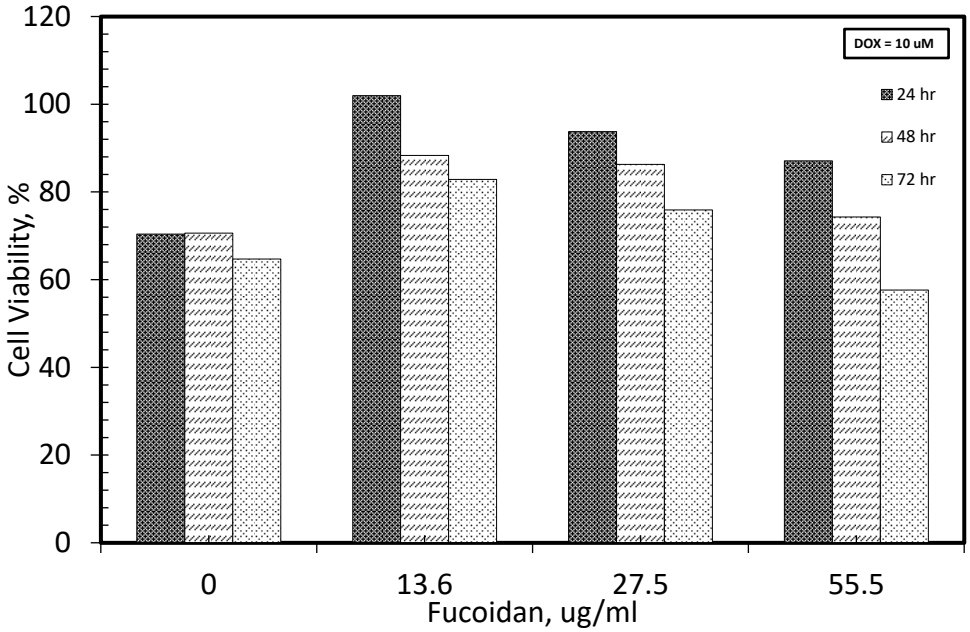

Figure 69. Cell viability of Fucoidan and Doxorubicin combination

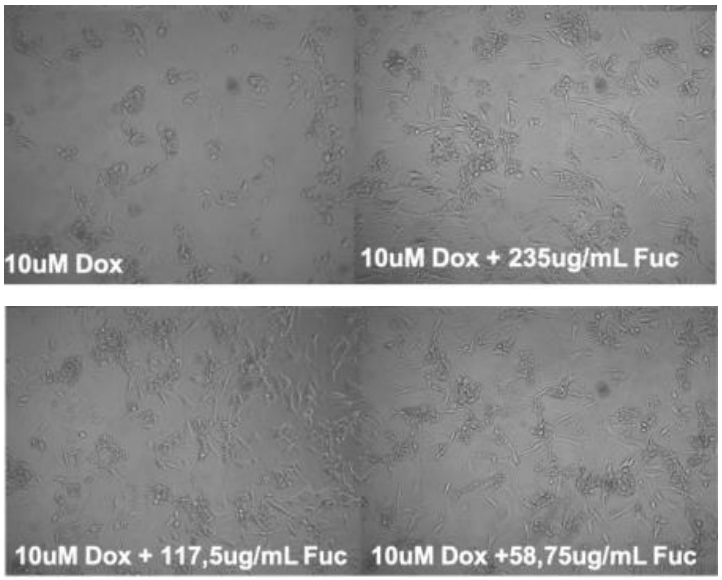

Figure 70. Microscopic image of Fucoidan and Doxorubicin combination

CHAPTER 5

CONCLUSION

In this thesis, the development of Tariquidar and Doxorubicin loaded liposomes composed of DSPC, Cholesterol, and DSTAP was studied. Fucoidan was coated on these liposomes to target the p-selectins expressed in MDA-MB-231 cells specifically.DSTAP was used as a cationic lipid to create cationic liposomes since fucoidan is a negatively charged polysaccharide. Zeta potential measurements were used to identify the most stable form of the liposomal solution with varying cationic lipid (DSTAP) concentrations while keeping the Cholesterol mol percent constant at 30%. Our findings showed that zeta potential increased with the increasing DSTAP percentage, resulting in Zeta potential values of +30 mV above 15% DSTAP. No matter how much DSTAP was included in the formulation, all liposomes had a size of about 200 nm, proving that the polycarbonate membrane's pore size determines the liposome's ultimate size. The Zeta potential measurements determined optimal liposome composition as DSPC/Cholesterol/DSTAP: 55/30/15.

Optimum Tariquidar loading was observed at a TRQ/Lipid molar ratio of 0.012, with encapsulation and loading efficiencies of 50% and 30%, respectively.

Doxorubicin was loaded into these liposomes by pH gradient (active loading).The presence of cationic DSTAP in the formulation decreased the DOX loading efficiency slightly, but the observed effect was DSTAP percentage independent, exhibiting an encapsulation efficiency of 70%. Tariquidar is loaded into the bilayer of liposomes, while DOX is in the core of liposomes. Because of its hydrophobic nature, TRQ is loaded into liposomes while making them (passive loading). However, Doxorubicin encapsulation efficiency was not affected significantly by the presence of TRQ in the bilayer. Loading of liposomes neither TRQ nor DOX did not affect the size and zeta potential of the liposomes.

Fucoidan was coated with electrostatic interaction onto the liposomes containing %15 DSTAP liposomes. Our results showed that the ratio of amounts of

Fucoidan to lipid is very important for successful coating. Agglomeration can occur at low Fucoidan/Lipid molar ratio because of partially coated liposomes (bridging flocculation). Agglomeration can also happen at a very high Fucoidan/Lipid molar ratio because of depletion flocculation. Zeta potential can be used as a guide to obtain the optimum Fucoidan/Lipid molar ratio.

REFERENCES

Abraham, Sheela A, Dawn N Waterhouse, Lawrence D Mayer, Pieter R Cullis, Thomas D Madden, and Marcel B Bally. 2005a. "[4] The Liposomal Formulation of Doxorubicin."

———. 2005b. "The Liposomal Formulation of Doxorubicin."

Alavi, Mehran, and Mehrdad Hamidi. 2019. "Passive and Active Targeting in Cancer Therapy by Liposomes and Lipid Nanoparticles," Drug Metabolism and Personalized Therapy, 34 (1). https://doi.org/doi:10.1515/dmpt-2018-0032.

Ale, Marcel Tutor, Jørn D. Mikkelsen, and Anne S. Meyer. 2011. "Important Determinants for Fucoidan Bioactivity: A Critical Review of Structure-Function Relations and Extraction Methods for Fucose-Containing Sulfated Polysaccharides from Brown Seaweeds." *Marine Drugs*. MDPI AG. https://doi.org/10.3390/md9102106.

Alekseyenko, T V, S Ya. Zhanayeva, A A Venediktova, T N Zvyagintseva, T A Kuznetsova, N N Besednova, and T A Korolenko. 2007. "Antitumor and Antimetastatic Activity of Fucoidan, a Sulfated Polysaccharide Isolated from the Okhotsk Sea Fucus Evanescens Brown Alga." *Bulletin of Experimental Biology and Medicine* 143 (6): 730–32. https://doi.org/10.1007/s10517-007-0226-4.

Barenholz, Yechezkel (Chezy). 2012. "Doxil® — The First FDA-Approved Nano-Drug: Lessons Learned." *Journal of Controlled Release* 160 (2): 117–34. https://doi.org/https://doi.org/10.1016/j.jconrel.2012.03.020.

Bax, Benjamin D., Garib Murshudov, Anthony Maxwell, and Thomas Germe. 2019. "DNA Topoisomerase Inhibitors: Trapping a DNA-Cleaving Machine in Motion." *Journal of Molecular Biology*. Academic Press. https://doi.org/10.1016/j.jmb.2019.07.008.

Bukowski, Karol, Mateusz Kciuk, and Renata Kontek. 2020. "Mechanisms of Multidrug Resistance in Cancer Chemotherapy." *International Journal of Molecular Sciences*. MDPI AG. https://doi.org/10.3390/ijms21093233.

Chawla, Sant P., Victoria S. Chua, Lita Fernandez, Dorris Quon, William C. Blackwelder, Erlinda M. Gordon, and Frederick L. Hall. 2010. "Advanced Phase I/II Studies of Targeted Gene Delivery in Vivo: Intravenous Rexin-g for

Gemcitabine-Resistant Metastatic Pancreatic Cancer." *Molecular Therapy* 18 (2): 435–41. https://doi.org/10.1038/mt.2009.228.

Cole, S P C, G Bhardwaj, J H Gerlach, J E Mackie, C E Grant, K C Almquist, A J Stewart, E U Kurz, A M V Duncan, and R G Deeley. 1992. "Overexpression of a Transporter Gene in a Multidrug-Resistant Human Lung Cancer Cell Line." *Science* 258 (5088): 1650–54. https://doi.org/10.1126/science.1360704.

Cumashi, Albana, Natalia A Ushakova, Marina E Preobrazhenskaya, Armida D'Incecco, Antonio Piccoli, Licia Totani, Nicola Tinari, et al. 2007. "A Comparative Study of the Anti-Inflammatory, Anticoagulant, Antiangiogenic, and Antiadhesive Activities of Nine Different Fucoidans from Brown Seaweeds." *Glycobiology* 17 (5): 541–52. https://doi.org/10.1093/glycob/cwm014.

Danhier, Fabienne, Olivier Feron, and Véronique Préat. 2010. "To Exploit the Tumor Microenvironment: Passive and Active Tumor Targeting of Nanocarriers for Anti-Cancer Drug Delivery." *Journal of Controlled Release* 148 (2): 135–46. https://doi.org/https://doi.org/10.1016/j.jconrel.2010.08.027.

Daraee, Hadis, Ali Etemadi, Mohammad Kouhi, Samira Alimirzalu, and Abolfazl Akbarzadeh. 2016. "Application of Liposomes in Medicine and Drug Delivery." *Artificial Cells, Nanomedicine, and Biotechnology* 44 (1): 381–91. https://doi.org/10.3109/21691401.2014.953633.

Das, Sabya Sachi, Priyanshu Bharadwaj, Muhammad Bilal, Mahmood Barani, Abbas Rahdar, Pablo Taboada, Simona Bungau, and George Z. Kyzas. 2020. "Stimuli-Responsive Polymeric Nanocarriers for Drug Delivery, Imaging, and Theragnosis." *Polymers*. MDPI AG. https://doi.org/10.3390/polym12061397.

Delfino, Ines, Nadia Diano, and Maria Lepore. 2021. "Advanced Optical Sensing of Phenolic Compounds for Environmental Applications." *Sensors*. MDPI. https://doi.org/10.3390/s21227563.

Fox, Elizabeth, Brigitte C. Widemann, Devang Pastakia, Clara C. Chen, Sherry X. Yang, Diane Cole, and Frank M. Balis. 2015. "Pharmacokinetic and Pharmacodynamic Study of Tariquidar (XR9576), a P-Glycoprotein Inhibitor, in Combination with Doxorubicin, Vinorelbine, or Docetaxel in Children and Adolescents with Refractory Solid Tumors." *Cancer Chemotherapy and Pharmacology* 76 (6): 1273–83. https://doi.org/10.1007/s00280-015-2845-1.

Fritze, Andreas, Felicitas Hens, Andrea Kimpfler, Rolf Schubert, and Regine Peschka-Süss. 2006. "Remote Loading of Doxorubicin into Liposomes Driven by a

Transmembrane Phosphate Gradient." *Biochimica et Biophysica Acta (BBA) - Biomembranes* 1758 (10): 1633–40. https://doi.org/https://doi.org/10.1016/j.bbamem.2006.05.028.

Fugit, Kyle D., Tian Xiang Xiang, Du H. Choi, Sogol Kangarlou, Eva Csuhai, Paul M. Bummer, and Bradley D. Anderson. 2015. "Mechanistic Model and Analysis of Doxorubicin Release from Liposomal Formulations." *Journal of Controlled Release* 217 (August): 82–91. https://doi.org/10.1016/j.jconrel.2015.08.024.

Gao, Weiwei, Che-Ming J Hu, Ronnie H Fang, and Liangfang Zhang. 2013. "Liposome-like Nanostructures for Drug Delivery." *Journal of Materials Chemistry B* 1 (48): 6569–85. https://doi.org/10.1039/C3TB21238F.

Gillet, Jean-Pierre, and Michael M Gottesman. 2010. "Mechanisms of Multidrug Resistance in Cancer." In *Multi-Drug Resistance in Cancer*, edited by Jun Zhou, 47–76. Totowa, NJ: Humana Press. https://doi.org/10.1007/978-1-60761-416-6_4.

Gokhalel, P C, B Radhakrishnan', S R Husain', D R Abernethy2, R Sacherl, A Dritschilo3, and A Rahman'. 1996. "An Improved Method of Encapsulation of Doxorubicin in Liposomes: Pharmacological, Toxicological and Therapeutic Evaluation." *Bridsh Journal of Cancer*. Vol. 74.

Gonzalez Gomez, Azucena, Saifuddin Syed, Kenji Marshall, and Zeinab Hosseinidoust. 2019. "Liposomal Nanovesicles for Efficient Encapsulation of Staphylococcal Antibiotics." *ACS Omega* 4 (6): 10866–76. https://doi.org/10.1021/acsomega.9b00825.

Gote, Vrinda, Anantha Nookala, Pradeep Kumar Bolla, and Dhananjay Pal. 2021. "Drug Resistance in Metastatic Breast Cancer: Tumor Targeted Nanomedicine to the Rescue." *International Journal of Molecular Sciences* 22 (April): 4673. https://doi.org/10.3390/ijms22094673.

Hamaguchi, Tetsuya, Yasuhiro Matsumura, Yukihiro Nakanishi, Kei Muro, Yasuhide Yamada, Yasuhiro Shimada, Kuniaki Shirao, et al. 2004. "Antitumor Effect of MCC-465, Pegylated Liposomal Doxorubicin Tagged with Newly Developed Monoclonal Antibody GAH, in Colorectal Cancer Xenografts." *Cancer Science* 95 (7): 608–13. https://doi.org/https://doi.org/10.1111/j.1349-7006.2004.tb02495.x.

Haran, Gilad, Rivka Cohen, Liliana K Bar, and Yechezkel Barenholz. 1993. "Transmembrane Ammonium Sulfate Gradients in Liposomes Produce Efficient

and Stable Entrapment of Amphipathic Weak Bases." *Biochimica et Biophysica Acta (BBA) - Biomembranes* 1151 (2): 201–15. https://doi.org/https://doi.org/10.1016/0005-2736(93)90105-9.

Hardiansyah, Andri, Ming Chien Yang, Ting Yu Liu, Chih Yu Kuo, Li Ying Huang, and Tzu Yi Chan. 2017. "Hydrophobic Drug-Loaded PEGylated Magnetic Liposomes for Drug-Controlled Release." *Nanoscale Research Letters* 12. https://doi.org/10.1186/s11671-017-2119-4.

Huang, Tse Hung, Yi Han Chiu, Yi Lin Chan, Ya Huang Chiu, Hang Wang, Kuo Chin Huang, Tsung Lin Li, Kuang Hung Hsu, and Chang Jer Wu. 2015. "Prophylactic Administration of Fucoidan Represses Cancer Metastasis by Inhibiting Vascular Endothelial Growth Factor (VEGF) and Matrix Metalloproteinases (MMPs) in Lewis Tumor-Bearing Mice." *Marine Drugs* 13 (4): 1882–1900. https://doi.org/10.3390/md13041882.

Immordino ML, Dosio F, and Cattel L. 2006. "Stealth Liposomes: Review of the Basic Science, Rationale, and Clinical Applications, Existing and Potential," 297–315.

Jafari, Mina, Vishnu Sriram, Zhenyuan Xu, Greg M Harris, and Joo-Youp Lee. 2020. "Fucoidan-Doxorubicin Nanoparticles Targeting P-Selectin for Effective Breast Cancer Therapy." *Carbohydrate Polymers* 249: 116837. https://doi.org/https://doi.org/10.1016/j.carbpol.2020.116837.

Kaul, Goldie, and Mansoor Amiji. 2002. "Long-Circulating Poly(Ethylene Glycol)-Modified Gelatin Nanoparticles for Intracellular Delivery."

Kim, Chang Hyun, Sangkil Lee, Ji Yeh Choi, Min Jeong Lyu, Hyun Min Jung, Yoon Tae Goo, Myung Joo Kang, and Young Wook Choi. 2022. "Simultaneous Delivery of Docetaxel and Tariquidar to Chemoresistance Cancer Cells Using Functionalized Lipid Nanocarriers." https://doi.org/10.21203/rs.3.rs-1880173/v1.

Kim, Eun J., So Y. Park, Jae Yong Lee, and Jung H.Y. Park. 2010. "Fucoidan Present in Brown Algae Induces Apoptosis of Human Colon Cancer Cells." *BMC Gastroenterology* 10 (August). https://doi.org/10.1186/1471-230X-10-96.

Kylin, Harald. 1913. "Zur Biochemie Der Meeresalgen." 83 (3): 171–97. https://doi.org/doi:10.1515/bchm2.1913.83.3.171.

Lara, Lorena Infante, Sabine Fenner, Steven Ratcliffe, Albert Isidro-Llobet, Michael Hann, Ben Bax, and Neil Osheroff. 2018. "Coupling the Core of the Anticancer Drug Etoposide to an Oligonucleotide Induces Topoisomerase II-Mediated

Cleavage at Specific DNA Sequences." *Nucleic Acids Research* 46 (5): 2218–33. https://doi.org/10.1093/nar/gky072.

Lasic, D D, B Čeh, M C A Stuart, L Guo, P M Frederik, and Y Barenholz. 1995. "Transmembrane Gradient Driven Phase Transitions within Vesicles: Lessons for Drug Delivery." *Biochimica et Biophysica Acta (BBA) - Biomembranes* 1239 (2): 145–56. https://doi.org/https://doi.org/10.1016/0005-2736(95)00159-Z.

Lewrick, Felicitas, and Regine Süss. 2010. "Remote Loading of Anthracyclines into Liposomes." In *Liposomes: Methods and Protocols, Volume 1: Pharmaceutical Nanocarriers,* edited by Volkmar Weissig, 139–45. Totowa, NJ: Humana Press. https://doi.org/10.1007/978-1-60327-360-2_9.

Liu, Peng, Guiliang Chen, and Jingchen Zhang. 2022. "A Review of Liposomes as a Drug Delivery System: Current Status of Approved Products, Regulatory Environments, and Future Perspectives." *Molecules*. MDPI. https://doi.org/10.3390/molecules27041372.

Lombardo, Domenico, and Mikhail A. Kiselev. 2022. "Methods of Liposomes Preparation: Formation and Control Factors of Versatile Nanocarriers for Biomedical and Nanomedicine Application." *Pharmaceutics*. MDPI. https://doi.org/10.3390/pharmaceutics14030543.

López Mendoza, Carlos Miguel, and Luz Eugenia Alcántara Quintana. 2022. "Smart Drug Delivery Strategies for Cancer Therapy." *Frontiers in Nanotechnology*. Frontiers Media S.A. https://doi.org/10.3389/fnano.2021.753766.

Luqmani, Y. A. 2005. "Mechanisms of Drug Resistance in Cancer Chemotherapy." In *Medical Principles and Practice,* 14:35–48. S. Karger AG. https://doi.org/10.1159/000086183.

Mao, Qingcheng, and Jashvant D. Unadkat. 2015. "Role of the Breast Cancer Resistance Protein (BCRP/ABCG2) in Drug Transport—an Update." *AAPS Journal* 17 (1): 65–82. https://doi.org/10.1208/s12248-014-9668-6.

Marei, Hany E. 2022. "Multimodal Targeting of Glioma with Functionalized Nanoparticles." *Cancer Cell International* 22 (1): 265. https://doi.org/10.1186/s12935-022-02687-8.

Maria P. Nikolova, Enamala Manoj Kumar, Murthy S. Chavali. 2022. "Liposomes for Drug Delivery and Their Production Methods." https://doi.org/10.3390/pharmaceutics14102195.

Menaa, Farid, Udari Wijesinghe, Gobika Thiripuranathar, Norah A. Althobaiti, Aishah E. Albalawi, Barkat Ali Khan, and Bouzid Menaa. 2021. “Marine Algae-Derived Bioactive Compounds: A New Wave of Nanodrugs?” *Marine Drugs*. MDPI. https://doi.org/10.3390/md19090484.

Mohamed, Esraa Ali, Nasser S M Ismail, Mohamed Hagras, and Hanan Refaat. 2021. “Medicinal Attributes of Pyridine Scaffold as Anticancer Targeting Agents.” *Future Journal of Pharmaceutical Sciences* 7 (1): 24. https://doi.org/10.1186/s43094-020-00165-4.

Mondal, Utpal K., and Marc A. Ilies. 2021. “Efflux Pumps, NHE1, Monocarboxylate Transporters, and ABC Transporter Subfamily Inhibitors.” *PH-Interfering Agents as Chemosensitizers in Cancer Therapy*, January, 95–120. https://doi.org/10.1016/B978-0-12-820701-7.00017-8.

Monteiro, Nelson, Albino Martins, Rui L Reis, and Nuno M Neves. 2014a. “Liposomes in Tissue Engineering and Regenerative Medicine.” *Journal of The Royal Society Interface* 11 (101): 20140459. https://doi.org/10.1098/rsif.2014.0459.

Monteiro, Nelson, Albino Martins, Rui L. Reis, and Nuno M. Neves. 2014b. “Liposomes in Tissue Engineering and Regenerative Medicine.” *Journal of the Royal Society Interface*. Royal Society of London. https://doi.org/10.1098/rsif.2014.0459.

Mourtas, Spyridon, Stela Duraj, Styliani Fotopoulou, and Sophia G. Antimisiaris. 2008. “Integrity of Liposomes in Presence of Various Formulation Excipients, When Dispersed in Aqueous Media and in Hydrogels.” *Colloids and Surfaces B: Biointerfaces* 61 (2): 270–76. https://doi.org/10.1016/j.colsurfb.2007.09.003.

Nieto Montesinos, Rita, Arnaud Béduneau, Alf Lamprecht, and Yann Pellequer. 2015. “Liposomes Coloaded with Elacridar and Tariquidar To Modulate the P-Glycoprotein at the Blood-Brain Barrier.” *Molecular Pharmaceutics* 12 (11): 3829–38. https://doi.org/10.1021/acs.molpharmaceut.5b00002.

Nikolova, Maria P., Enamala Manoj Kumar, and Murthy S. Chavali. 2022a. “Updates on Responsive Drug Delivery Based on Liposome Vehicles for Cancer Treatment.” *Pharmaceutics*. MDPI. https://doi.org/10.3390/pharmaceutics14102195.

———. 2022b. “Updates on Responsive Drug Delivery Based on Liposome Vehicles for Cancer Treatment.” *Pharmaceutics*. MDPI. https://doi.org/10.3390/pharmaceutics14102195.

Nkanga, Christian Isalomboto, Alain Murhimalika Bapolisi, Nnamdi Ikemefuna Okafor, and Rui Werner Maçedo Krause. 2019. “General Perception of Liposomes: Formation, Manufacturing and Applications.” In *Liposomes*, edited by Angel Catala, Ch. 3. Rijeka: IntechOpen. https://doi.org/10.5772/intechopen.84255.

Nussbaumer, Susanne, Pascal Bonnabry, Jean Luc Veuthey, and Sandrine Fleury-Souverain. 2011. “Analysis of Anticancer Drugs: A Review.” *Talanta*. Elsevier B.V. https://doi.org/10.1016/j.talanta.2011.08.034.

Oakman, Catherine, Erica Moretti, Francesca Galardi, Libero Santarpia, and Angelo Di Leo. 2009. “The Role of Topoisomerase IIα and HER-2 in Predicting Sensitivity to Anthracyclines in Breast Cancer Patients.” *Cancer Treatment Reviews* 35 (8): 662–67. https://doi.org/https://doi.org/10.1016/j.ctrv.2009.08.006.

Oliveira, Catarina, Andreia S Ferreira, Ramon Novoa-Carballal, Cláudia Nunes, Iva Pashkuleva, Nuno M Neves, Manuel A Coimbra, Rui L Reis, Albino Martins, and Tiago H Silva. 2017. “The Key Role of Sulfation and Branching on Fucoidan Antitumor Activity.” *Macromolecular Bioscience* 17 (5): 1600340. https://doi.org/https://doi.org/10.1002/mabi.201600340.

Olusanya, Temidayo O.B., Rita Rushdi Haj Ahmad, Daniel M. Ibegbu, James R. Smith, and Amal Ali Elkordy. 2018. “Liposomal Drug Delivery Systems and Anticancer Drugs.” *Molecules*. MDPI AG. https://doi.org/10.3390/molecules23040907.

Pan, Yuanwei, Suqiong Zhou, Yan Li, Badri Parshad, Wenzhong Li, and Rainer Haag. 2021. “Novel Dendritic Polyglycerol-Conjugated, Mesoporous Silica-Based Targeting Nanocarriers for Co-Delivery of Doxorubicin and Tariquidar to Overcome Multidrug Resistance in Breast Cancer Stem Cells.” *Journal of Controlled Release* 330: 1106–17. https://doi.org/https://doi.org/10.1016/j.jconrel.2020.11.015.

Parchekani, Jalil, Abdollah Allahverdi, Majid Taghdir, and Hossein Naderi-Manesh. 2022. “Design and Simulation of the Liposomal Model by Using a Coarse-Grained Molecular Dynamics Approach towards Drug Delivery Goals.” *Scientific Reports* 12 (1). https://doi.org/10.1038/s41598-022-06380-8.

Park, Kinam. 2014. “Controlled Drug Delivery Systems: Past Forward and Future Back.” *Journal of Controlled Release*. Elsevier B.V. https://doi.org/10.1016/j.jconrel.2014.03.054.

Patel, Niravkumar R., Alok Rathi, Dmitriy Mongayt, and Vladimir P. Torchilin. 2011a. "Reversal of Multidrug Resistance by Co-Delivery of Tariquidar (XR9576) and Paclitaxel Using Long-Circulating Liposomes." *International Journal of Pharmaceutics* 416 (1): 296–99. https://doi.org/10.1016/j.ijpharm.2011.05.082.

———. 2011b. "Reversal of Multidrug Resistance by Co-Delivery of Tariquidar (XR9576) and Paclitaxel Using Long-Circulating Liposomes." *International Journal of Pharmaceutics* 416 (1): 296–99. https://doi.org/10.1016/j.ijpharm.2011.05.082.

Rana, Abhilash, and Seema Bhatnagar. 2021a. "Advancements in Folate Receptor Targeting for Anti-Cancer Therapy: A Small Molecule-Drug Conjugate Approach." *Bioorganic Chemistry* 112: 104946. https://doi.org/https://doi.org/10.1016/j.bioorg.2021.104946.

———. 2021b. "Advancements in Folate Receptor Targeting for Anti-Cancer Therapy: A Small Molecule-Drug Conjugate Approach." *Bioorganic Chemistry* 112 (July): 104946. https://doi.org/10.1016/J.BIOORG.2021.104946.

Rani, Kirti, Saurabh Paliwal, and Rani Kirti. 2014. "A Review on Targeted Drug Delivery: Its Entire Focus on Advanced Therapeutics and Diagnostics." *Scholars Journal of Applied Medical Sciences (SJAMS) Sch. J. App. Med. Sci* 2 (1C): 328–31. https://doi.org/10.36347/sjams.2014.v02i01.0069.

Redmond, Kelly Marie, Timothy Richard Wilson, Patrick Gerard Johnston, and Daniel Broderick Longley. 2008. "Resistance Mechanisms to Cancer Chemotherapy." *Frontiers in Bioscience*. Vol. 5138.

Rocca, G La, I Pucci-Minafra, A Marrazzo, P Taormina, and S Minafra. 2004. "Zymographic Detection and Clinical Correlations of MMP-2 and MMP-9 in Breast Cancer Sera." *British Journal of Cancer* 90 (7): 1414–21. https://doi.org/10.1038/sj.bjc.6601725.

Saha, Sounik, Ritankar Majumdar, Akhtar Hussain, Rajan R. Dighe, and Akhil R. Chakravarty. 2013. "Biotin-Conjugated Tumour-Targeting Photocytotoxic Iron(III) Complexes." *Philosophical Transactions of the Royal Society A: Mathematical, Physical and Engineering Sciences* 371 (1995). https://doi.org/10.1098/rsta.2012.0190.

Sawant, Rupa R., and Vladimir P. Torchilin. 2012. "Challenges in Development of Targeted Liposomal Therapeutics." *AAPS Journal*. https://doi.org/10.1208/s12248-012-9330-0.

Shen, Peili, Zongmei Yin, Guiyan Qu, and Chunxia Wang. 2018. “11 - Fucoidan and Its Health Benefits.” In *Bioactive Seaweeds for Food Applications*, edited by Yimin Qin, 223–38. Academic Press. https://doi.org/https://doi.org/10.1016/B978-0-12-813312-5.00011-X.

Silverman, Jeffrey A., and Steven R. Deitcher. 2013. “Marqibo® (Vincristine Sulfate Liposome Injection) Improves the Pharmacokinetics and Pharmacodynamics of Vincristine.” *Cancer Chemotherapy and Pharmacology*. https://doi.org/10.1007/s00280-012-2042-4.

Stavrovskaya, A A. 2000. “Cellular Mechanisms of Multidrug Resistance of Tumor Cells.” *Biochemistry. Biokhimiia* 65 (1): 95–106. http://www.ncbi.nlm.nih.gov/pubmed/10702644.

Sur, Surojit, Anja C. Fries, Kenneth W. Kinzler, Shibin Zhou, and Bert Vogelstein. 2014. “Remote Loading of Preencapsulated Drugs into Stealth Liposomes.” *Proceedings of the National Academy of Sciences of the United States of America* 111 (6): 2283–88. https://doi.org/10.1073/pnas.1324135111.

Teruya, Takeshi, Teruko Konishi, Shuntoku Uechi, Hajime Tamaki, and Masakuni Tako. 2007. “Anti-Proliferative Activity of Oversulfated Fucoidan from Commercially Cultured Cladosiphon Okamuranus TOKIDA in U937 Cells.” *International Journal of Biological Macromolecules* 41 (3): 221–26. https://doi.org/https://doi.org/10.1016/j.ijbiomac.2007.02.010.

Tewabe, Ashagrachew, Atlaw Abate, Manaye Tamrie, Abyou Seyfu, and Ebrahim Abdela Siraj. 2021. “Targeted Drug Delivery — from Magic Bullet to Nanomedicine: Principles, Challenges, and Future Perspectives.” *Journal of Multidisciplinary Healthcare*. Dove Medical Press Ltd. https://doi.org/10.2147/JMDH.S313968.

Thorn, Caroline F., Connie Oshiro, Sharon Marsh, Tina Hernandez-Boussard, Howard McLeod, Teri E. Klein, and Russ B. Altman. 2011a. “Doxorubicin Pathways: Pharmacodynamics and Adverse Effects.” *Pharmacogenetics and Genomics* 21 (7): 440–46. https://doi.org/10.1097/FPC.0b013e32833ffb56.

———. 2011b. “Doxorubicin Pathways: Pharmacodynamics and Adverse Effects.” *Pharmacogenetics and Genomics* 21 (7): 440–46. https://doi.org/10.1097/FPC.0b013e32833ffb56.

Valent, Peter, Bernd Groner, Udo Schumacher, Giulio Superti-Furga, Meinrad Busslinger, Robert Kralovics, Christoph Zielinski, et al. 2016. “Paul Ehrlich

(1854-1915) and His Contributions to the Foundation and Birth of Translational Medicine." *Journal of Innate Immunity*. S. Karger AG. https://doi.org/10.1159/000443526.

Wang, Yu, Maochen Xing, Qi Cao, Aiguo Ji, Hao Liang, and Shuliang Song. 2019. "Biological Activities of Fucoidan and the Factors Mediating Its Therapeutic Effects: A Review of Recent Studies." *Marine Drugs* 17 (3). https://doi.org/10.3390/md17030183.

Warchal, Scott J., John C. Dawson, and Neil O. Carragher. 2016. "Development of the Theta Comparative Cell Scoring Method to Quantify Diverse Phenotypic Responses between Distinct Cell Types." *Assay and Drug Development Technologies* 14 (7): 395–406. https://doi.org/10.1089/adt.2016.730.

Waterhouse, Dawn N, Paul G Tardi, Lawrence D Mayer, and Marcel B Bally. n.d. "A Comparison of Liposomal Formulations of Doxorubicin with Drug Administered in Free Form Changing Toxicity Profiles."

Xia, Yuqiong, Mei Fang, Jingyu Dong, Chunzhong Xu, Zhen Liao, Pengbo Ning, and Qi Zeng. 2018. "PH Sensitive Liposomes Delivering Tariquidar and Doxorubicin to Overcome Multidrug Resistance of Resistant Ovarian Cancer Cells." *Colloids and Surfaces. B, Biointerfaces* 170 (October): 514–20. https://doi.org/10.1016/j.colsurfb.2018.06.055.

Yamasaki-Miyamoto, Yumi, Masao Yamasaki, Hirofumi Tachibana, and Koji Yamada. 2009. "Fucoidan Induces Apoptosis through Activation of Caspase-8 on Human Breast Cancer MCF-7 Cells." *Journal of Agricultural and Food Chemistry* 57 (18): 8677–82. https://doi.org/10.1021/jf9010406.

Zamani, Parvin, Amir Abbas Momtazi-Borojeni, Maryam Ebrahimi Nik, Reza Kazemi Oskuee, and Amirhossein Sahebkar. 2018. "Nanoliposomes as the Adjuvant Delivery Systems in Cancer Immunotherapy." *Journal of Cellular Physiology* 233 (7): 5189–99. https://doi.org/https://doi.org/10.1002/jcp.26361.

Zhang, Wei, Tatsuya Oda, Qing Yu, and Jun O. Jin. 2015. "Fucoidan from Macrocystis Pyrifera Has Powerful Immune-Modulatory Effects Compared to Three Other Fucoidans." *Marine Drugs* 13 (3): 1084–1104. https://doi.org/10.3390/md13031084.

Zhang, Yilin, Shravan Kumar Sriraman, Hilary A. Kenny, Ed Luther, Vladimir Torchilin, and Ernst Lengyel. 2016. "Reversal of Chemoresistance in Ovarian Cancer by Co-Delivery of a P-Glycoprotein Inhibitor and Paclitaxel in a

Liposomal Platform." *Molecular Cancer Therapeutics* 15 (10): 2282–93. https://doi.org/10.1158/1535-7163.MCT-15-0986.